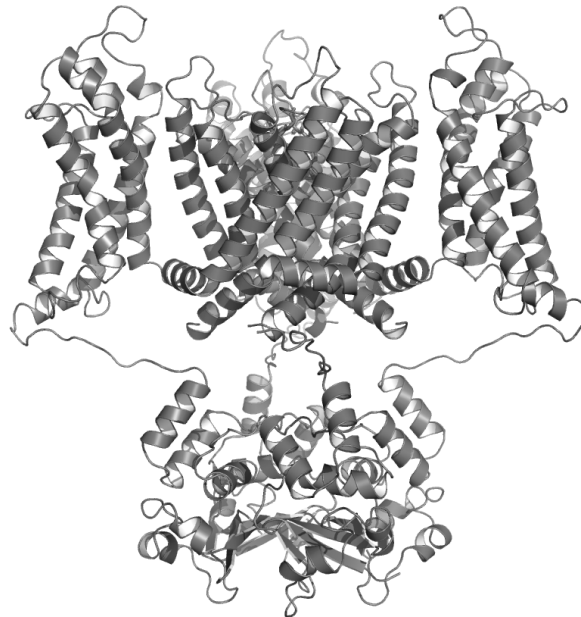


SÖREN WACKER

MOLECULAR DYNAMICS STUDY OF POTASSIUM CHANNELS,  
THEIR INTERACTION WITH NON-AMINO ACID COMPOUNDS  
AND PEPTIDIC SCORPION TOXINS  
PARAMETERIZATION AND BINDING AFFINITIES

DIPLOMARBEIT



MOLECULAR DYNAMICS STUDY OF POTASSIUM CHANNELS,  
THEIR INTERACTION WITH NON-AMINO ACID COMPOUNDS  
AND PEPTIDIC SCORPION TOXINS

-

PARAMETERIZATION AND BINDING AFFINITIES

DIPLOMARBEIT

VERFASST VON

SÖREN WACKER

AUS

STADTHAGEN

ANGEFERTIGT IN DER

ABTEILUNG FÜR THEORETISCHE UND COMPUTERGESTÜTZTE BIOPHYSIK  
AM MAX PLANCK INSTITUT FÜR BIOPHYSIKALISCHE CHEMIE

GÖTTINGEN, DEN 30.10.2008

# Contents

<b>1</b>	<b>Introduction</b>	<b>3</b>
<b>2</b>	<b>Potassium channels</b>	<b>4</b>
2.1	The action potential . . . . .	4
2.2	Classification and nomenclature . . . . .	5
2.3	Physiology . . . . .	6
2.4	Structure and function . . . . .	8
2.4.1	The selectivity filter . . . . .	8
2.4.2	Occupation and conduction . . . . .	9
2.4.3	Snug-fit . . . . .	9
2.4.4	The $\alpha$ -subunit . . . . .	10
2.4.5	Gating . . . . .	10
2.4.6	Inactivation and recovery from inactivation . . . . .	11
2.4.7	The adjacent $\beta$ -subunits . . . . .	12
<b>3</b>	<b>Crystal-structures and model channels</b>	<b>13</b>
3.1	KcsA-WT and KcsA-K <sub>V</sub> 1.3 . . . . .	13
3.2	The “paddle-chimera channel”: K <sub>V</sub> 1.2-2.1 . . . . .	14
3.3	KvAP . . . . .	15
<b>4</b>	<b>Inhibitors</b>	<b>16</b>
4.1	Toxic peptides . . . . .	16
4.2	Tetraethylammonium . . . . .	16
4.3	4-Aminopyridine . . . . .	17
<b>5</b>	<b>Theory</b>	<b>18</b>
5.1	Molecular Dynamics Simulations . . . . .	18
5.2	Force Fields . . . . .	19
5.2.1	The all-atom force field for organic molecules and peptides (OPLSAA) . . . . .	19
5.2.2	AMBER and GAFF . . . . .	20
5.3	Temperature-Enhanced Essential Dynamics - TEEREX . . . . .	21
5.4	Estimating Binding Free Energies . . . . .	21
5.4.1	First Principles Docking . . . . .	22
5.4.2	Linear Interaction Energy . . . . .	23
5.4.3	Umbrella Sampling and the Potential of Mean Force . . . . .	23
5.5	IC <sub>50</sub> estimation . . . . .	24

<b>6</b>	<b>Inhibition of Potassium Channels</b>	<b>25</b>
6.1	Material & Methods . . . . .	25
6.2	KcsA-Kv1.3 and KTX . . . . .	26
6.2.1	Simulations . . . . .	27
6.2.2	Analysis of the conformational changes observed in MD simulation . . . . .	28
6.2.3	KTX binding relation to C-type inactivation . . . . .	28
6.3	K <sup>+</sup> channels and TEA . . . . .	28
6.3.1	The distribution of TEA1 and TEA2 is quasi fixed in simulations . . . . .	30
6.3.2	TEA - First Principles Docking . . . . .	30
6.4	Conclusions . . . . .	32
<b>7</b>	<b>The parameterization of non-amino acid compounds</b>	<b>33</b>
7.1	Parameterization Process . . . . .	33
7.2	Charge determination . . . . .	35
7.2.1	Partial charges, conformational space and chemical structure . . . . .	35
7.3	TEA . . . . .	37
7.4	Nifedipine: Sampling . . . . .	37
7.4.1	Sampling approaches . . . . .	39
7.5	Cisapride: Self-convergence . . . . .	40
7.6	Pentamidine: Flexibility . . . . .	42
7.7	4-Fluorosulfonylpiperidine: The influence of the environment. . . . .	43
7.8	Conclusions . . . . .	47
<b>8</b>	<b>Potential of Mean Force and the estimation of IC<sub>50</sub> values</b>	<b>48</b>
8.1	Methods . . . . .	48
8.2	Binding of TEA on the K <sub>V</sub> 1.2-2.1 receptor . . . . .	49
8.2.1	Calibration of the sampling conditions . . . . .	49
8.2.2	Binding of TEA on the extracellular K <sub>V</sub> 1.2-2.1 receptor site . . . . .	53
8.2.3	Binding of TEA on the intracellular K <sub>V</sub> 1.2-2.1 receptor site . . . . .	55
8.3	Validation of a hERG-homology model . . . . .	56
8.4	Conclusions . . . . .	56
<b>9</b>	<b>Discussion</b>	<b>57</b>

# Abstract

The subject of this thesis are inhibitory interactions between potassium channels and various molecules. The main findings are based on molecular dynamics simulations supported by quantum-mechanical calculations. The aim of this thesis is to develop a method for the prediction of affinities between drugs and transmembrane channel proteins. An initial study focused on the binding of a peptidic scorpion toxin (KTX) to a potassium channel chimera (KcsA-K<sub>v</sub>1.3). In collaboration with experimental groups, we established the molecular mechanism underlying the inhibition of the channel chimera due to KTX. Subsequently, simulations with a potassium channel blocking compound (TEA) have highlighted the necessity of the automatic generation of robust simulation parameters for arbitrary molecules. In particular, the influence of a compound's conformation on the calculated charge distribution was investigated. A method for the generation of *force field parameters* for non-amino acid compounds is described and a methodology is presented from which a self-consistent set of partial charges can be derived taking into account the possible conformations of a compound. Finally, the estimation of IC<sub>50</sub> concentrations based on *umbrella simulations* was tested suggesting a feasible simulation protocol for the prediction of binding affinities that can be directly compared to the experiment.

# Abriss

Das Thema der vorliegenden Arbeit sind inhibitorische Wechselwirkungen zwischen Kaliumkanälen und verschiedenen Molekülen. Die Hauptresultate dieser Arbeit basieren auf Molekular-Dynamic Simulationen sowie quantenmechanischen Berechnungen. Ziel dieser Arbeit ist die Entwicklung einer Methode für die Vorhersage der Affinitäten zwischen Medikamenten und transmembranen Kanalproteinen. Eine erste Studie behandelte die Bindung eines peptidischen Toxins (KTX) aus dem Gift eines Scorpions an eine Kaliumkanal-Chimäre (KcsA-K<sub>v</sub>1.3). In Zusammenarbeit mit experimentellen Gruppen konnten essentielle molekulare Mechanismen ermittelt werden, die der Hemmung der Kanalfunktion durch KTX zu Grunde liegen. Anschließende Simulationen mit einem bekannten Hemmstoff für Kaliumkanäle (TEA) verdeutlichten die Notwendigkeit einer automatisierten Generierung von akkuraten Kraftfeldparametern für beliebige Moleküle. Zu diesem Zweck wurde insbesondere die Abhängigkeit der Partialladungsverteilung von der Konformation verschiedener Moleküle untersucht. Eine Methode für die Generierung von Kraftfeldparametern wird beschrieben und eine Methodik wird präsentiert mit deren Hilfe selbstkonsistente Partialladungen unter Einbeziehung der möglichen Konformationen erzeugt werden können. Zuletzt wurde eine Methode zur Abschätzung von IC<sub>50</sub> Konzentrationen getestet, welche möglicherweise ein geeignetes Protokoll für die Vorhersage von Bindungsaffinitäten darstellt den direkten Vergleich mit experimentellen Befunden erlaubend.

# Chapter 1

## Introduction

Signal transduction processes are processes by which a cell converts one kind of signal or stimulus into another. They are essential for both monocellular and multicellular organisms because they allow the cell to react to changes of the cellular environment. In multicellular organisms signal transduction is also important for converting inner and outer stimuli. Complex organisms like humans or even flies like the fruit fly *Drosophila*, the most studied organism in biological research, require a rapid and accurate system of information exchange among cells. In nature, these networks are realized by a wide variety of proteins, enzymes, ligands, second messengers, hormones, neurotransmitter and ions. Roughly, half of the 25 grand gene-families of the human genome is used for the processing of information.

One special kind of signal transduction proteins are potassium channels. Their function is the regulation of the permeability of plasmamembranes for  $K^+$  ions in order to change the electrochemical gradient which in turn originates the ions tendency to move across the membrane. This tendency is caused by the entropically conditioned exertion to reduce concentration differences on the one hand and the compensation of electrostatic potential between the inner- and the extracellular side of the membrane on the other hand. This gradient is, for example, essential for the intercellular transduction of signals and represents the driving force for the motion of ions in biological systems. Voltage gated ion channels contribute to changes of the electrostatic potential and are at the same time themselves controlled by changes of this potential.

The distortion of ion channels, e.g. due to the blockade of a drug or a mutation, can change the form of the action potential and evoke malfunctions of the overall system the the cell is part of. The inhibition of the human ERG  $K^+$  channel (hERG) highly expressed in muscle cells of the heart, as a side effect of certain drugs can cause an elongation of the plateau of the cell's action potential. That can cause cardiac arrhythmia or even sudden death. This channel gave the motivation for the thesis at hand. The comprehension of the mechanisms that underly this inhibition could qualify us to make reasonable suggestions for new drugs that do not have this side effect. Unfortunately, the structure of the hERG channel is unknown and the overall sequence identity to known structures is below 30% which makes a homology modelling difficult. A reliable method for the prediction of binding affinities of drugs to receptors requires on the one hand a solid model for both the receptor and the drug and on the other hand a method for the accurate calculation of binding energies. This thesis focuses on the methods for the generation of *force field parameters* for non-amino acid residues and the prediction of binding affinities to receptors whose structure is already known and well parameterized.

## Chapter 2

# Potassium channels

With more than 140 members the voltage gated ion channels are one of the largest superfamilies of signal transduction proteins that perform many different tasks in both eukariotic and procariotic cells. The superfamily include  $K^+$ ,  $Na^+$ ,  $Ca^{2+}$  and  $Cl^-$  channels. They form membrane spanning pores which conduct predominantly their eponymous ion [49]. These channels enable cells to generate spontaneous bursts of action potentials, to make long plateaus in the action potential, to regulate the overall excitability of the cell or to generate regular pacemaker potentials [39]. The founding member of this superfamily of ion channels are the voltage-gated sodium channels which resemble in their structure the voltage-gated calcium channels. The voltage-gated potassium channels form the second structural architecture of this superfamily. They appear in virtually all living organisms and play a crucial role in the partly controlling live-sustaining functions like, for example, the transduction of nerve impulses and the regulation of the heart beat frequency [49].

### 2.1 The action potential

The action potential is a membrane potential change caused by the flow of ions through selective ion channels in the membrane. It is defined as the inside potential  $V_{in}$  minus the outside potential  $V_{out}$ .

$$V_{action} = V_{in} - V_{out} \quad (2.1)$$

Often  $V_{out}$  is treated as the ground potential  $V_o = 0$  mV. For the resting potential a value of about  $-70 \pm 30$  mV is typical. Electrically excitable cells can respond to changes of the applied potential in an all-or-nothing manner. If the action potential depolarizes (becomes more positive) and overcomes a critical value, the potential shortly becomes positive and then repolarizes (returns to the resting potential). These changes are accompanied by consecutive changes in the membrane conductances for different ions due to changes of the selective permeabilities [39]. The equilibrium membrane potential depends on the inner  $c_i^i$  and outer concentrations  $c_i^o$  of the ions and the specific permeabilities  $P_i$  and can be approximated with the Goldman-equation. As an example the Goldman-equation is shown for a system with three kinds of ions ( $K^+$ ,  $Na^+$ ,  $Cl^-$ ) in eq. 2.2. If the inner and outer concentration for the ion  $i$  is known it is possible to calculate the equilibrium potential for that ion with the Nerst-equation (eq. 2.3).

$$V_{eq} = k_B T \ln \left( \frac{P_K c_K^o + P_{Na} c_{Na}^o + P_{Cl} c_{Cl}^i}{P_K c_K^i + P_{Na} c_{Na}^i + P_{Cl} c_{Cl}^o} \right) \quad (2.2)$$

$$V_{eq,i} = k_B T \ln \left( \frac{c_i^i}{c_i^o} \right) \quad (2.3)$$

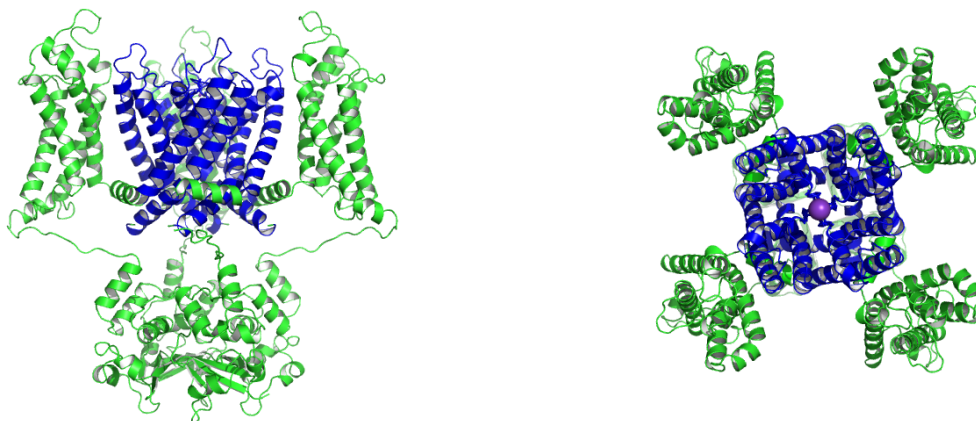


Figure 2.1: A model of a  $K^+$  channel crystal structure in cartoon representation. The  $K^+$  pore domain is colored blue. One of the four voltage sensing domains is removed in the lateral view (left) for clarity. The top view (right) shows where the  $K^+$  ions (purple balls) march through the channel.

The resulting equilibrium potential lies somewhere between the equilibrium potentials for each ion, weighted with the specific permeabilities. If the specific permeability for ion  $i$  increases, then the equilibrium potential is forced closer to  $V_{eq,i}$ . The action potential shows in general the following behavior: Firstly, the membrane becomes more permeable to  $Na^+$  ions. Therefore the equilibrium potential is closer to  $V_{eq,Na} \sim +60$  mV that causes an inwardly directed flux of  $Na^+$  ions. Depolarization forces the voltage gated potassium channels in the open state. Their opening increases the permeability for  $K^+$  ions and an outwardly directed flux of  $K^+$  ions repolarizes the membrane. The specific form of an action potential varies in dependence of the attending ions and channels.

## 2.2 Classification and nomenclature

The Database of the International Union of Pharmacology (IUPHAR) lists 78 different voltage gated potassium channel receptors: 40  $K_v$  channels, 15 two-pore channels, 15 inward rectifier and 8 calcium activated channels. The sequencing of the human genome initially identified 67 human  $K^+$  channel proteins [49]. The architectures of  $K^+$  channel families consists of diverse variations build upon a common pore-forming structure. The primary criterion for the classification of  $K^+$  channels is the number of transmembrane helices (TM-helices) per molecule [44]. Four classes of potassium channels have been described so far, which differ in the number of TM-helices and pores [33]. These are in detail:

- Those channels containing six transmembrane helices and one pore forming region (c.t. 2.1). This group contains voltage gated  $K^+$  channels ( $K_V$ ), KQT-type channels, nucleotide gated calcium-activated channels ( $K_{CNG}$ ), *ether-a-go-go*-related channels (eag, erg, elk) and the related small- and intermediate-conductance  $Ca^{2+}$ -activated  $K^+$ -channels ( $K_{Ca}$ ).
- The group with two transmembrane helices and one pore forming region contains the *inward rectifiers* ( $K_{IR}$ ), the ATP-activated  $K^+$  channels ( $K_{ATP}$ ) and G protein-coupled  $K^+$  channels.
- A class with eight transmembrane helices and two pore forming regions ( $K_{2P}$ ).
- The large-conductance calcium-activated  $K^+$  channels that contain 7 TM helices.

Slowly inactivating or non-inactivating  $K_V$  channels are commonly referred to as *delayed rectifiers* while rapidly inactivating  $K_V$  channels are referred to as *A-type channels* [49]. The  $K^+$  channels with 7 TM-helices per subunit are admittedly defined as a separate structural class, because contrary to the 6TM-channels and 2TM-channels the N-terminus of the 7TM-channels is situated on the extracellular side of the membrane [49, 33]. Sequence conservation among all kinds of  $K^+$  channels, as well as  $K_{CNG}$  channels is strongest for the amino acids corresponding to the pore region (cf. section 2.4.4) [22].

In the course of time there were three systems of  $K^+$  channel nomenclature available. The original nomenclature that created subfamilies  $K_V1$ - $K_V6$  has not been updated for several years. Another system, called the *KCN system*, established by the *Human Gene Nomenclature Committee* ignores completely the structural and phylogenetic relations between the channels and therefore lacks an intuitive comprehensibility [49, 33]. The current system takes into account structural and functional relationships of the channels. For example, the 6TM-channels are split up into two distinct groups, i.e. the  $K_{Ca}$  and  $K_V$  channels. This notion follows a combination of two numbers separated by a dot (e.g.  $K_V1.7$ ). The first numbers denotes the channel a subgroup and the second gives the order of investigation. Channels within the same group (e.g.  $K_{IR}$ ) exhibit functional similarity whereas channels within a certain subgroup are phylogenetic related [33]. The diversity of  $K^+$  channels could further be increased due to the mix and match of different subunits forming heteromeric potassium channels with different subunit stoichiometry. It seems clear that only members of the same subfamily can coassemble and form heteromeric channels [43]. Furthermore, it could be shown that on the basis of one gene different  $K^+$  subunits can be transcribed due to different splicing of the genetic information [39].

There are a few further terms that should be explained here: *Shaker* is one of four  $K^+$  channel coding genes in the genome of *Drosophila*: *Shaker*, *Shal*, *Shab* and *Shaw*. The *Shaker* gene product, the Shaker channel or Shaker, was the first predicted 6TM  $K^+$  channel. Shaker was the first channel where the amino acid residues forming the selectivity filter (cf. section 2.4.1) were clearly identified. The subfamilies  $K_V1$ ,  $K_V2$ ,  $K_V3$  and  $K_V4$  are vertebrate homologues of the channels encoded by *Shaker*, *Shal*, *Shab* and *Shaw*. The bacterial gene *KcsA* from the Gram-positive eubacterium *Streptomyces lividans* encodes the *KcsA* channel, a 2TM  $K^+$  channel that is overall more similar to Shaker than to *inward rectifiers* (cf. section 2.3) and whose pore is an excellent model of eukaryotic  $K^+$  channels, even if its *gating* (cf. section 2.4.5) is apparently quite different. *Shaker* gives rise to at least five different transcripts for channel subunits derived by different splicing [39].

## 2.3 Physiology

Before the first x-ray structure was solved by Doyle et al. in 1998 [22], potassium channels were studied intensively by physiology and mutagenesis experiments. Initially Hodgkin coined the term *delayed rectifier* for  $K^+$  channels of axons of the squid that change the membrane potential with a delay. Actually all

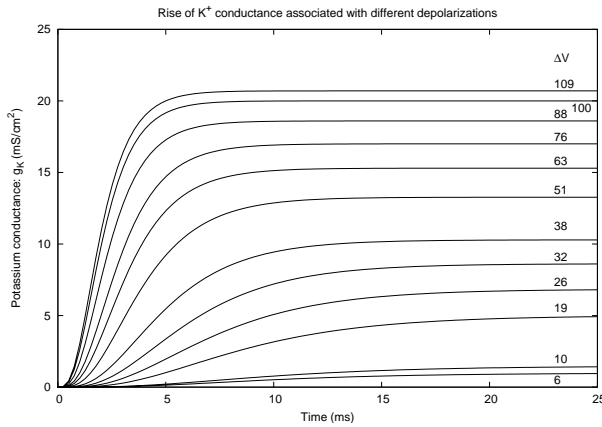


Figure 2.2: Rise of the outward directed  $K^+$  conduction associated with different depolarizations according to equation 2.4 with the original data for  $g_{K_\infty}$ ,  $\tau_n$  and  $\Delta V$  from [40]. The number on each curve gives the depolarization in mV. These curves show the change of the conductance due to the opening of many channels. The opening of a single channel contributes a discrete value to the conductance.

potassium channels exhibit a delayed rectification after depolarization [39]. In 1949 Hodgkin and Huxley were the first who measured the complete action potential of axons with a refined voltage clamping method of Cole and Marmont. They characterized the voltage- and time-dependent changes in  $Na^+$  and  $K^+$  currents that underly the action potential, the primary electrical signal generated by excitable nerve cells when sending signals and created the first mathematical construct for the electrical response of a cell to changes of the membrane potential. Hodgkin and Huxley observed a conspicuously non-linear rise in  $K^+$  conductance after depolarization which they described with eq. 2.4.

$$g_K = \left[ g_{K_\infty}^{1/4} - (g_{K_\infty}^{1/4} - g_{K_0}^{1/4}) \exp\left(-\frac{t}{\tau_n}\right) \right]^4 \quad (2.4)$$

$g_{K_0}$  is the value of the conductance at time  $t = 0$  and  $g_{K_\infty}$  is the value which the conductance finally attains.  $\tau_n = (\alpha + \beta)^{-1}$  has unit  $s^{-1}$  and is the inverse of the sum of the rate constants  $\alpha$  and  $\beta$  with which the time dependent behavior of the proportion of the ions at the inside of the cell  $n$  is described: [40]:

$$\frac{dn}{dt} = \alpha(1 - n) - \beta n \quad (2.5)$$

As these channels allowed outward rather than inward directed ion currents they were also-called *outward rectifier* [44, 40]. The second rectifying  $K^+$  conductance directed in opposite direction to the *outward rectifier*, was identified in 1949 by Katz and was termed *inward rectifier* [44]. All potassium channels exhibit similar ion permeability characteristics. The permeability of  $K^+$  and  $Rb^+$  for example is roughly the same whereas the permeability of  $Na^+$  and  $Li^+$  is much smaller those of  $Cs^+$  lies between these extremes. *Inward rectifiers* are blocked by cytoplasmic  $Mg^{2+}$  ions [39]. Therefore they conduct preferably inwardly directed currents. Potassium channels conduct potassium about 1000-fold more than  $Na^+$  and allow conduction rates of potassium up to  $10^8$  ions per second [91, 22]. Most of the voltage gated ion channels are closed at the normal resting potential of a cell ( $\sim -70$  mV). Depolarization of the membrane increases the probability for a channel to obtain the open state. Some channels show a subsequent decrease of conductance due to inactivation. After the repolarization of the membrane potential most ion channels revert to the closed state [7]. Physiological experiments revealed remarkably deep insight into the ion channel structures. Already MacKinnon and Yellen have predicted a cavity at the intracellular side due to the voltage dependence of a common  $K^+$  channel blocker tetraethylammonium<sup>1</sup> (TEA) and could show that 80% of the transmembrane electric potential falls across only eight amino acids situated in the loop connecting

<sup>1</sup>TEA traversed 5% of the applied transmembrane electric field from the outside and 15% from the inside to reach its binding site in the Shaker channel [92].

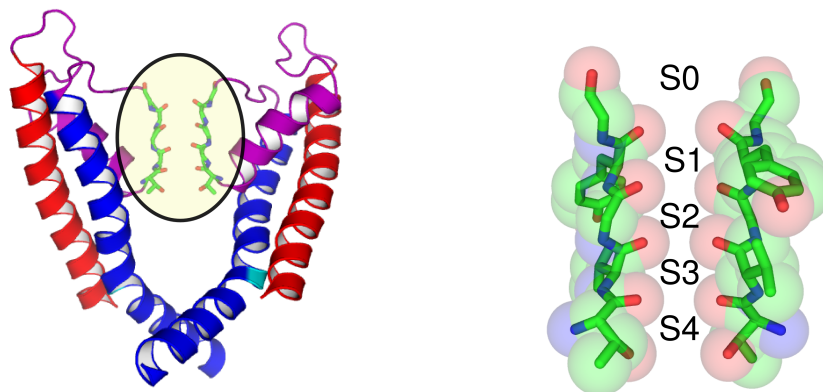


Figure 2.3: Left: Two opposed  $\alpha$ -subunits in the *open state*. The red colored outer helices (corresponding to S6 in 6TM channels and TM2 in 2TM channels) are connected with the blue colored inner helices (corresponding to S5 in 6TM channels and TM1 in 2TM channels) over the pore loop which is colored purple. The selectivity filter backbone atoms which are shown in stick representation have a separate color code: green for carbon, blue for nitrogen and red for oxygen atoms. The SF is the narrowest part of a  $K^+$  channel. The inner helices are colored blue. Right: The SF in the conductive conformation depicted in stick representation without hydrogens. The van-der-Waals spheres of the atoms are shown transparently. The binding sites S0 to S4 are labelled.

the S5 and S6 TM-segments [92]. The pore building domain was firstly defined with pore-blocking toxins by MacKinnon and Miller in 1989 in a site-directed mutagenesis study. They replaced defined amino acids and located the residue sites and amino acids that strongly influence the binding affinity of the toxin [66]. Based on results of experiments with *Agitoxin* it was also assumed that the receptor sites on both KcsA and Shaker  $K^+$  channels are similar. Due to the assumption that KcsA structurally resembles eukaryotic  $K^+$  channels, it was taken into consideration for the first crystallization of a  $K^+$  channel [22, 65]. Many of the presumptions basing on mutagenesis and physiology studies were confirmed by the first x-ray structures.

## 2.4 Structure and function

### 2.4.1 The selectivity filter

There is a highly conserved motif of eight amino acids (TXXTXGXG) in  $K^+$  channels situated in the loop connecting the S5 and S6 transmembrane segments which is used as a signature for the identification of possible  $K^+$  channel coding genes [34, 76]. The x-ray-structure of the 2TM potassium channel KcsA from *Streptomyces lividans* solved by Doyle et al. in 1998 [22] revealed that five of these amino acids (TVGYG in KcsA) are situated on an elongated region of the pore loop near the extracellular vestibule of the channel. This arrangement is conserved in other  $K^+$  channels [22, 45, 55, 98, 63] and is termed the *selectivity filter* (SF). Several studies have shown that this narrow part of the pore can adopt different atomic structures depending on the concentration and the kind of cations in the extra- and intracellular solution. Bathed in solutions with a concentration of  $K^+$  or  $Na^+$  of over 40 mM the SF preferably adopts a conformation where it is able to conduct cationic currents. Here the amino acids are arranged in a way that the backbone peptide carbonyl groups point towards the center of the tetrameres with little lateral displacement, where the carbonyl oxygen atoms form a ring mimicking the coordination of the hydration

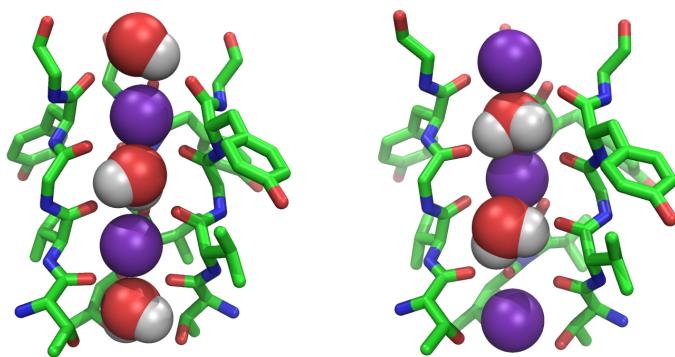


Figure 2.4: The selectivity filter in occupation states [sksks] and [ksksk] which are thought to be the essential states during ion conduction. The SF backbone is shown from three of four subunits for the sake of clarity.

shell oxygen atoms of a cation in water (cf. fig. 2.4.1). Such an arrangement has been shown to allow the dehydration of small cations, which are strongly bound to water molecules in bulk solution, with a reduced free energy barrier [98]. The spaces between the oxygen atoms serve as binding sites termed S0 to S4 for cations and water. Due to their adjacent arrangement along the pore more than one  $K^+$  ion can be bound at the same time.

In this thesis a special notation is used for the occupation state of the SF. The scheme of this notation are five letters in brackets. Thereby every site stands for a certain binding site: [S0 S1 S2 S3 S4]. E.g. [ssksx] means that S0, S1 and S3 are occupied by water, S2 by potassium and S4 is not occupied. “t” stands for tetraethylammonium and x means “not occupied”. If an ion is situated within the cavity, it is marked by a letter behind the closing bracket e.g. [sssss]k means that the SF is fully occupied by water and a potassium ion is situated within the cavity. Water molecules are permanently situated within the cavity, therefore solvent molecules in the cavity are not separately noted.

## 2.4.2 Occupation and conduction

It has been suggested that under physiological conditions mostly two of the binding sites of the SF are simultaneously occupied by  $K^+$  and that the ions are separated by a single water molecule. Crystal structures solved in solvents with low  $K^+$  concentration exhibit a SF in a collapsed conformation that contains only one cation [98]. MD-simulation studies revealed a conduction mechanism (*knock-on-mechanism*) in KcsA [6, 51] which states that the SF is occupied by two  $K^+$  ions separated by water molecules oscillating around their equilibrium positions (i.e. the states [ssksk] and [sksks]), when a cation from the inner cavity diffuses to the entrance of the SF, where it interacts with the ions inside the SF due to the mutual electrostatic repulsion. This lowers the affinity for cations at the inner sites. Therefore the ion in the cavity pushes the ions in the SF to the extracellular side. This induces eventually a concerted movement of the ions in the SF, whereby the ion from the cavity occupies the inner binding site. Then the SF is in the state [ksksk] with three ions. The ion closest to the outer vestibule of the channel finally escapes into the bulk and is rapidly replaced by a water molecule from the bulk or from the SF [93]. The whole cycle of the ion translocation is almost barrier-less and ion conduction of other  $K^+$  channels is also assumed to take place according to this mechanism [6].

## 2.4.3 Snug-fit

In 1972 Benzanilla and Armstrong [8] described the so-called *snug-fit* mechanism that is generally consulted for the explanation of the selectivity of  $K^+$  channels in respect to  $Na^+$  and  $K^+$  ions. According to that theory the selectivity bases on different dehydration energies for the various ion types. The carbonyl oxygen atoms mimicking perfectly the oxygens of the hydration shell of a  $K^+$  ion. As the distance of the

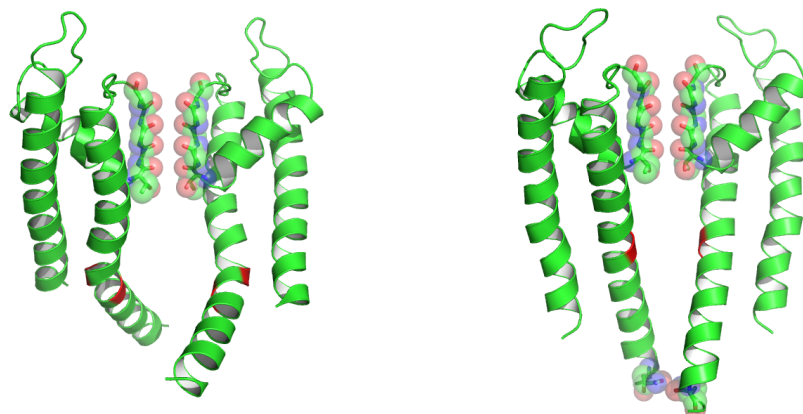


Figure 2.5: Two opposed  $\alpha$ -subunits from  $K_V1.2$  in open (left) and  $KcsA$  in closed conformation (right). The putative gating hinges, which are a highly conserved PVP motive in eukariotic channels and a certain glycine residue, respectively, in the inner helix, are colored red. The selectivity filter shows the same structure in both crystal structures.

oxygen is too large for  $Na^+$  ions, the coulombic energy for the hydration is larger making an entering unlikely. The difference of the ion's atom radius is only  $0.38 \text{ \AA}$ . Therefore this approach meets with criticism. The opposer of the *snug-fit* mechanism believe that the SF is too flexible to satisfy the requirements of *snug-fit*, because the root mean square fluctuations of the atoms lining the SF is about  $0.8 \text{ \AA}$  [74]. Nevertheless, *snug-fit* is a broadly accepted theory for the explanation for selectivity properties of  $K^+$  channels.

#### 2.4.4 The $\alpha$ -subunit

The four molecules of  $K^+$ -channel tetramers provide in general a domain whose structure is almost conserved in all  $K^+$  channels. This domain is called  $\alpha$ -subunit and consists of two TM- $\alpha$ -helices (termed TM1 and TM2 in 2TM-channels; S5 and S6 in 6TM-channels) and a loop, which connects the helices at the extracellular site and contains an amphipatic  $\alpha$ -helix. Coming from the outer helix the backbone enters the extracellular medium and re-enters the transmembrane region as an  $\alpha$ -helix that is tilted by about  $45^\circ$  with respect to the membrane-water surface normal. Then the peptide chain continues as a coil that forms the selectivity filter which is connected with the inner helix. Four of such  $\alpha$ -subunits build the central pore with fourfold symmetry in homotetrameric channels. The pore is the origin of the *gating*, the opening and closing mechanisms of the channel.

#### 2.4.5 Gating

Ion channels in general control the membrane potential by regulating selective permeabilities of the membrane for different ion types by a spectrum of mechanisms, which are abstracted as *gating*. Gating involves quite different mechanisms called *opening*, *closing*, *inactivation* and *recovery from inactivation*. When a channel is in the *closed state*, its permeability for all kinds of ions and water is roughly zero, whereas in the *open state* an ion channel can conduct certain ions, e.g.  $K^+$  and water. The open channel can change its conduction behavior via a mechanism called *inactivation* to the non-conducting *inactivated state*. The

opposite mechanism i.e. the transition from the *inactivated state* to the *activated state* is termed *recovery from inactivation*. The diversity of ion channels differ mainly in the transition kinetics between these states and their dependencies on other factors like the membrane potential, the pH-value or the binding of ligands. Ion channels are diverse proteins exhibiting a wide variety of gating properties like voltage-, pH- or ligand-dependent gating and differ also in properties like the transit time from the open to the inactivated state and the time for the recovery from inactivation. The transition from the closed to the open state and vice versa is probably controlled by a conformational change of the inner helices, which depend on the flexibility in the middle of the helix, caused by a highly conserved glycine (G) residue or a proline-valine-proline (PVP) motive, respectively, which is referred to as the *gating hinge* [45, 55]. Mutagenesis studies with the bacterial sodium channel NaChBac have shown that substitution of proline for this glycine dramatically enhances activation and slows pore closure, providing evidence for bending at this position as an important step in opening and closing the pore [96, 97]. Glycine is known to induce flexibility  $\alpha$ -helices, whereas proline residues induce kinks. However, in other channel types (e.g.  $K_{CNG}$  channels), the establishment of a cytoplasmic gate analogous to the inner helix crossing of the KcsA channel remains questionable [30, 56].

#### 2.4.6 Inactivation and recovery from inactivation

In the *inactivated state* an ion channel is in an open, but non-conducting state. Commonly there are two distinguished types of inactivation. The first is called *N-type inactivation*. It depends on the N-terminal residues and is responsible for the fast inactivation in *A-type channels*. According to the *ball and chain mechanism* the N-terminal “ball” which is connected to the rest of the protein by a very flexible “chain” occludes the pore from the cytoplasmic side after the channel opens [49]. *N-type inactivation* can be abolished by deletion of the N-terminus and can be restored by applying exogenous peptides derived from the N-terminus or added to channels without *N-type inactivation* in chimeric constructs. One channel can contain multiple *N-type inactivation* domains (cf. sec 2.4.7), which behave roughly independently from each other. Binding of both intracellular TEA and *N-type inactivation* slows down the gating charge return after repolarizing. This assumes that the binding of both stabilizes the open state of the channel and simultaneously delays the return of the voltage sensing domain to its configuration in the closed state [56]. Point mutations in the S4-S5-linker have been shown to slow down or remove the *N-type inactivation* suggesting that the S4-S5-linker is part of the binding site for the N-terminal ball [49].

*C-type inactivation* is much slower than *N-type inactivation* and was first observed after deleting the N-terminus and with it the *N-type inactivation* from the Shaker channel. It is caused by conformational changes within the SF and the extracellular entrance of the pore. It emerges with prolonged depolarization and leads likewise to a decreased current flow. A crystal structure solved in a solution with low  $K^+$  concentration solved in 2001 exhibits such a conformational rearrangement [98]. In Shaker *C-type inactivation* is retarded by elevated concentrations of extracellular  $K^+$  [10] and accelerated in minimal extracellular  $K^+$  concentration [41]. Similar observations have been confirmed also in a mammalian Shaker homologue [28]. These results suggest that the outer binding sites of the SF have to be unoccupied to allow *C-type inactivation* which is fundamentally affected by ion occupancy of the pore. Mutations within the extracellular region near the pore dramatically alter *C-type inactivation*. In contrast to *N-type inactivation* presumably all four subunits contribute to *C-type inactivation* [56]. *Recovery from inactivation* is unaffected from the presence of *N-type inactivation* causing N-Terminal domains. Therefore it is *C-type inactivation* that controls the time course of *recovery from inactivation* and *N-type inactivation* that governs the time course of *inactivation* [56].

Inactivation mechanisms that persist after the deletion of the N-terminus have been classified by default as *C-type inactivation*. However, the characteristics of the *C-type inactivation* described for Shaker and

Shaker related channels often fail for other  $K_V$ -channels. For example, the inactivation from  $K_V2.1$  is accelerated in elevated concentrations of extracellular  $K^+$  and exhibits a certain dependency from the membrane potential [56], whereas Shaker does not.

#### 2.4.7 The adjacent $\beta$ -subunits

The function of the so-called  $\beta$ -subunits (the transmembrane segments S1-S4 in 6 TM-channels) is mainly the modification of the channel's gating-kinetics. For example,  $\beta$ -subunits can confer the channel voltage or ligand dependent gating. The mechanism of voltage-dependent gating is unknown in detail, but there are some suggestions on how it works. Commonly the S4-helices are understood to serve as the primary voltage sensors, because they contain a repeated motif of one positively charged amino acid followed by two hydrophobic residues [94] and mutations of these amino acids have a large influence on gating. The voltage dependent opening is accompanied by small transient currents of charges trapped in the membrane electric field, which likely come from a repositioning of the charges of the S4-helices. Possibly such conformational rearrangement increases the open probability by exerting a force onto the S6-helices [7]. The different  $\beta$ -subunits mainly cause the wide diversity of potassium channels, since they are responsible for the various voltage- and ligand-dependencies of the gating. This diversity can be extended by combining various subunits and the pores from different ion channels [70].

## Chapter 3

# Crystal-structures and model channels

The solution of various potassium channel structures via *x-ray crystallography* and *nuclear magnetic resonance* (NMR) has provided so far the deepest insight into the atomic assembly of these proteins and highlighted essential structural elements which underly their functionality. The knowledge of such structures in combination with modern computer performance has afforded the investigation of the dynamics of these proteins inside their biological environment on an atomic scale. In this section the ion channel structures that are used in the thesis at hand are described in detail.

### 3.1 KcsA-WT and KcsA-K<sub>V</sub>1.3

The *KcsA* gene found in the Gram-positive bacterium *Streptomyces lividans* codes a 2TM K<sup>+</sup> channel subunit of 160 amino acids that exhibit 32% amino acid identity with the core region of Shaker. The pore loop is nearly identical to that in Shaker-related channels and human K<sub>V</sub> channels [22]. The crystal structure of the wild type KcsA channel (KcsA-WT) solved by Doyle et al. in 1998 includes the entire transmembrane region but lacks the first 22 N-terminal and the last 41 C-terminal residues. Wild type means that the channel is in its native form without any mutation. The channel is a homotetramer. The TM1 segment crosses the membrane from the cytoplasmic side to the outside as an  $\alpha$ -helix. The peptide backbone continues after a short loop, re-enters the membrane area as a short amphipathic  $\alpha$ -helix and sweeps back to the extracellular medium as a chain building the SF. Finally, the backbone goes over into the third  $\alpha$ -helical part, the TM2 segment that crosses the membrane to the intracellular side. The length of the pore amounts 45 Å and its diameter varies between 1.8 Å in the SF and 10 Å in the inner cavity. The inner helix, the TM2 segment, is closer to the pore than the TM1 segment, the outer helix, and lines the inner half of the pore. The inner helices are tilted with respect to the membrane-water surface normal by about 25° and are slightly bent [22, 39]. The structure shows amino acids with aromatic rings near the water-membrane surfaces (W26, Y45, W87, W113 and F114), which anchor the channel in the membrane. Both, the intra- and the extracellular entryway of the pore are flanked with negatively charged amino acids. Residues lining the cavity and the internal pore are predominantly hydrophobic whereas the SF consists rather of hydrophilic residues. The KcsA channel is similar to the pore regions of other K<sup>+</sup> channels including vertebrate and invertebrate voltage-dependent K<sup>+</sup> channels, vertebrate *inward rectifier* and Ca<sup>2+</sup>-activated K<sup>+</sup> channels, K<sup>+</sup> channels from plants and bacteria, and cyclic nucleotide-gated cation channels [22].

KcsA-K<sub>V</sub>1.3 is a potassium channel chimera created by Legros et al. in 2000 [61]. They replaced certain regions in the TM1-TM2-linker of KcsA with regions in the S5-S6-linker of K<sub>V</sub>1.3 and showed that the chimera is a high affinity receptor for at least two scorpion toxins (i.e. *Kalimotoxin* and *Hogotoxin*

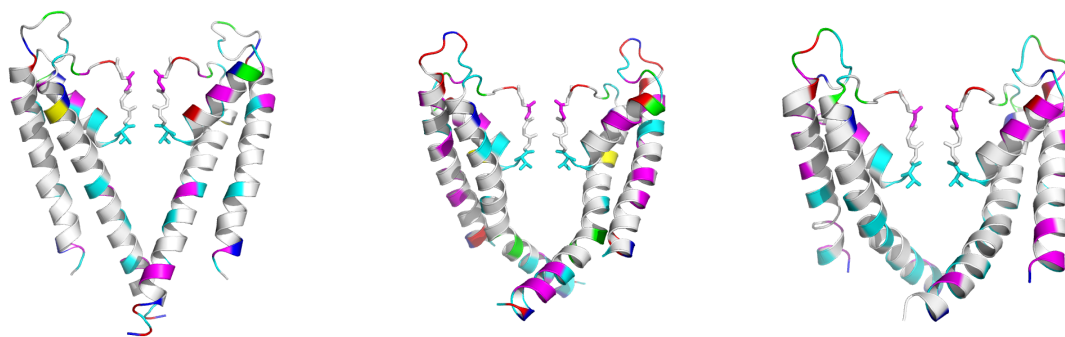


Figure 3.1: Two opposed  $\alpha$ -subunits from each the bacterial KcsA (left), the mammalian Kv1.2 channel (middle) and the also bacterial KvAP (right) in cartoon representation. Atoms which significantly contribute to the functionality of the selectivity filter are illustrated in stick representation. The residues are colored in dependence of their chemical properties. Hydrophobic residues are colored white, aromatic residues purple, positively charged blue and negatively charged red. Hydrophilic amino acids are colored cyan. Proline is colored green. The inner cavities are flanked by mostly hydrophobic residues, whereas hydrophilic residues are preferably situated at the protein-water surfaces.

1), which bind specifically to  $K_V1.3$ . The study has revealed that the complete toxin receptor of a human  $K_V$  channel can be transferred to a bacterial  $K^+$  channel.

### 3.2 The “paddle-chimera channel”: $K_V1.2-2.1$

In 2007 Long et al. solved the x-ray structure of an almost complete voltage gated  $K^+$  channel chimera in which a structural motif comprising the S3 and S4 helices of the voltage sensor paddle from  $K_V2.1$  was transferred to the Shaker related channel  $K_V1.2$  from rat. Therefore the structure is called the *paddle-chimera channel*. The crystal-structure reveals complete  $\alpha$ - and  $\beta$ -subunits and N-terminus of the homotetramer embedded in a membrane lipid environment. Altogether 514 residues per chain from the  $K^+$  channel are contained. The first 31 N-terminal residues and the last 24 C-terminal residues fail. The N-terminal residues are arranged in a ball with hydrophilic surface. It contains three  $\alpha$ -helices of different lengths and four short  $\beta$ -sheets. A loop of 29 amino acids containing an amphipathic  $\alpha$ -helix connects the ball with the first helix transmembrane segment S1 which is one of the four transmembrane helices that build the 169 amino acids spanning voltage sensing domain. A loop of 18 amino acids lengths containing likewise an  $\alpha$ -helical part which is strongly hydrophilic connects the S1 with the S2 helix segment. Like S3 the S4 helix the assumed voltage sensor is slightly kinked and contains furthermore four positively charges arginines. An  $\alpha$ -helix lying in the membrane-water surface, called S4-S5-linker, connects the S4 helix with the  $\alpha$ -subunit that has a similar structure analogous to that of KcsA described in section 3.1. An interesting difference between both pore domains lies in the kink of the S6 helix which corresponds to the TM2 segment in KcsA, nearby the highly conserved PVP motive in certain  $K_V$  channels. A glycine residue is located at a corresponding position in KcsA. Apparently, the structure is in the *open state*, because the inner helices are much less crossed compared to KcsA so that the narrowest part lies within the SF that has roughly the same conformation compared to KcsA structure solved in a solution of 200mM KCl concentration [98, 63]. Since the presence of the S4-S5-linker holds the system slightly closer to the crystal structure, the simulation system was primarily chosen to consist of the  $\alpha$ -subdomains and the

S4-S5-linkers, but also simulations without the linker or with the voltage sensor were performed. For simulations the N-terminal region as well as the voltage sensing domains were removed and the ends of the peptide chains were capped with neutral groups to prevent unphysiological interactions.

### 3.3 KvAP

The x-ray structure of the voltage dependent  $K^+$  channel KvAP from *Aeropyrum pernix*, a species of *Archaea*, solved by Jiang et al. in 2003 [46] at a resolution of 3.2 Å in a complex with monoclonal Fab fragments gave reason for heated debates, because of the unexpected arrangement of its voltage sensor paddles. Due to this structure the group hypothesized a new mechanism for movement of the gating charges. The structure is in the open conformation and has a broader pore entrance than the chimera [46].

## Chapter 4

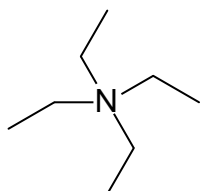
# Inhibitors

Prior to sequencing the classification of  $K^+$  channels was on the basis of properties of its activation (e.g., by membrane depolarization), its conductance and its susceptibility to blocking by peptide toxins, tetraethylammonium and 4-aminopyridine. All these inhibitors have been invaluable in the study of  $K^+$  channel function [44]. In the following these historically important compounds were introduced.

### 4.1 Toxic peptides

$K^+$  channel blocking scorpion toxins in scorpion venoms are polypeptides of about 30-45 amino acids that exert their toxic effect by binding with a 1:1 stoichiometry to the extracellular entrance of  $K^+$  channels and thereby blocking ion conduction [38, 32]. The affinities between these toxins and potassium channels are governed by electrostatic interactions and belong to the strongest of all known protein-protein complexes [32]. Residues that are crucial for the binding of the toxins cluster on one side of the peptides. At least two of these toxins (KTX and CTX) exhibit a lysine whose side chain competes with  $K^+$  for a binding site near or within the SF [24]. These toxins possess three to four disulfide bridges in the core which maintain a ridged and compact tertiary structure with 3 antiparallel  $\beta$ -strands linked to an  $\alpha$ -helical part [24, 32].

### 4.2 Tetraethylammonium

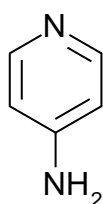


Tetraethylammonium (TEA) is a small compound composed of 29 atoms. It consists of four ethyl groups bound to a central nitrogen atom. The molecule adopts two main conformers. In the TEA1 conformation the end carbon atoms form an irregular tetrahedron with side lengths of about 3.5 and 4.5 Å, while in the TEA2 conformer the nitrogen atom and the end carbon atoms nearly lie in the same plane. TEA2 is predicted to be slightly more stable than TEA1 (by 2.5 – 3.8 kJ mol<sup>-1</sup>) both in vacuum and in a high dielectric continuum [64, 18]. Crouzy et al. also included the solvation free energy difference of both conformations and obtained an energy difference of

7.5 kJ mol<sup>-1</sup> [18]. The pores of most of the known  $K^+$  channels can be blocked by TEA [35]. TEA binds to KcsA from the intra- and extracellular side. The extracellular binding site is selective for TEA in comparison with other quaternary-ammonium (QA) derivatives. External tetramethylammonium (TMA) binds very ineffectively and external tetrapropylammonium (TPA) binds with about a tenfold lower affinity [35]. TEA is thought to be an ideal plug for the extracellular binding site of  $K^+$  channels. Electrophysiological experiments revealed a linear relationship between the extracellular binding affinity for TEA and the num-

ber of aromatic residues near the outer mouth of the channel<sup>1</sup>. The dissociation constant with four Y449 in Shaker channel is 0.65 mM and 0.22 mM after substitution by four threonines [35]. It was suggested that these residues interact simultaneously with a TEA molecule by cation- $\pi$ -interactions. However, the x-ray structure of KcsA revealed that these residues form a square of 11.8 Å side. The diameter of TEA is about 6 Å. Therefore the distance between the aromatic side chains is too large to allow simultaneous interactions of the aromatic side chains with one TEA molecule [22]. It was shown by molecular dynamics simulations that the radial water density around TEA is lowest, if it is bound to KcsA-Y82 as compared to the KcsA-Y82T mutant and TEA in bulk water [18]. So hydrophobic effects may play an important role in the stabilization of extracellular blocking by TEA. The intracellular binding affinity rises with the hydrophobicity of the compound [62]. It was shown that internal TEA blocks only open K<sup>+</sup> channels and that TEA stabilizes the open state [2]. Hyperpolarization and increasing of the external K<sup>+</sup> concentration help to clear QA ions from the blocked channels [58, 2]. The very rapid *N-type inactivation* is affected by intracellular TEA, which generally slows down the *N-type inactivation* by presumably competing with the N-terminus for identical, overlapping or nearby binding sites.

### 4.3 4-Aminopyridine



4-Aminopyridine (4AP) is smaller than TEA and acts on the cytoplasmic side of K<sup>+</sup> channels. It only binds to open or inactivated channels having greater affinity in *delayed rectifiers* than in rapidly inactivating K<sub>V</sub> channels [49]. This can be explained in the light of the mechanism of fast inactivation. The N-terminal ball that interrupts the ion current competes with 4AP for the same or adjacent binding sites within the inner cavity. The potencies of K<sub>V</sub> channels for intracellular 4AP range between micromolar and millimolar concentrations [49]. A subsequent study of *delayed rectifiers* suggested that 4AP block the channel in its open state and becomes trapped in the channel when it closes [12]. The binding site for 4AP in K<sub>V</sub> channels is seems to be close enough to the pore to allow the molecule to be trapped when the channel closed. If the channel is closed prior to the application of 4AP the binding site is inaccessible for the compound. Mutagenesis studies have suggested that the binding site for 4AP lies more to the cytoplasmic site compared to TEA [75].

<sup>1</sup>Position 82 in KcsA and 449 in Shaker

# Chapter 5

## Theory

### 5.1 Molecular Dynamics Simulations

Biological systems are often many-particle systems for which, contrary to crystalline or solid state systems, no straightforward reduction to a few degrees of freedom is possible. As the temperature of such systems typically lies close to 300 K, also entropic effects contribute to the state of the system. Hence, for this kind of systems explicit treatments of many degrees of freedom are required in order to adequately describe their state [86]. The high dimensionality and complexity render an *ab initio* treatment of these systems still impossible. Therefore, a number of approximations is required for the handling of these systems.

The first approximation from an *ab initio* treatment is the removal of the electronic degrees of freedom from the system. The separation of the electronic and the nuclear degrees of freedom is done according to the *Born-Oppenheimer approximation*. This approximation assumes that the wave function of the electrons alters adiabatically with the potential generated by the nuclei and that the electrons are in the ground state. A second approximation is the classical treatment of the molecular system as a system of balls with point charges in their center and which are connected with springs. Then the numeric integration of the *newtonian equations of motion* allows the calculation of the dynamics of the nuclei in terms of classical instead of quantum dynamics. Empirical effective pair potentials, so called *force fields*, allow for a manageable number of spring constants and other parameters that describe the energy of the system for any configuration represent the third approximation used in MD simulations.

The reliability of a MD simulation depends on the particular force field, the type of system and the question that should be answered. One force field may be parameterized in order to predict transition temperatures and others in order to predict relative conformational energies. Therefore, the choice of a particular force field depends on the system properties which are of interest. The usually chosen functional form of the atomic interaction's description does not allow the breaking or the building of covalent bonds and therefore cannot describe chemical reactions. Furthermore, this description fails for systems at low temperatures, where quantum effects play a crucial role, as the nature of the system cannot be described with the laws of classical mechanics anymore.

In general, the approximations described above can lead to reliable predictions of thermodynamic properties and dynamics (In comparison to *ab initio* calculations at the RHF/6-31G\* level, the bond lengths predicted with the OPLSAA force field (cf. sec. 5.2.1), for example, differ by about 0.01 Å in average. The average differences of the bond angles and dihedral angles are of the order of 2° and 1°, respectively.). Average errors for heats of vaporization and for densities were 2% in comparison with experimental data. Computations of the free energy of hydration of tested molecules with OPLSAA parameters and TIP4P water showed average errors of less than 0.5 kJ mol<sup>-1</sup> [47].

Generally, the size of the system is kept as small as possible in order to allow for a sufficient sampling.

Modern molecular dynamics simulations cover typically simulation times of several tens of nanoseconds at system-sizes of typically 100,000 atoms. For small simulation systems simulation times of the order of several milliseconds are possible. The largest all-atom simulation systems contain about one million particles were already simulated for over 50 ns [31], but the handling of such large systems already requires a lot of effort and is on the limit of modern MD simulation's capabilities. Slow processes are still out of reach nowadays, but the folding of small and rapidly folding proteins, for example, has become possible in the last years [81].

## 5.2 Force Fields

There is a broad variety of force fields available that approximate the nature of multiatomic systems at different levels of abstractness. The parameters of a *force field* and the functional form of the energy function give the potential energy between all pairs of interaction sites and therefore the overall potential energy of any configuration of the system. Often these energy functions use simple harmonic terms for the description of bond stretching and angle bending energies. Such force fields are called *harmonical force fields*. The interaction site of a force field can stand for a single atom like in *all-atom force fields*, a group of atoms like it is done in *united-atom force fields* or even whole molecules like it is done, for example, in some coarse-grained simulations. The parameters of *all-atom force fields* separately describe covalent and electrostatic interactions, induced dipole interactions and forces that result from the *Pauli exclusion principle*. *Polarizable force fields* approximate the polarizability of the atoms as point polarizabilities [86, 87], whereby in *non-polarizable force fields* the polarizabilities are neglected and only the mean polarization is effectively included in the *force field parameters*.

The functional form of the energy function can vary from one force field to another. For example, the non-bonded and non-electrostatic interactions can be described by a Lennard-Jones potential or a Buckingham-potential, where the repulsive part that results from the *Pauli exclusion principle* is modeled with an exponential term. Furthermore, it is possible to modify these functions further by using a *cut-off* or a *reaction field* in order to prevent the calculation of the energy terms between atoms far away from each other which contribute little to the overall energy, and in that way save computational effort. The mean forces resulting from quantum mechanical interactions between electrons and atoms as well as non-bonded interactions can thereby very well be described by a classical Hamiltonian. In this thesis *non-polarizable harmonical all-atom force fields* are used except for the lipid bilayer molecules from Berger et al. [5] which are described with an *united-atom force field*.

In this thesis different force fields were used. At first the OPLSAA force field was chosen for all simulations, since it reproduces most accurately energetic properties of solvated molecules. Unfortunately, there is no straightforward way to generate *force field parameters* for the OPLSAA force field for non-amino acid compounds. For the AMBER99 [88] and AMBER03 [23] force fields there is the recently developed *generalized amber force field* (GAFF) [90] which can generate *force field parameters* for a broad range of non-amino acid and residue and non-residue compounds. An all-atom lipid bilayer model has been already parameterized by Siu et al. [79] with GAFF, that allowed a fully consistent simulation system in this force field. These facts made the AMBER force fields attractive for our requirements.

### 5.2.1 The all-atom force field for organic molecules and peptides (OPLSAA)

The *all-atom force field for organic molecules and peptides* OPLSAA was developed in 1996 basing on a partially united-atom model (OPLS-UA), where sites for nonbonded interactions were all non-hydrogen atoms and hydrogens attached to heteroatoms or carbons in aromatic rings [47]. The bond stretching and angle bending parameters have been adopted mostly from the AMBER *all-atom force field*, whereas

torsional parameters were determined by fitting to rotational energy profiles obtained from *ab initio* calculations (at the RHF/6-31G\*\*//RHF/6-31G\* level) for more than 50 organic molecules and ions and the nonbonded parameters by calculating thermodynamic and structural properties for 34 pure organic liquids in conjunction with Monte Carlo statistical mechanics. The OPLS-AAff is therefore in part an *empirical force field* [47].

### 5.2.2 AMBER and GAFF

Contrary to OPLS the AMBER force field parameters are solely fitted to *ab initio* calculated energies [23] the *generalized amber force field* GAFF is compatible with existing AMBER force fields for proteins and nucleic acids and contains parameters for most organic molecules being composed of H, C, N, O, S, P, and halogens. It uses a simple functional form and applies the same harmonical energy function as the AMBER force fields do [89]:

$$E_{pair} = \sum_{bonds} K_r(r - r_{eq})^2 + \sum_{angles} K_{\Phi}(\Phi - \Phi_{eq})^2 + \sum_{dihedrals} \frac{v_n}{2} \times [1 + \cos(n\Phi - \gamma)] + \sum_{i < j} \left[ \frac{A_{ij}}{R_{ij}^{12}} - \frac{B_{ij}}{R_{ij}^6} + \frac{q_i q_j}{\epsilon R_{ij}} \right]$$

GAFF is intended for the generation of *force field parameters* of arbitrary organic molecules. It uses 35 basic and 22 special atom types. For example, there are six different hydrogen, five different carbon and eight nitrogen types, which are required as in force fields for molecular dynamics different chemical environments are encoded as different atom types. The topologies are generated with an auxiliary module called ANTECHAMBER in the AMBER package. It assigns atom types, bond types and generates topologies that encode all *force field parameters* for the molecules. These parameters are developed by reproducing the experimental data of a training set of molecules and high-level *ab initio* data. The derived parameters were subsequently compared to a test set of molecules outside the training set [89]. The ANTECHAMBER package factors the atomic number, the number of bonded atoms, the number of attached hydrogen atoms and for hydrogens also atoms connected to the atom the hydrogen is bonded to, chemical environments and properties like the kind of a ring system into the assignment of the atom types. There are five aromatic types defined for ring atoms and ten ring types. Furthermore, there are seven bond types defined, from which a model for a specific molecule is build upon. This scheme works fine for a broad variety of molecules without conjugated/aromatic rings attached to large aliphatic rings, and can easily be applied in an automated fashion [90]. The ANTECHAMBER package includes several subprograms which are usually automatically started by the main program *antechamber*. These subprograms fulfill different tasks: *atomtype* factors the atomic number, *bondtype* the number of bonded atoms and *parmchk* assigns missing *force field parameters*, *resp* refines the charges calculated *ab initio* and *prepgen* can generate amino acid-like residue topologies. If the compound is composed of repeating subunits like amino acids, it is common to not generate an over-all topology but a topology for every subunit individually in order to make the topology code as compact as possible. The parameters of all standard amino acids are already contained in the AMBER force fields and also parameters for several established water models like TIP4P [48] and TIP3P [48] are included. Below the generation of partial charges for small non amino acid compounds is described, using the AMBER03 port for GROMACS [82].

#### AMBER99/03 partial charge generation

The generation of *force field parameters* used in a simulation should be performed in an equivalent manner to yield consistency. As we wanted to set up simulation systems with a combination of GAFF and AMBER parameters, we looked on how the partial charges are generated for the force fields AMBER99, AMBER03. The 6-31G\* basis set was used for the generation of the AMBER99 partial charges [17].

The partial charges of the AMBER03 force field were obtained by fitting to the quantum mechanical derived ESP using the B3LYP/cc-pVTZ//HF//6-31G\*\* method, where each amino acid was represented by a dipeptide fragment consisting of the amino acid group and the terminal groups ACE- and -NME. The ESP was calculated for two conformations representing the  $\alpha$ -helical and the extended ones. These conformers were then geometry optimized at the RHF/6-31G\*\* level of QM theory. Single-point calculations were done using the density functional theory (DFT) method and the B3LYP exchange and correlation functionals with the cc-pVTZ basis set. Furthermore, an implicit solvent environment was applied with  $\epsilon = 4$ . The ESP of the peptides was saved and used in the charge fitting using the RESP method in two steps. At the first step the ESP charges of the two conformers were averaged and in the second step chemically equivalent atoms were set to have the same charges [23]. The same parameterization approach according to AMBER99 was used for the parameterization. The same approach was used by Siu et al. [79] for the parameterization of DOPC lipids.

### 5.3 Temperature-Enhanced Essential Dynamics - TEEREX

*Temperature-Enhanced Essential Dynamics Replica Exchange* is a combination of *essential dynamics* (ES) and replica exchange (REX). It alleviates the problem of limited conformational sampling. In standard REX simulations multiple simulations at different temperatures are performed. Except for one all simulations are coupled to higher temperatures. The conformational states of these trajectories are regularly exchanged, if a certain exchange condition is fulfilled: the potential energy of the trajectory performed at higher energy  $E_j$  at temperature  $T_j$  is lower than that of the trajectory with lower energy  $E_i$  at temperature  $T_i$ , the states will be exchanged. Otherwise an exchange will take place with the probability  $P_{ex}$ :

$$P_{ex} = \exp\left[-\left(\beta_j - \beta_i\right)\left(E_j - E_i\right)\right] \quad (5.1)$$

$$\beta_k := \left(k_B T_k\right)^{-1} \quad (5.2)$$

A prerequisite for efficient exchange is therefore an overlapping potential energy distribution between two simulations. The trajectories with higher temperature allow the system to overcome energy barriers with higher probability. The TEEREX method excites not the whole system but only the essential collective modes of motion contributing significantly to the overall motion of the system. These modes are the eigenvectors of the covariance matrix  $C_{ij}$ .  $m_i$  is the mass of particle  $i$ .

$$C_{ij} = \left\langle \mu_{ii}^{1/2} (x_i - \langle x_i \rangle) \mu_{jj}^{1/2} (x_j - \langle x_j \rangle) \right\rangle \quad (5.3)$$

$$\mu := \text{diag}(m_1, m_2, \dots) \quad (5.4)$$

This selective excitation allows the exchange between simulations with higher temperature differences, because the fraction of the solvent is not longer the dominating term of the potential energy. Therefore TEEREX is an efficient method for the conformational sampling that approximately preserves the thermodynamic ensemble [53].

### 5.4 Estimating Binding Free Energies

The free energy is generally considered as the most important concept in physical chemistry. The Helmholtz free energy  $F = U - TS$  belongs to an ensemble with a constant number of particles  $N$ , volume  $V$  and temperature  $T$ . The free enthalpy  $G = U - TS - pV$  or Gibbs free energy in contrast, belongs to an ensemble of constant number of particles  $N$ , pressure  $P$  and temperature  $T$ . As most of the experiments are rather

proceeded at constant pressure as at constant volume, the Gibbs free energy is often of major interest. In this thesis most of the simulations are proceeded at constant pressure. The free energy of a molecular system describes affinities and tendencies to react. The free energy is a sum of the Boltzmann weights of all of the energy levels of the system. Treated in this way, the calculation of the free energy requires an integration over  $3N$  degrees of freedom, where  $N$  is the number of atoms in the system. Fortunately, frequently only the differences between free energies of various states are important for the description of biological systems, alleviating the need to compute absolute values. The free energy difference of two related systems is represented by the fundamental equation of *free energy perturbation* (FEP) (eq. 5.5), where  $H_i$  represents the Hamiltonian of the  $i$ th system and  $\langle \rangle_i$  an ensemble average of system described with the Hamiltonian  $H_i$ .

$$\Delta G_{A,B} = G_B - G_A = -RT \ln \left( \left\langle \exp \left[ -\frac{H_B - H_A}{RT} \right] \right\rangle_A \right) \quad (5.5)$$

Equation 5.5 in practice holds only for systems with small differences between the systems that are described by the Hamiltonians  $H_1$  and  $H_2$ . This approach can be generalized to more complex systems by inducing the parameter  $\lambda$  and the following Hamiltonian:

$$H(\lambda) = \lambda H_B + (1 - \lambda) H_A \quad (5.6)$$

$$\Delta G = G_B - G_A = \sum_{\lambda=0}^1 -RT \ln \left( \left\langle \exp \left[ -\frac{\Delta H'}{RT} \right] \right\rangle_{\lambda} \right) \quad (5.7)$$

Here  $\lambda$  varies from 0 to 1 and  $\Delta H' = H_{\lambda+d\lambda} - H_{\lambda}$ . An alternative to FEP is *thermodynamic integration*. This approach requires the ensemble average of the derivative of the Hamiltonian with respect to  $\lambda$  at various values of  $\lambda$ . Then FEP methods are used to calculate  $\Delta G$ :

$$\Delta G = \int_{\lambda=0}^1 d\lambda \left\langle \frac{\partial H(\lambda)}{\partial \lambda} \right\rangle_{\lambda} \quad (5.8)$$

In the *slow growth* method  $\lambda$  is viewed as incremental and changes its value in each step of a simulation.  $\Delta G$  can be calculated then with eq 5.9:

$$\Delta G = \sum_{\lambda=0}^1 (H_{n+1} - H_n) \quad (5.9)$$

[50, 60]

### 5.4.1 First Principles Docking

It is possible to estimate the free energy differences between two states, for example bound state and an unbound state, with the help of the probabilities for the system to be in the bound  $P_{bound}$  and in the unbound state  $P_{unbound}$ . The free energy between these states can be calculated with eq. 5.10.

$$\Delta G = -RT \ln \left( \frac{P_{bound}}{P_{unbound}} \right) \quad (5.10)$$

The probabilities can in principle be estimated from a MD trajectory. This requires that the system changes frequently enough between the two states. The method gives limited results if the energy barrier

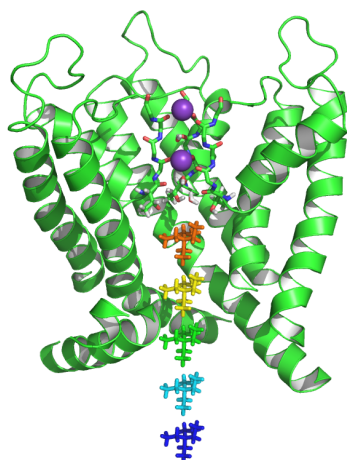


Figure 5.1: An example for an umbrella simulation. The binding of intracellular *tetraethylammonium* on a  $K^+$  channel in the *open state*. The pore axis serves as reaction coordinate. Each umbrella calculation would contain only one TEA molecule.

between the  $S_{bond}$  and  $S_{unbond}$  is too high to allow fluctuations and the system stays in one of the states over long periods of the trajectory after taking the state one time. In this case it would require very much computational effort or even render the estimation of probabilities impossible.

#### 5.4.2 Linear Interaction Energy

The Linear Interaction Energy (LIE) is a method that builds an empirical linear model from computed interaction energy terms and attempts to compute  $\Delta G$  by examining the end states without carrying out computationally expensive FEP calculations. The binding free energy between a ligand and a receptor is then derived using formula 5.11 or related formulas.

$$\Delta G = \alpha \langle \Delta U_{vdw} \rangle + \beta \langle \Delta U_{el} \rangle + \gamma \langle \Delta SASA \rangle \quad (5.11)$$

$\alpha$ ,  $\beta$  and  $\gamma$  are constants that were derived using a linear regression fitting to a set of known binding free energies. It can be shown that  $\beta$  has a value of about 0.5. It has been argued that this value can vary depending upon the structural and polar properties of the ligand as well as on the employed force field [85]. The third term that represents the energetic costs of creating a cavity in the receptor is not always taken into account [80].  $SASA$  is the *solvent-accessible surface area* of the inhibitor. There are also alternative approaches where the  $\gamma \langle SASA \rangle$  is supplied by a constant [80].

#### 5.4.3 Umbrella Sampling and the Potential of Mean Force

The *potential of mean force* (PMF) is a free energy surface along a chosen inter- or intramolecular reaction coordinate. The procedures described above allow the estimation of the free energy differences of chemical modifications. Often the mutation pathways in common FEP calculations are non-physical. In contrast, the PMF is usually calculated along physically feasible pathways. A simple example is the free energy change as a function of the separation of two particles. The reaction coordinate could be chosen to be the distance between the particles  $r$ . Then the free energy change along  $r$  can be calculated according to the following relationship between the free energy  $\Delta G$  and the radial distribution function  $g(r)$ :

$$G(r) = -k_B T \ln [g(r)] + C \quad (5.12)$$

Unfortunately, standard MD simulations do not adequately sample regions in configuration space with higher potential energies. If the PMF varies by several multiples of  $k_B T$ , an adequate sampling is unlikely

or cannot be reached, leading to inaccurate values for the PMF. To avoid this sampling problem one can use the so-called *umbrella sampling* method, where due to a modification of the potential function  $V(r)$  by a weighting function or biasing potential  $W(r)$  the unfavorable states are sampled systematically. In most cases the applied biasing potential is a simple harmonic potential. Each *umbrella calculation* samples a histogram for the reaction coordinate in vicinity of each sampling point which is affected both by the biasing potential and the underlying free energy landscape. Depending on the PMF in this area the histogram is shifted to higher or lower values than this of the minimum of the biasing potential. The unbiased PMF can be finally reconstituted by several methods [60]. In this thesis the so-called *weighted histogram analysis method* (WHAM) [54] was used. The resulting PMF with respect to the reaction coordinate  $z$  is denoted as  $G(z)$ .

## 5.5 IC<sub>50</sub> estimation

The IC<sub>50</sub> is the concentration of an antagonist of a receptor where 50% of the receptors are inhibited. In contrast, the EC<sub>50</sub> value is the concentration of an agonist of a receptor where 50% of the receptors are activated. The IC<sub>50</sub> and EC<sub>50</sub> values serve in general as a characterization of a molecule's interaction with a certain receptor. As the drugs and toxins treated in this thesis are antagonists of potassium channels, it is the IC<sub>50</sub> in which we are interested. It is possible to estimate the IC<sub>50</sub> from a PMF  $G(z)$  taking  $e^{-G(z)/RT}$  as the density of the probability to find the drug at a value  $z$  along the reaction coordinate. The drug can be considered as bound if the distance to the center of mass of the receptor is smaller than  $z_B$ , then the probability for the drug for being bound is

$$P_B = N^{-1} \int_0^{z_B} dz e^{-G(z)/RT} \quad (5.13)$$

The probability for being unbound is

$$P_U = N^{-1} \int_{z_B}^L dz e^{-G(z)/RT} \quad (5.14)$$

Where  $N$  is a normalization constant. Applying  $P_B = P_U$  and solving for  $L$  allows the estimation of the corresponding  $IC_{50} = (1000 \cdot N_A \pi r_c^2 L)^{-1}$  in mol per liter, where  $r_c$  is the radius of the slice and the drug is allowed to diffuse freely around the reaction coordinate (cf. sec. 5.4.3).

## Chapter 6

# Inhibition of Potassium Channels

### 6.1 Material & Methods

The following simulations were carried out using the GROMACS simulation software [83] and the OPLSAA force field for the proteins, the TEA molecules, the ions and the solvent atoms. Lipid parameters for palmitoylcholine lipids (POPC) and a template for the POPC-membrane were taken from Berger et al. [5], enlarged and equilibrated for 2 ns. The membrane-water surface was perpendicular to the z-axis. The proteins were inserted into the bilayer using the *makehole-plugin* for GROMACS<sup>1</sup>. The protein coordinates of the protein were fitted to the membrane and a protein surface was generated with the program *MSMS* from Michael Sanner. Lipids of the membrane positioned with their phosphorus atom within the protein surface were removed. Remaining lipids and water were pressed out of the protein volume at first with an additional potential with a force constant of  $10 \text{ kJ mol}^{-1} \text{ nm}^{-2}$  for 30 ps. A buffer zone around the protein surface of  $1.5 \text{ \AA}$  was applied. In the following the force constant was increased to a value of  $100 \text{ kJ mol}^{-1} \text{ nm}^{-2}$  for 10 ps. The force acted on water molecules in the x-,y- and z-direction and for membrane lipids in the x- and y-direction. An additional force with a force constant of  $10 \text{ kJ mol}^{-1} \text{ nm}^{-2}$  perpendicular to the membrane-water surface was applied on all membrane-lipids in order to avoid the lipids to diffuse into the bulk. The neighbor list for atoms within the offset of the surface was updated every 50 steps. The membrane and the water molecules were separately coupled to a temperature bath of 300 K with a Berendsen thermostat [4]. No pressure coupling was applied.

Afterwards the membrane-solvent system was equilibrated for 2 ns. During the equilibration the protein atoms were kept fixed by position restraints with a force constant of  $1000 \text{ kJ mol}^{-1} \text{ nm}^{-2}$ . Terminal ACE- and NME-caps were applied to the ends of fragmentary polypeptide chains in order to avoid unphysiological interaction, firstly using the software *pymol* [21] and *yasara* [52]. Chloride, sodium and potassium ions were added to yield a physiological salt concentration around 150 mM NaCl or KCl, respectively. Long-range electrostatic interactions were calculated at every time step with the particle-mesh Ewald method (PME) [20, 27]. Short-range attractive and repulsive interactions were described by a Lennard-Jones potential, which was cut off at 1 nm. The settle algorithm [67] was used to constrain bond lengths and angles of water molecules, and Lincs [37] was used to constrain all other bond lengths, allowing an integration time step of 2 fs. The temperature was kept constant by weak Berendsen coupling of the protein, lipids and solvent separately to a temperature bath of 300K [4]. The pressure was kept constant by a weak, semiisotropic Berendsen coupling to a pressure bath of 1 bar with a time constant of  $\tau = 1 \text{ ps}$  in x- and y-directions [4]. Periodic boundary conditions in all directions were applied. TIP4P [48] was used as water model. The neighbor list was updated all 10 steps with the grid search method [83].

---

<sup>1</sup> Available at [www.gromacs.org](http://www.gromacs.org)

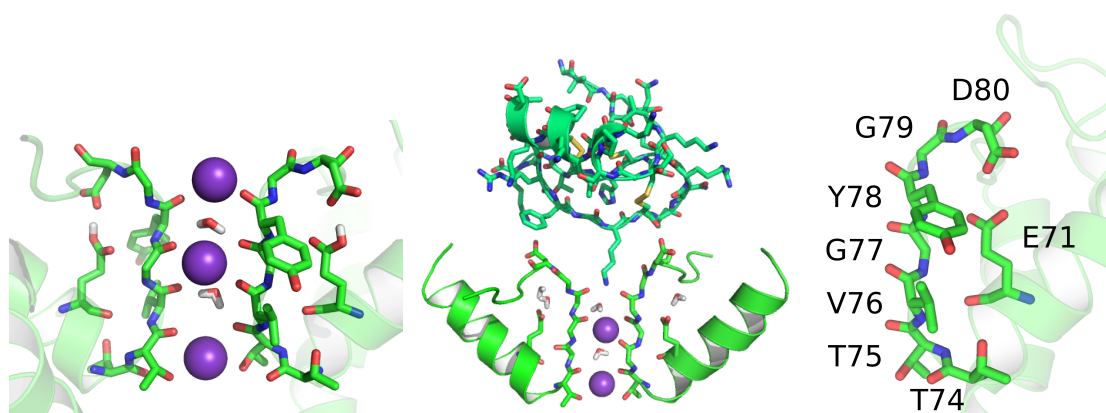


Figure 6.1: In simulations the binding of KTX to the pore of KcsA-Kv1.3 induces a shift in the orientation of the side chain D80.

For simulations with AMBER/GAFF the DOPC model for the lipid bilayers was used from Siu et al. [79]. The system was increased to a size of 280 lipid molecules. As water model TIP3P [48] was used. After an energy minimization the system was equilibrated and simulated for 70 ns. The system remained stable over the whole trajectory. Simulations of a solution with 75 mM NaCl and 75 mM KCL solvated in water (TIP3P) revealed that the parameters from the AMBER force fields result in an unsatisfying behavior of the ions which aggregate even in simulations with temperatures of about 300 K. This is a well known problem and improved van-der-Waals parameters are already available [19]. Therefore, the parameters from Dang et al.[19] were tested and used for simulations with AMBER. The same procedure mentioned above was used for the insertion of the protein into the membrane bilayer.

## 6.2 KcsA-Kv1.3 and KTX

*Kalimotoxin* (KTX) is a 38 residue peptide from the venom of the scorpion *Androctonus mauretanicus mauretanicus* and specifically blocks the voltage-gated  $K^+$  channel  $K_V1.3$ . KTX contains a short  $\alpha$ -helix and two parallel  $\beta$ -strands that are connected by three disulfide bonds [59]. KTX binds to KcsA-K $V$ 1.3 with an affinity of 30 pM [59, 1]. The binding of Kalimotoxin (KTX) on a chimeric  $K^+$  channel (KcsA-K $V$ 1.3) was the object of investigation of a *solid-state nuclear magnetic resonance* (ssNMR) study by Lange et al. [59]. With an approach that combines both the analysis of chemical-shift perturbation and proton-proton distances, they could verify that the high-affinity binding is associated with significant structural rearrangements in both molecules. It was assumed that the largest backbone changes occur at G77, Y78 and G79, which are located in the extracellular entrance of the selectivity filter (SF). They also observed chemical-shift changes for E71 and D80 that form carboxyl-carboxylate pairs on the back side of the SF. E71 is a residue of the pore helix, situated close to the SF and its side chain points to the extracellular side. D80 is located opposed to E71 at the extracellular side of the protein. Their side chains can form a hydrogen bond that potentially stabilizes the structure of the SF. They share a proton whose probability is higher at the E71 as reported by a recent quantum chemical study [9]. Conformational changes involving the E71-D80 pair apparently play an important role in *C-type inactivation* [14, 13]. The mutation of E71 to alanine (denoted as E71A) allows the D80 side chain to rotate fully into the bulk and prevents the channel from entering the *inactivated state* [14, 13]. The protonation of E71, when the side chain of D80 is flipped to the bulk, seems rather unfavorable [9] and experimental findings have suggested that the side chains of E71 are not permanently protonated [13]. A recent study has shown that the distance between

the side chains of E71 and D80 is the major determinant of *C-type inactivation* [15]. With bound toxin the observed chemical-shifts resembled those of the conductive conformation, but the arrangement of residues Y78 and G79 seemed to approximate the collapsed state of the SF [59]. Therefore the structure of the SF in this state remained unclear. We have performed MD simulations in order to explore the origin of the observed chemical-shifts and to illuminate the mechanisms playing the major part in KTX:K<sup>+</sup>-channel complex building. These studies were performed together with Ulrich Zachariae who has done the major contributions in collaboration with the Baldus group from the Max Planck Institute for Biophysical Chemistry in Göttingen (ssNMR experiments) and the group of Olaf Pongs from the Center for Molecular Neurobiology Hamburg (ZNMH) (physiological experiments).

### 6.2.1 Simulations

The model channel for KcsA-K<sub>V</sub>1.3 was embedded in a POPC membrane and surrounded by water and solvated Na<sup>+</sup> and Cl<sup>-</sup> ions at physiological concentration (about 150 mM). The KTX model was then inserted at random positions into the extracellular bulk phase at a distance of at least 25 Å from the receptor. The hypothetical active site K27 pointed to the extracellular binding site S0 (cf. 2.4.1). Initially eight simulations of 10 to 20 ns length were performed. In three simulations a spontaneous and stable toxin binding was observed. The simulation with K27 bound closest to the binding site S0 was taken for further analysis. The binding of K27 was in accordance with previous suggestions made on the basis of double mutant cycles, electrophysiological studies and docking calculations [26, 65, 72].

The side chain nitrogen atom of K27 formed a hydrogen bond to G79 of one subunit. In simulations the largest side chain changes occurred at E71 and D80. The side chain of D80 was unprotonated and was found to rotate frequently from the protonated E71 to the bulk [95]. The fivefold positively charged KTX or cations (K<sup>+</sup>, Na<sup>+</sup>, TEA<sup>+</sup>) near the extracellular entrance of the pore facilitated this motion. Furthermore, the probability for this motion is higher, the fewer cations are located in the SF. In light of the ssNMR study showing substantial rearrangements in this region, the effect of side chain deprotonation of D71 with respect to binding of KTX was studied. In simulations the deprotonation of E71 led to a fast rotation of the D80 side chains to the bulk which can be explained by the mutual electrostatic repulsion. When both residues E71 and D80 are deprotonated, they are negatively charged. This rotation leads to a distortion of the residues of the extracellular entrance of the SF (G77 to G79) and created a cavity in each subunit next to the SF's back side. In this "flipped state" the side chains of all D80 build saltbridges or hydrogen bonds with basic or polar residues of KTX [95]. The new contacts stabilize the bound state. As a result the K27 side chain from KTX is drawn about 4 Å deeper into the SF where it is bound to the carbonyl oxygen atoms of two Y78. The other two Y78 underwent a backbone flip that caused its carbonyl oxygen atoms to point into the cavity originally occupied by the E80 side chains. The effect of reprotonation of E71 led to a destabilization of the complex and the L27 side chain returned to its prior position. Subsequently, the rearrangement observed at the entrance of the SF was reversed [95].

The conformational changes observed when E71 and D80 become deprotonated were compatible with the ssNMR data from Lange et al. [59], whereas the changes after reprotonation were not compatible. Therefore it seems that both E71 and D80 side chains are charged in the KTX complex [95]. Ten simulations with initially deprotonated E71 side chains were set up. KTX was inserted at random positions and with random orientations. The simulations were carried out for 5 to 15 ns. None of these simulations has shown a binding of K27 to S0. Instead the toxin was attracted in most cases by negatively charged side chains located in the TM1-TM2-linker. Once the toxin was bound to the linker it remained there for the rest of the simulation. These results might suggest that the deprotonation of E71 is induced first when the toxin is close to the pore entrance.

### 6.2.2 Analysis of the conformational changes observed in MD simulation

Changes in the expectation value of the <sup>13</sup>C chemical-shifts for each frame of the trajectory were calculated using the *SHIFTX* software [69]. The results were compared to the measured chemical-shifts by ssNMR [59]. In the simulations only Y78 showed large backbone changes in the SF that led to remarkable deviations of the calculated chemical-shifts. The originally unimodal signal with a maximum at  $\delta = 60.2$  ppm split into two separated contributions at  $\delta = 58 - 60$  ppm and  $\delta = 56$  ppm. The latter was the most striking change, probably originating from the Y80 backbone flips, because these changes are strongly correlated with the observed  $\Psi$  dihedral angle transitions at Y78. In the ssNMR experiment the C <sub>$\alpha$</sub>  chemical-shift of Y78 were particularly affected by KTX binding. The peak in the spectrum at 61.7 ppm of the free channel which has been assigned to the C <sub>$\alpha$</sub> -C <sub>$\beta$</sub>  correlation of Y78 is split up in the bound state, with the Y78 C <sub>$\alpha$</sub>  signal shifted to 63.2 ppm. The magnitude and direction of the changes were consistent with the predictions made with *SHIFTX* within the accuracy limits of the program [69]. The calculated changes of the chemical-shifts from the trajectories favorably agree with the data from the experiment [95].

### 6.2.3 KTX binding relation to C-type inactivation

Since conformational changes associated with KTX:KcsA-K<sub>V</sub>1.3 complex formation involve the E71-D80 pair, we hypothesized that *C-type inactivation* may reduce the KTX-binding of K<sup>+</sup> channels. In collaboration with the group of O. Pongs the influence of *C-type inactivation* on KTX binding was investigated. The group performed physiological experiments with the K<sub>V</sub>1.3 channel expressed in the *Xenopus oocyte* expression system. Two different pulse protocols were used to force the channel into the open, closed and the *C-type inactivated state*, respectively. The first applied protocol<sup>2</sup> forced the channels into the open and closed states where an EC<sub>50</sub> of 0.06 nM was observed, in agreement with previous reports [59]. The second protocol<sup>3</sup> allowed the channels to fully enter into *C-type inactivation*. The latter protocol lowered the KTX binding affinity for K<sub>V</sub>1.3 20-fold (EC<sub>50</sub> = 1.2 nM) suggesting that *C-type inactivation* indeed changes the interaction surface with KTX.

## 6.3 K<sup>+</sup> channels and TEA

The models for TEA parameterized with OPLSAA force field were taken from ref. [68]. The partial charges in units of an electron charge  $e = 1.60217733C$  were 0.16 for the central nitrogen, 0.049 for the CX1-atoms and -0.27 for the CX2-atoms (cf. fig. 6.3). The hydrogens of the CX1-atoms had a charge of 0.06 and the hydrogens of the CX2-atoms a charge of 0.1. Five trajectories with the KcsA-Kv1.3 chimera and 25 TEA1 molecules in physiological solution were performed. The simulations had a length of about 10 ns and contained around 83000 atoms, about 150 mM NaCl and 241 POPC membrane lipids. The initial structures mainly differed in the occupation state of the SF in order to investigate the influence of the occupation state on the binding affinity of TEA. Based on the estimated affinity difference (cf. sec. 4.2), it was expected that the TEA molecules would take a distribution of TEA1 and TEA2 conformation of 1:3 while equilibrating, but none of the contained TEA molecules showed a transition into the TEA2 conformer during the whole simulation.

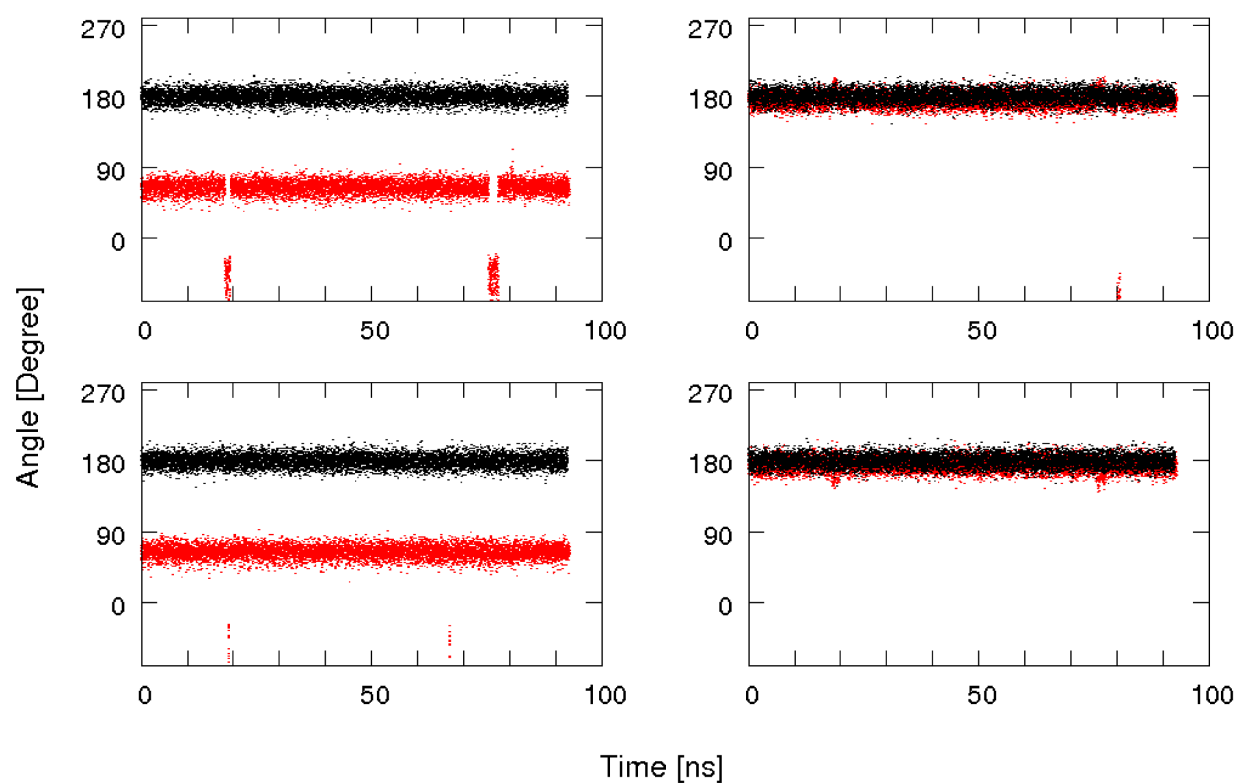


Figure 6.2: Dihedral angles between atoms  $CB1 - N - CA1 - CA2$  (top, left),  $CA1 - N - CB1 - CB2$  (top, right),  $CD1 - N - CC1 - CC2$  (down, left) and  $CC1 - N - CC1 - CC2$  (down, right) of TEA1 (red) and TEA2 (black), stay in their initial position over the whole trajectory. Only TEA1 shows short transitions into metastable states, whereas the structure of TEA2 is completely stable.

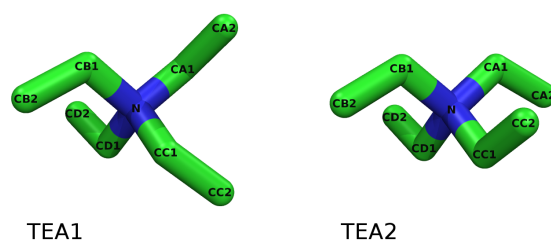


Figure 6.3: Tetraethylammonium in configurations TEA1 (left) and TEA2 (right). Both configurations turn into each other by turning two non-opposing side chains around the  $N-CX1$  axis. The panels show the nomenclature of the carbon (green) and nitrogen (blue) atoms of TEA. Hydrogen atoms are removed for clarity.

Receptor	SF occupation state	Inhibitor
KcsA-WT	[sskss] and [skskss]	TEA1, TEA2, mixture
KcsA-Kv1.3	[sskssk] [xsssk] [ssssk] [xssks]	TEA1
KvAP	[sskss] and [skskss]	TEA1, TEA2
Kv1.2-2.1	[sskss] and [skskss]	TEA1, TEA2
Kv1.2-2.1 with $\beta$ -subunits	[sssss]	mixture

Table 6.1: Overview of the simulations with TEA and OPLSAA parameters.

### 6.3.1 The distribution of TEA1 and TEA2 is quasi fixed in simulations

To focus on the behavior of the TEA model two trajectories with a length of about 100 ns were set up, each with 5 solvated TEA molecules. The configuration comprised about 4000 water molecules, 4 Na<sup>+</sup> ions and 9 Cl<sup>-</sup>. One configuration contained only molecules in the TEA1 conformation and the other contained just TEA2 conformers. The time step was chosen to 2 fs. None of the ten molecules has shown a transition from one into the other configuration. Whereas the TEA1 conformers exhibit short transitions into metastable states, the TEA2 conformers rest in their initial configuration. Figure 6.2 shows a representative example for both a TEA1- and a TEA2-molecule. The dihedral angles between the nitrogen, two C1 atoms of oppositely situated side chains and a C2 atom of one of these side chains were taken as observable, respectively. To get an impression of the height of the energy barrier between TEA1 and TEA2 a simulation in vacuum containing just one TEA2 in molecule was carried out. Position restraints of 4500 kJmol<sup>-1</sup>nm<sup>-2</sup> were applied on the nitrogen atom as well as all carbon atoms except for the carbon atom corresponding to CC2 in fig. 6.3. As a reference structure acted a TEA1 conformer, which was fitted onto the TEA2 structure. In that way a transition from TEA2 to TEA1 was enforced. The transition of the A-side chain was achieved after 3.88 ps. The C-side chain followed after a further 0.4 ps. Afterwards snapshots of the trajectory were taken from a point in time a short time before and after the transition of the side chains took place (i.e. at 3.9 ps and 4.0 ps). 100 free molecular dynamic simulations were performed for each snapshot with different initial velocities in concordance with a Boltzman distribution at 300 K. Those trajectories that contained a transition into the TEA1 or TEA2 state were taken for further analysis. These simulations revealed a third stable state between TEA1 and TEA2 with just one side chain pair in the trans-configuration. The energy of this third configuration (TEA3) was about 20 kJ mol<sup>-1</sup> higher than that of TEA1 and TEA2 calculated with GROMACS. The highest potential energy of those trajectories were assumed to reflect the energy of the transition states between the transitions from TEA1 to TEA3 and from TEA2 to TEA3. The energies of both transition states were estimated to be about 140 ± 10 kJ mol<sup>-1</sup> higher than that of the TEA2 ground state.

### 6.3.2 TEA - First Principles Docking

Nineteen free molecular dynamic simulations with a length of 20 ns were performed. The simulation systems contained different potassium channels (KcsA-WT, KcsA-Kv1.3, KvAP, Kv1.2-2.1 and also Kv1.2-2.1 with voltage sensing domains) embedded in a POPC bilayer. The cubic simulation boxes with edge lengths up to 12 nm where filled with KCl solution. As water model TIP4P [48] was used. The systems were equilibrated in the same manner as described in sec. 6.1. Boxes containing solvated TEA molecules were added to the pre equilibrated systems. The occupation states of the channels were modified manually.

<sup>2</sup>Repeatedly depolarized from a holding potential of -80 mV for 50 ms to +60 mV at 10 s intervals.

<sup>3</sup>The second protocol used test pulses of 60 s

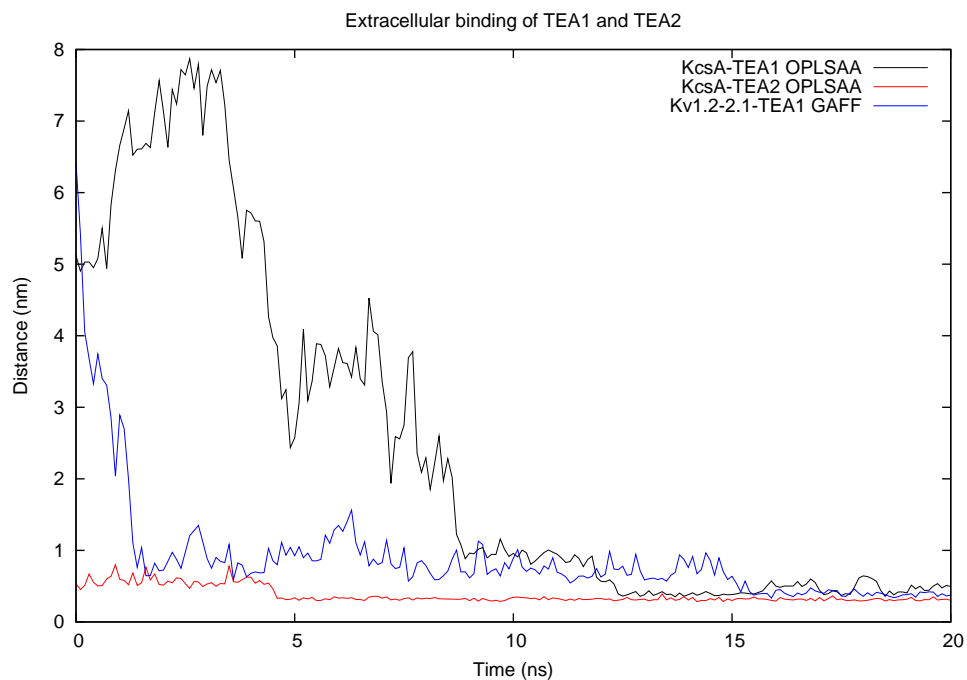


Figure 6.4: The distances between the central nitrogen of TEA and binding sites S0 of KcsA-WT and  $K_V1.2-2.1$  for the OPLSAA and the AMBER simulation, respectively.

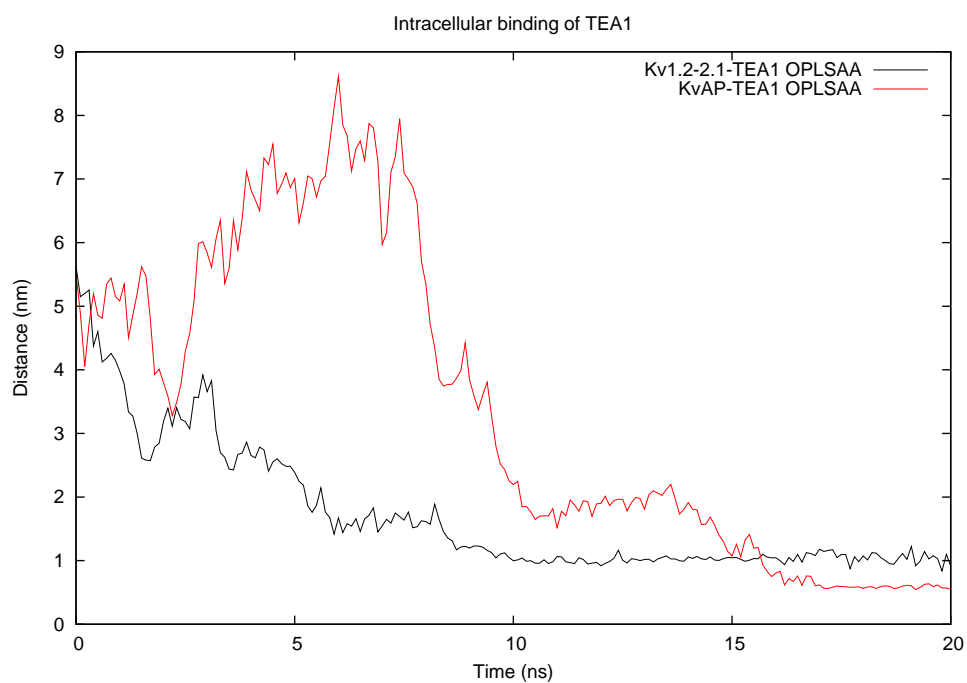


Figure 6.5: The distances between the central nitrogen of TEA and binding sites S4 of KvAP and  $K_V1.2-2.1$ , respectively, of the observed intracellular binding events.

The systems were subsequently energy minimized according to the *conjugate gradient* method.

The behavior of the channels in the OPLSAA and the AMBER/GAFF simulation exhibited no significant differences in the 20 ns of the simulation. TEA was found to bind in the most cases spontaneously at the extracellular receptor site. No extracellular binding was observed when site S0 was occupied by K<sup>+</sup>. The cation located deeper inside the SF did not affect extracellular TEA binding. In both simulations with a mixture of TEA1- and TEA2 conformers it was TEA2 that bound to S0. The side chains of Y81 stayed in a symmetric composition while TEA2 was bound. In the bound state TEA2 was situated central to the pore axis. In the case of TEA1 the side chains were in the majority of cases asymmetrically positioned. TEA1 toggled from one Y81 side chain to the other. One simulation with AMBER and GAFF parameters was performed with TEA1. TEA1 bound on the extracellular binding site. In contrast to simulations with OPLSAA the binding exerted direct influence to the occupation state of the receptor. As TEA1 bound to the extracellular site the occupation state changed from [kxsk] to [tkxsk]. One methyl group pointed into the SF and the compound was situated central to the pore axis. Figure 6.3.2 shows the distance of the central nitrogen of TEA for representative binding events of TEA1 and TEA2 on KcsA-WT and for the AMBER simulation. The curve of TEA1 exhibits more fluctuations suggesting that TEA1 is less stable, bound at the extracellular receptor site than TEA2. TEA2 binds about 0.7 Å closer to S0 than TEA1.

In two cases TEA1 diffused into the intracellular pore (KvAP [sskss], Kv1.2-2.1 with voltage sensing domains), whereas TEA2 does not. Figures 6.4 illustrates the intracellular binding events. The distance between the central nitrogen of TEA and S4 is plotted over time. In both cases the molecules “knocked on” before they diffuse into the cavity and stayed stable at a distance of about 2 nm from S4 for 3 to 4 ns before they reached the final position. In the final state the nitrogen was 5.5 Å away from S4 in the case of KvAP and 10 Å in the case of Kv1.2-2.1. In further simulations with TEA inside the central cavity of KvAP and Kv1.2-2.1 both TEA1 and TEA2 stayed stable inside the cavity over whole 20 ns of the trajectories.

## 6.4 Conclusions

The free molecular dynamics simulations performed with KTX provided a reliable model for the chemical shift changes observed with ssNMR upon KTX binding to KcsA-Kv1.3. The simulations highlighted structural rearrangements that potentially play a crucial role for the binding. The opening of the selectivity filter entrance and the rotation of the E80 side chains increase the number of intimate contacts with KTX and represent the basis for the attractive interactions that significantly increase the affinity. The results of the analysis with SHIFTX correspond almost perfectly to the ssNMR data. The simulations with TEA provided an insight into the binding of extra- and intracellular TEA in different conformations, but could not be used for a reliable estimation of binding affinities due to the lack of frequent binding and unbinding events. Nevertheless, they provide a model for the differences of the binding of TEA in the conformations TEA1 and TEA2. TEA2 is an ideal plug for the extracellular entrance of the channel and binds central to the pore axis. TEA1 seems to fit better into the intracellular entrance, but for a more accurate conclusion more simulations are required to yield better statistics. The analysis of TEA revealed an energy barrier between the conformers that is too high for frequent transitions during simulations. Therefore, the concentration of TEA1 and TEA2 conformers has to be chosen in the initial configuration of the simulation system.

## Chapter 7

# The parameterization of non-amino acid compounds

Ideally, the *force field parameters* of all components in a simulation system should be consistent. For the OPLSAA force field, which was introduced in section 5.2.1, no automatic protocol for the parameterization of non-amino acid molecules with an adequate accuracy is available yet. In 2004 Wang et al. developed the *general amber force field* (GAFF)[90]. In combination with the AMBER03 force field and a conversion script that converts AMBER topologies into GROMACS topologies, GAFF can be an accurate alternative for OPLSAA, providing a complete force field for proteins and nucleic acids as well as an approach to generate consistent parameters for arbitrary compounds. In this chapter, an approach that was developed for the automated generation of *force field parameters* for non-amino acid compounds is described. Furthermore, the dependence of the generated parameters on the conformation of the molecule was investigated and a strategy for the generation of a self-consistent (i.e. independent on the configuration) set of partial charges was successively developed by its iterative application on molecules with increasing complexity and different chemical composition.

### 7.1 Parameterization Process

Starting with a file containing the atomic coordinates of a compound (e.g. a PDB or MOL2 file), one can calculate and assign all required parameters with the software packages AMBER 9, ANTECHAMBER and GAUSSIAN03 (G03). The latter is needed for the *ab initio* calculation of partial charges. *Antechamber*, a program of the ANTECHAMBER software package, can generate input files for G03 from files in different formats that contain the partial structure (and the atom names) of a molecule. The default input for G03 generated by *Antechamber* has the following form:

```
#HF/6-31G* SCF=tight Test Pop=MK iop(6/33=2) iop(6/42=6) opt
```

```
1 1
N
C 1 b2
H 2 b3 1 a3
H 2 b4 3 a4 1 t4
C 2 b5 4 a5 1 t5
```

```
b2=0.8123
```

```
b3=0.7645
```

```
...
```

The line that begins with the '#' symbol contains the keywords which specify the type of calculation to be performed by G03. The meanings of the keywords are in detail:

**HF/6-31G\*** A Hartree-Fock Hamiltonian is used with a standard basis set 6-31G\*. This method is known to overestimate the polarizability, an effect which is exploited to implicitly include polarizability effects in a *non-polarizable force field*.

**SCF=tight** By default single point direct SCF<sup>1</sup> calculations are run with modest convergence criteria automatically to enhance efficiency. The keyword 'tight' requests the most precise convergence.

**Test** This keyword suppresses the automatic creation of an archive entry (formerly intended for the browse Quantum Chemistry Database System).

**Pop=MK** This properties keyword controls printing of molecular orbitals and several types of population analysis and atomic charge assignments. MK produces charges fitted to the electrostatic potential at points selected according to the Merz-Singh-Kollman scheme [78]. ESP and MerzKollman are synonyms for MK.

**IOP(6/33)=2** Makes Gaussian write out the grid points used for calculation of the electrostatic potential and the corresponding values of the potential.

**IOP(6/42)=6** Controls the density of the grid points.

**opt** Performs a geometry optimization according to the *Berny algorithm* until a stationary point on the potential surface is found, before the charge assignment. The algorithm constructs an approximate Hessian at the beginning of the optimization to reduce computational costs and then uses the forces on the atoms to predict energetically more favorable structures [77, 71].

The keyword section is followed by a line specifying the overall charge the multiplicity. The multiplicity is 1 for all cases considered here, because we treat systems in the singlet ground state. Subsequently a description of the geometry of the molecule follows. By default the geometry is specified in internal coordinates in the z-matrix format with variables b, a and t describing distances, angles and dihedral angles, respectively. With these options G03 performs a geometry optimization, calculates the atomic orbitals and calculates the electrostatic potential. Then a set of atom-centered point charges is generated (ESP charges) that reproduce as accurately as possible the *ab initio* electrostatic potential at grid points located at the

<sup>1</sup>SCF (*self consistent field*) methods [25] are required to determine the electronic orbitals of a many electron system.

van-der-Waals surface of the molecule. This is required because the electrostatics of atoms in MD simulations are represented by point charges at the center of mass of the atoms. In MD simulations the initial charge distribution is conserved over the whole trajectory, but the steric conformation is not. Therefore it is required to give sterically equivalent atoms (e.g. the hydrogens of a methyl group) the same partial charge. Furthermore, the ESP fitting process tends to give poor results for atoms buried in the center of a molecule. These charges therefore have to be scaled. Such a refined set of ESP charges is called RESP charges where RESP stands for *refined electrostatic potential*. The calculation of RESP-charges can automatically be carried out with a program called *resp* from the ANTECHAMBER package, which is also called by *antechamber*. The program *leap* from the AMBER 9 package was used afterwards to generate AMBER molecule topologies, which were converted into GROMACS topology format with the perl script *amb2gmx.pl* available at the home page of the Department of Chemistry and Biochemistry at the California State University Long Beach<sup>2</sup>.

## 7.2 Charge determination

### 7.2.1 Partial charges, conformational space and chemical structure

The partial charges calculated for a molecule by a procedure as used in GAFF may be different for different configurations of a molecule, and therefore depend on its flexibility. Different conformations will exhibit different interactions between the atoms of a molecule. For the parameters of the amino acids in AMBER03 two different conformations were taken into account [23]. Especially for larger and more flexible molecules various distributions of the partial charges at different conformers are conceivable. To give an example for the parameterization of a highly flexible molecule, Siu et al. [79] averaged over the RESP charges of 72 different conformers in order to obtain reasonable charges for DOPC. DOPC is a very flexible molecule with two tails which take very different conformations. In contrast, many therapeutic drugs are smaller and/or less flexible than DOPC. Their configurational space is smaller and therefore fewer conformers are presumably required for averaging to get an adequate set of charges. An appropriate approach for the parameterization might be to adjust the number of configurations to the number of atoms and the expected flexibility. An additional requirement is that the configurations of the compound have to be representative for the molecule. A configuration which is unlikely should be taken into account less than a configuration which is more probable. The weighting needs to be taken into account during averaging.

At first, the sampling problem was addressed. After initial parameterization based on a single configuration three sets of ten conformations each were generated for the first compound *nifedipine* (cf. sec. 7.4). For other compounds the conformations were generated by simulating the compound for 20 ns in vacuum using an initial set of parameters. To easier overcome conformational energy barriers, the simulations were performed at enhanced temperatures (i.e. 500 K) and snapshots from every 2 nanoseconds were taken. After a conjugate gradient energy minimization with maximally 1500 steps and a convergence criterion of  $1 \cdot 10^{-4}$  kJ mol<sup>-1</sup>, these snapshots were subjected again to the parameterization algorithm as schematically depicted in fig. 7.1. The ten charge sets generated in this way were taken and averaged to yield the final charge set. The final charge sets then were compared to the initially generated ones. To check whether the charges converge, this approach was repeated with the final charges in the case of *cisapride*. An improved sampling algorithm with an explicit water box was applied in the case of *4-Fluorosulfonylpiperidine*.

<sup>2</sup><http://chemistry.csulb.edu/ffamber/tools.html>

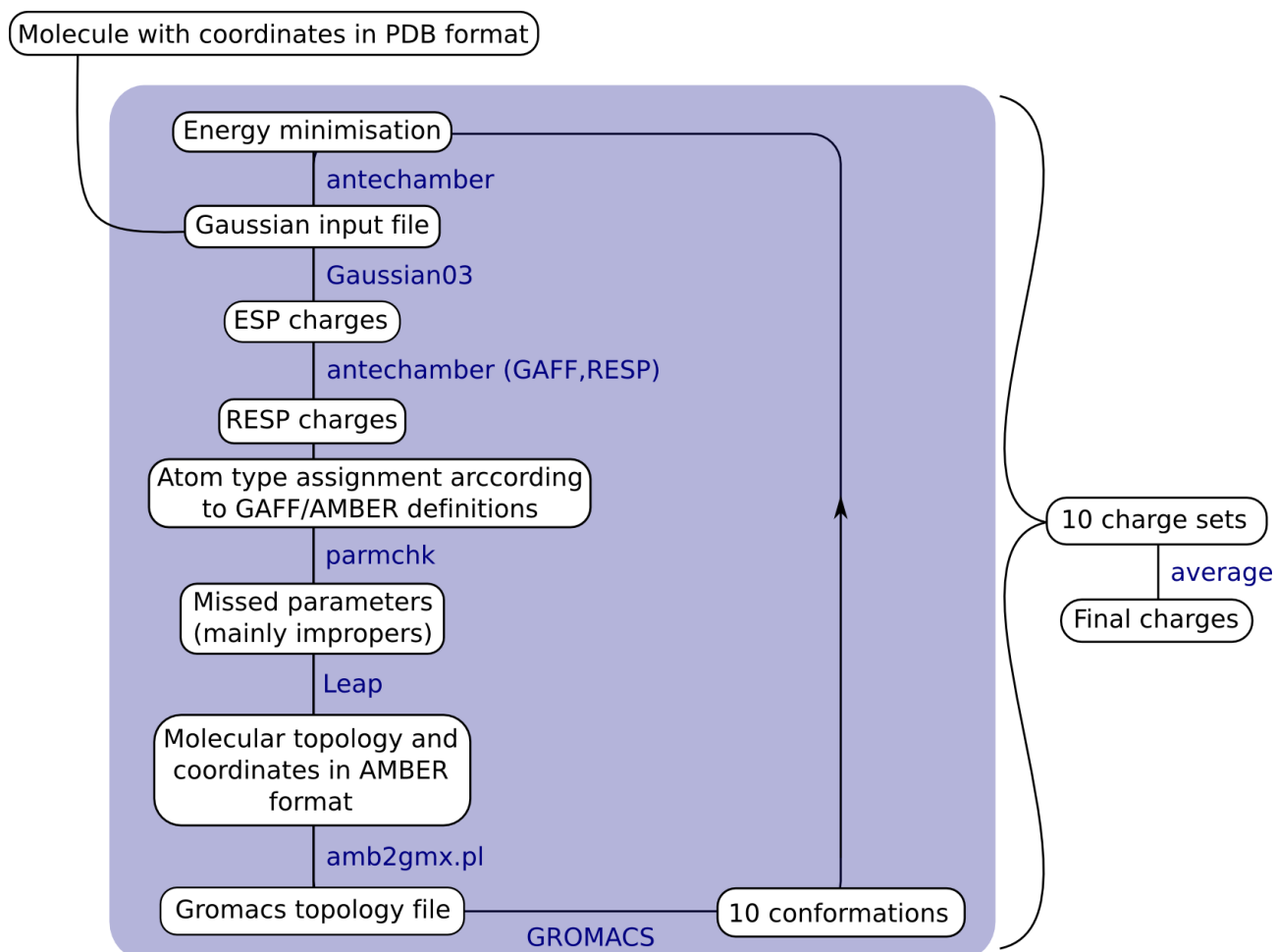


Figure 7.1: Schematic illustration of the parameterization scheme. In blue the programs are listed which are used in the particular step. For the initial structure no energy minimization could be performed because of the lack of a topology. With *antechamber* input files for G03 are created to calculate the ESP charges. *Antechamber* makes a RESP fit on the ESP charges. *Parmchk* generates missing *force field parameters*. The RESP charges and the parameters generated by *parmchk* and *antechamber* then are combined by *leap* that creates an AMBER topology. This topology is subsequently translated into GROMACS format by the perl script *amb2gmx.pl*. Using the GROMACS topology 10 conformations were generated by an MD simulation. For all of these conformations an energy minimization was performed initiating a new iteration. The ten generated charge sets then were finally averaged to yield a final set of charges. In the case of *4-Fluorosulfonylpiperidine* configurations were also generated in a simulation with explicit water.

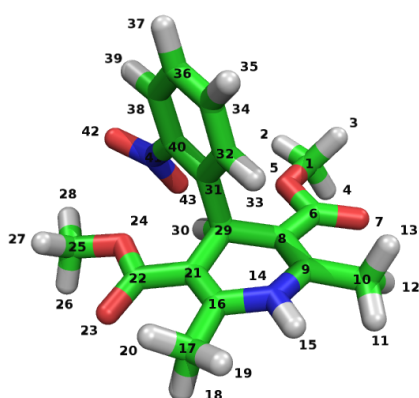
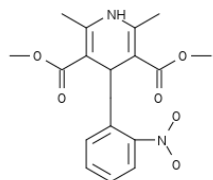


Figure 7.2: Structure and associated atom numbers of the calcium channel blocker *nifedipine*.

### 7.3 TEA

The 500 K-approach of generating partial charges was applied to TEA1. As mentioned in sec. 6.3, TEA is a relatively rigid molecule and also in the simulations at 500 K TEA exhibits no transition into the quasi-planar conformation (i.e. TEA2). The charges of the initial structures of TEA1 completely conform to the average from ten generated structures indicating that conformational flexibility does not affect the parameterization of charges in the case of TEA significantly. As TEA1 is more flexible than TEA2, TEA2 was expected to yield similar results and was not tested.

### 7.4 Nifedipine: Sampling



*Nifedipine*<sup>3</sup> is a calcium channel blocker used to treat high blood pressure, but it also interacts with *erg related* potassium channels (cf. 2.2). With 43 atoms *nifedipine* is also a small compound comparable to TEA in size but less symmetric. Figure 7.2 shows a three dimensional model in stick representation of *nifedipine* where the atom numbers are labeled. The two methyl ester groups and the nitro group can take several spatial conformations and the energy barriers between these states are small enough to allow transitions during simulations already at room temperature.

Therefore this is a proper test case for the investigation of the influence of the conformational flexibility on the calculated charge distribution. The states could be separated in classes defined by the configurations of the chemical groups mentioned above. The all atom root mean square deviation (RMSD<sup>4</sup>) with respect to the initial configuration is depicted in fig. 7.3 This makes *nifedipine* an optimal candidate for the analysis of different sampling approaches for the generation of representative, preferably Boltzman distributed, set of different conformers. For each conformation a new charge set was calculated and in the following the charge sets was averaged. Three sampling approaches were tested and are described in the conclusion.

<sup>3</sup>Dimethyl-2,6-dimethyl-4-(2-nitrophenyl)-1,4-dihydropyridine-3,5-dicarboxylate

<sup>4</sup>The RMSD is a measure of the difference between values, here between the conformation of a molecule at time  $t$  described by the time dependent vector  $\mathbf{r}(t) = (r_1(t), r_2(t), \dots, r_N(t))$  and a time independent reference structure described by the vector  $\mathbf{r}_0 = \mathbf{r}(t=0) = (r_{0,1}, r_{0,1}, \dots, r_{0,N})$ , where  $N$  is the number of atoms of the molecule:

$$RMSD(t) := \sqrt{\langle (\mathbf{r}(t) - \mathbf{r}_0)^2 \rangle} \quad (7.1)$$

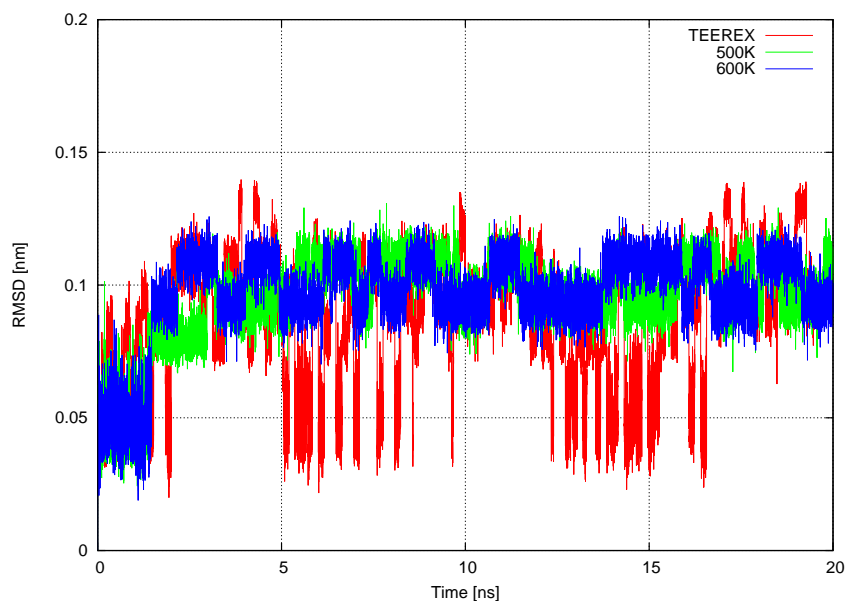


Figure 7.3: RMSD as a measure of the conformational variability. The TEEREX approach shows the best sampling, whereas the 500 K and 600 K approaches sample more or less the same configurational space.

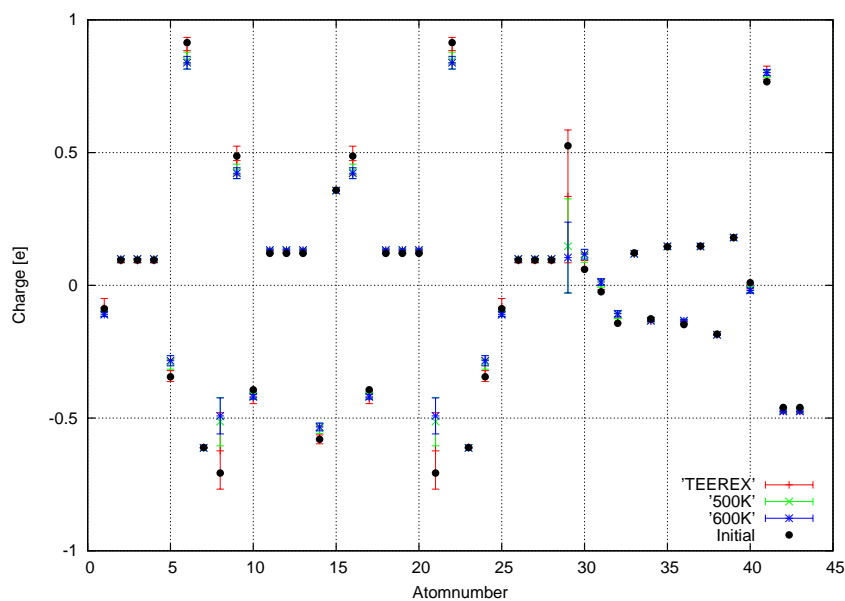


Figure 7.4: A comparison of three sets of partial charges based on structures generated with three different sampling approaches. The error bars are the standard deviation (STD) of the charge distribution for each atom. Qualitatively the standard deviations of all approaches exhibit the same tendency.

Atom/Approach	500 K		600 K		TEEREX	
	Charge	STD	Charge	STD	Charge	STD
C9	0.43	0.03	0.42	0.02	0.47	0.05
C21	-0.51	0.09	-0.49	0.07	-0.62	0.14
C29	0.15	0.18	0.1	0.13	0.34	0.25

Table 7.1: Comparison of the charges and the standart deviations (STD) of a subset of atoms based on different sampling approaches for *nifedipine*. Data given in units of  $e$ .

### 7.4.1 Sampling approaches

First of all a TEEREX (cf. 5.3) simulation of a solvated molecule over 20 ns was performed with a time step of 2 fs [53]. Every 2 picosecond a snapshot was taken for the analysis. The simulation was performed in a cubic simulation box with an edge length of about 3 nm. 876 water molecules and one model compound were included. As water model the TIP3P [48] model was used. Periodic boundary conditions were applied in all directions. The electrostatic interactions were calculated with the PME method [20, 27] and other non-bonded interactions with a Lennard-Jones potential with a cut-off radius of 1 nm. Furthermore, two trajectories of a molecule in vacuum, one at a temperature of 500 K and the other at 600 K, respectively, were calculated for a length of 20 ns each. No periodic boundary conditions and no pressure coupling were applied in these cases. The center of mass motion was removed in order to fix the molecule at the center of the simulation box. Figure 7.3 shows the RMSDs of the different approaches. The error bars in fig. 7.3 are the standard deviations STD of the charges.

$$STD := \sqrt{\langle (x_i - \langle x \rangle)^2 \rangle} \quad (7.2)$$

The variability is largest for the charge of the carbon atom with atom number 29 (C29), followed by C8 and C21, both situated directly beside C29 and then C6 and C22 which are sterically equivalent. These changes are likely to be induced by rotations of the highly electronegative oxygens O42 and O43 around the C40-C41-bond and by rotations of the side chains around the C6-C8- and C21-C22-bonds. The initial value of the charges, calculated for a single configuration, lies inside the standard deviation of the charge sets, except for C29, for which the value lies always within the standard deviation (STD) of the TEEREX trajectory, but not within the STD of the vacuum trajectories. Whereas the 500 K- and 600 K-simulations have sampled more or less the same region in configuration space, the TEEREX simulation frequently sampled also configurations the vacuum approach has not reached. Table 7.1 shows the STD of a subset of atoms for the different sampling approaches. The sets exhibit a similar behavior in the STD of the charge distribution. For most of the atoms the STD is close to zero. This is not the case for the atoms C8, C21 and C29 whose variability is the largest for all sampling approaches. The STD of C8 and C21 is roughly the same, which is expected, because both atoms are positioned at symmetrically equivalent positions. In all cases the STD is smallest for the 600 K-vacuum approach, and largest for the TEEREX approach. Furthermore, the compound appears more polar when snapshots are used from the TEEREX simulation, because the absolute values of the charges are frequently larger than those of the vacuum approaches. The reason for this effect is unknown.

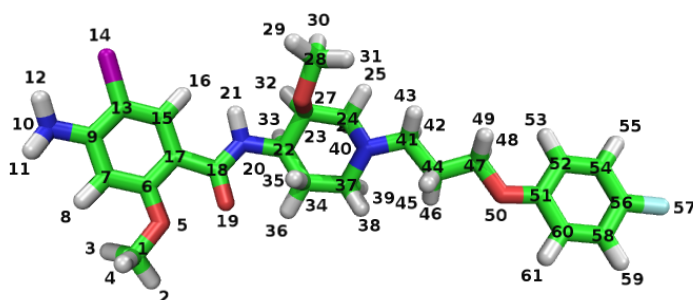
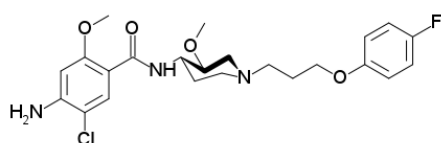


Figure 7.5: *Cisapride*, a drug for the treatment of nighttime heartburn. As a side effect it blocks the hERG potassium channel.

## 7.5 Cisapride: Self-convergence



*Cisapride*<sup>5</sup> is a drug which is used to treat symptoms of nighttime heartburn for people who have not responded to other treatments. As a side effect *cisapride* can prolong the plateau of the action potential of muscle cells in the human heart by binding to the human ERG receptor which controls the rapid component of the delayed rectifying potassium current ( $I_{Kr}$ ), a key component

of cardiac repolarization. The inhibition of this potassium current causes a prolongation of the so-called QT-interval, the time between depolarization and repolarization of the action potential of the heart cells, and increases the probability for the incidence of a life-threatening ventricular arrhythmia called *Torsades de Pointes*. Figure 7.5 shows the structure of cisapride. With 61 atoms *cisapride* is roughly double the size of TEA.

For the parameterization of this compound the vacuum approach at 500 K described in section 7.4 was used, because it is computationally cost efficient and the 600 K approach did not exhibit a significantly enhanced sampling in the case of *nifedipine* (cf. 7.4). The distribution was taken over 10 and 20 charge sets, respectively, in order to assess the minimum number of snapshots needed for the convergence of the partial charges. The charge set based on 10 structures is termed '10av', whereas the set based on 20 structures is termed '20av'. In fig. 7.6 the averages and the initial charge distribution are compared to each other. For all atoms the calculated partial charges of the '10av' set lie within the standard deviation of '20av' and vice versa. For most atoms, especially for the hydrogens, the charges are roughly identical. The initial charges also lie within the standard deviations of both charge sets in most of the cases. A histogram of the absolute values of the differences of the partial charges of both charge sets is depicted in fig. 7.6. There are five atoms with a difference in the partial charge of more than 0.02 e. The largest differences are observed for C22 and C17, both located between the two rings containing methoxyl groups. Smaller differences are observed for C114, C37 and N20. The region around the peptide bond between C22 and C17 is relatively rigid and polar. In simulations the aromatic ring and the peptide bond rest in the same plane. '20av' was taken for a convergence test. The parameterization process was repeated using '20av' as initial charges into the parameterization algorithm. The set generated in that way was termed 'SC1-10av'. In addition, the procedure was repeated with the 'SC1-10av' set to generate the 'SC2-10av' charge set and so on. In the case of convergence, the differences between the input and output charges should become smaller within every iteration step. In fig. 7.6 the development of the partial charges is illustrated. The histograms on the right side quantify the differences of the partial charges between subsequent steps in absolute values. The differences become smaller in every step. Thus it appears that the charges converge. Already in the second cycle the changes are at maximum around 0.05 e.

<sup>5</sup>4-amino-5-chloro-N- [1-[3-(4-fluorophenoxy)propyl]- 3-methoxy-4-piperidyl]-2-methoxy- benzamide

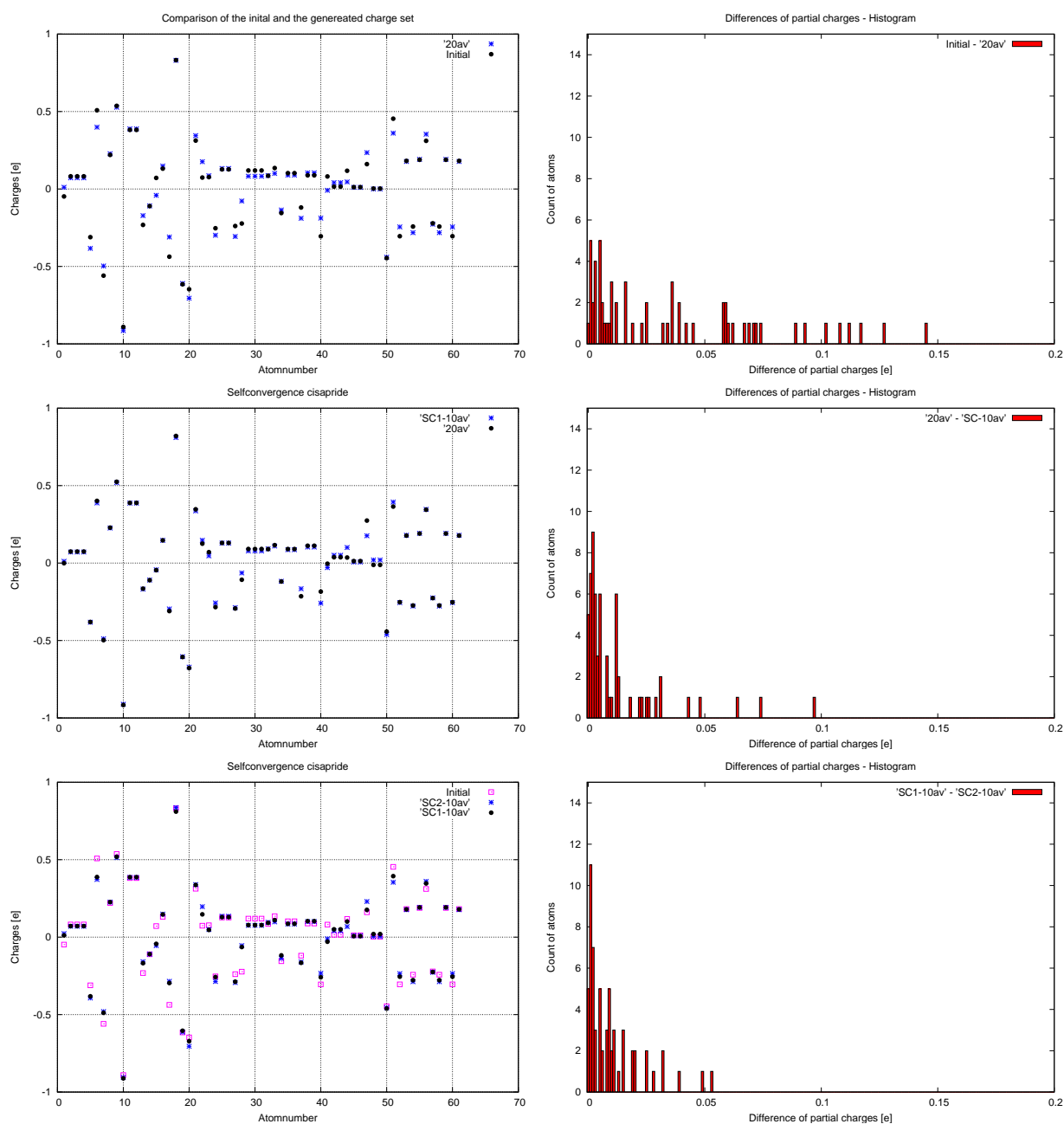


Figure 7.6: Difference between input and generated charge sets. The difference between the '20av' charges and the 'SC1-10av' set is larger than the difference between the '20av' and the 'SC1-10av' sets as one can deduce from the distribution of the histograms showing how many atoms exhibit a certain difference in the partial charge. The self-consistency of the partial charges has increased with an additional iteration cycle.

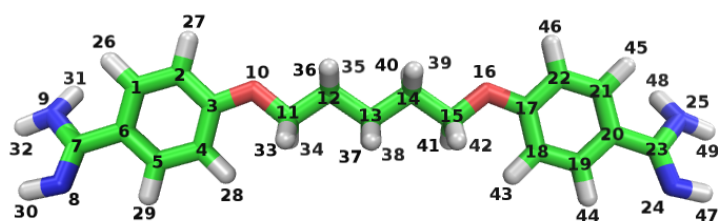
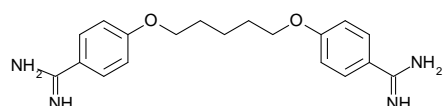


Figure 7.7: Structure and associated atomnumbers of the antiprotozoal *pentamidine*.

## 7.6 Pentamidine: Flexibility



*Pentamidine*<sup>6</sup> is an antiprotozoal, a drug against infectious disease caused by monocellular organisms. It interacts with DNA and therefore represses the synthesis of RNA and proteins. It also prolongs the QT-interval by blocking the hERG with an  $IC_{50}$  of  $252 \mu\text{M}$  [16, 57]. It is possible that *pentamidine* inhibits hERG currents also by repressing the expression of the hERG channel [16]. It is a onefold symmetrical drug with a very flexible central part. The sampling in vacuum generates a set of conformations in which a strongly kinked conformation is strongly overrepresented. This kinked conformation is relatively infrequently sampled in a MD simulation with explicit water molecules. The generated conformations are fitted and depicted in fig. 7.6. Despite those strong differences compared to the initial conformation, no dramatic redistribution of the partial charges was observed. Figure 7.6 shows the 10av charge set. The 10av charges roughly match with the initial charges. The largest differences between the initial values and the generated ones are about  $0.06 e$  and were observed in the vicinity of the oxygen atoms O10 and O16 at the carbon atoms C11 and C15 and also for the carbons of the carbodiimides C7 and C23. The variability is largest for the charge of C13, but the difference between the initial value and the generated one is only about  $0.02 e$ .

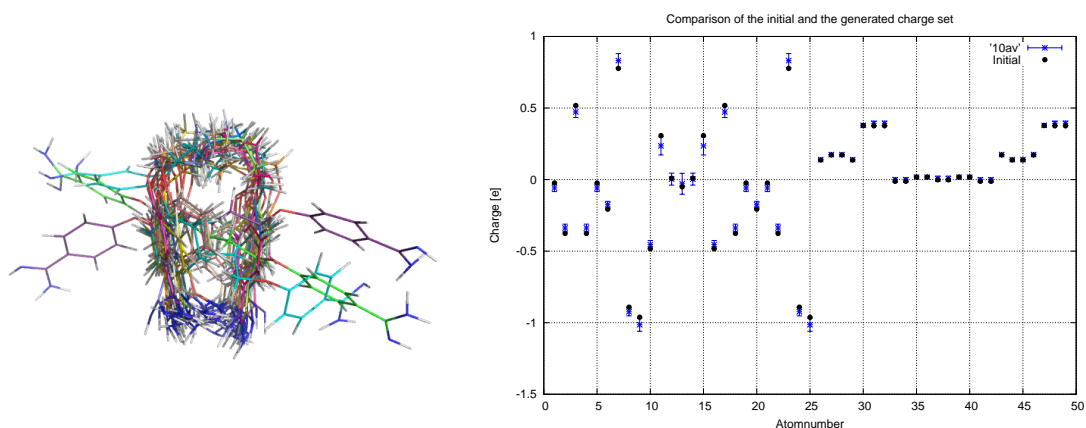


Figure 7.8: The fitted conformations of *pentamidine* on the left side. The approach in vacuum overestimates a strongly kinked conformation. However, the initial and the generated charge set strongly resemble each other.

<sup>6</sup>4-[5-(4-carbamimidoylphenoxy) pentoxy]benzenecarboximidamide

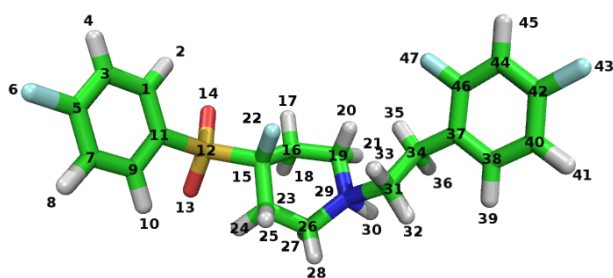
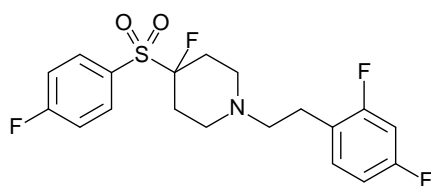


Figure 7.9: Structure and associated atom numbers of a hERG-optimized drug 4-Fluorosulfonylpiperidine.

## 7.7 4-Fluorosulfonylpiperidine: The influence of the environment.



4-Fluorosulfonylpiperidine is a hERG-optimized preparation of the isomeric *fluorophenylsulfone* and yields a more than 10-fold reduction of hERG activity [29, 42]. Both drugs differ only in a swap of fluorine F6 and the hydrogen H10 in one of the aromatic rings (cf. fig. 7.9). 4-Fluorosulfonylpiperidine is one-fold positively charged and has roughly the same size as *cisapride*. It is flexible like *pentamidine* and contains many atoms with high electronegativity i.e. four fluorine atoms and a sulfonyl group.

Therefore an increased variability of the partial charges and a higher dependence on the molecules conformation is expected. Like *pentamidine* it adopts a strongly kinked structure in the vacuum simulation (cf. 7.6).

Figure 7.10 shows the development of the partial charges in four iteration steps<sup>7</sup>. The number of atoms with differences in its partial charges of more than 0.05 e stayed stable at around 10. The set of partial charges differed in every step by about the same magnitude from the input data. As one can see on the left side of fig. 7.10, there are certain atoms, i.e. in particular the atoms C11, C19, C26, N29, H30 and C31, whose charges have changed between two distinct values for each iteration step. The difference between these occupied values went up to 0.2 e. Notably H30 exhibited substantial variability in its partial charge.

As no accurate convergence could be reached with the 500 K-vacuum approach in four iteration steps, the vacuum approach was considered as insufficient in this case, and it was decided to improve the sampling algorithm. In the following the input structures for the calculation of the partial charges were taken from a more physiological system i.e. a simulation box with explicit water molecules. The temperature was set to 300 K in order to create a set of conformations that is representative for physiological system. The simulation length was 20 ns. Starting structures were taken from every 2 nanoseconds of the trajectory. AV-solvent denotes the charge set of the first iteration step and SC1-solvent those for the second step. Figure 7.11 shows the results. The histograms in fig. 7.11 indicate that from the first step the charges differ less than the charges in the fourth iteration step with the 500 K vacuum approach. Already in the second iteration step, differences are less than 0.03 e. There was only one outlier with a value of about 0.063 e corresponding to C31, but its value in AV-solvent lies within the STD of the SC1-solvent charge set's deviation indicating that also for C31 a convergence takes place. Taking the highest difference as indicator, accurate convergence was reached in a single iteration step. In comparison to the vacuum approach the convergence was obviously increased.

<sup>7</sup>The notation is the same as in sec. 7.5

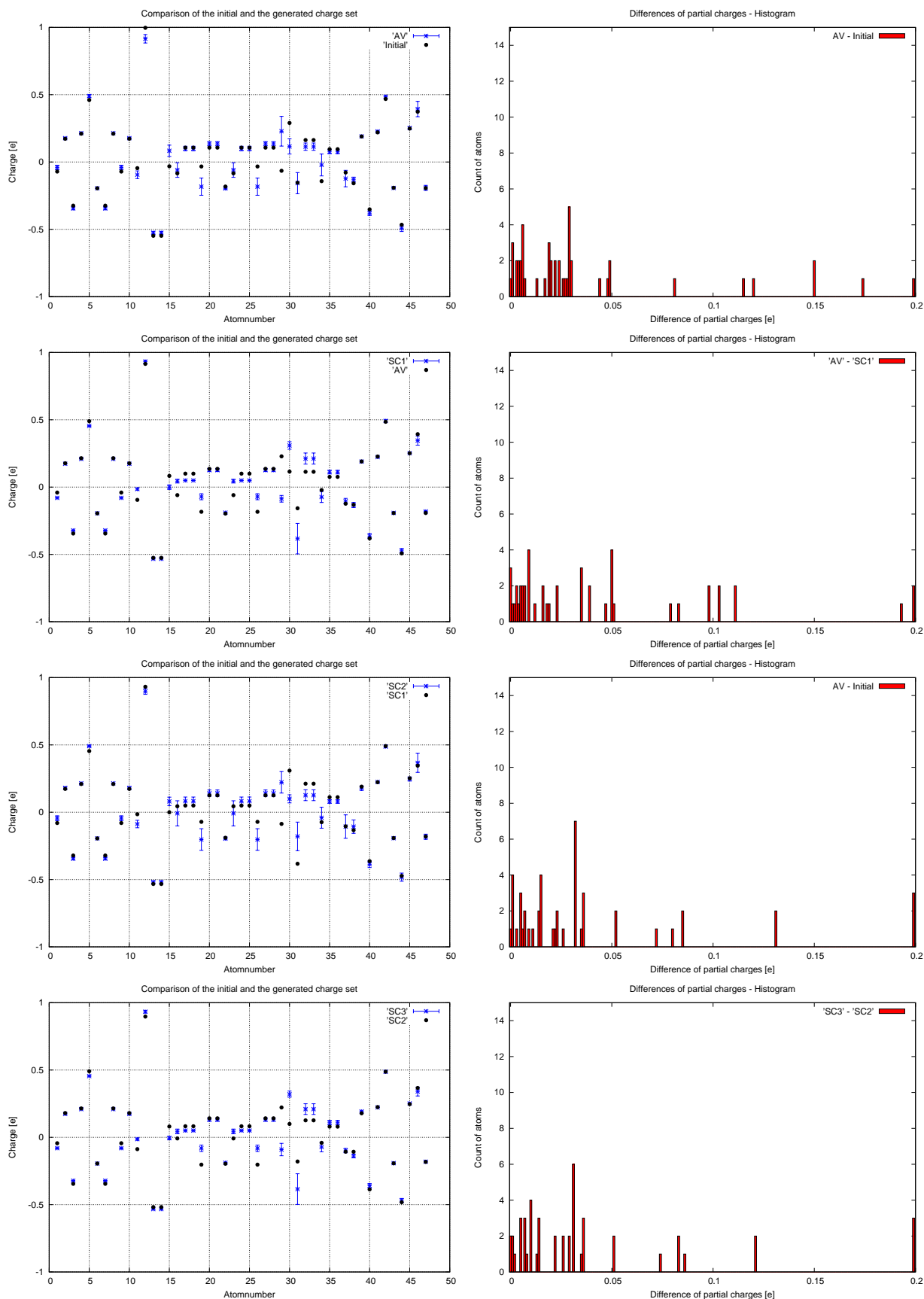


Figure 7.10: The development of *4-Fluorosulfonylpiperidine*'s partial charges basing on structures generated in a vacuum simulation at 500 K, exhibits two attraction points in the charge space.

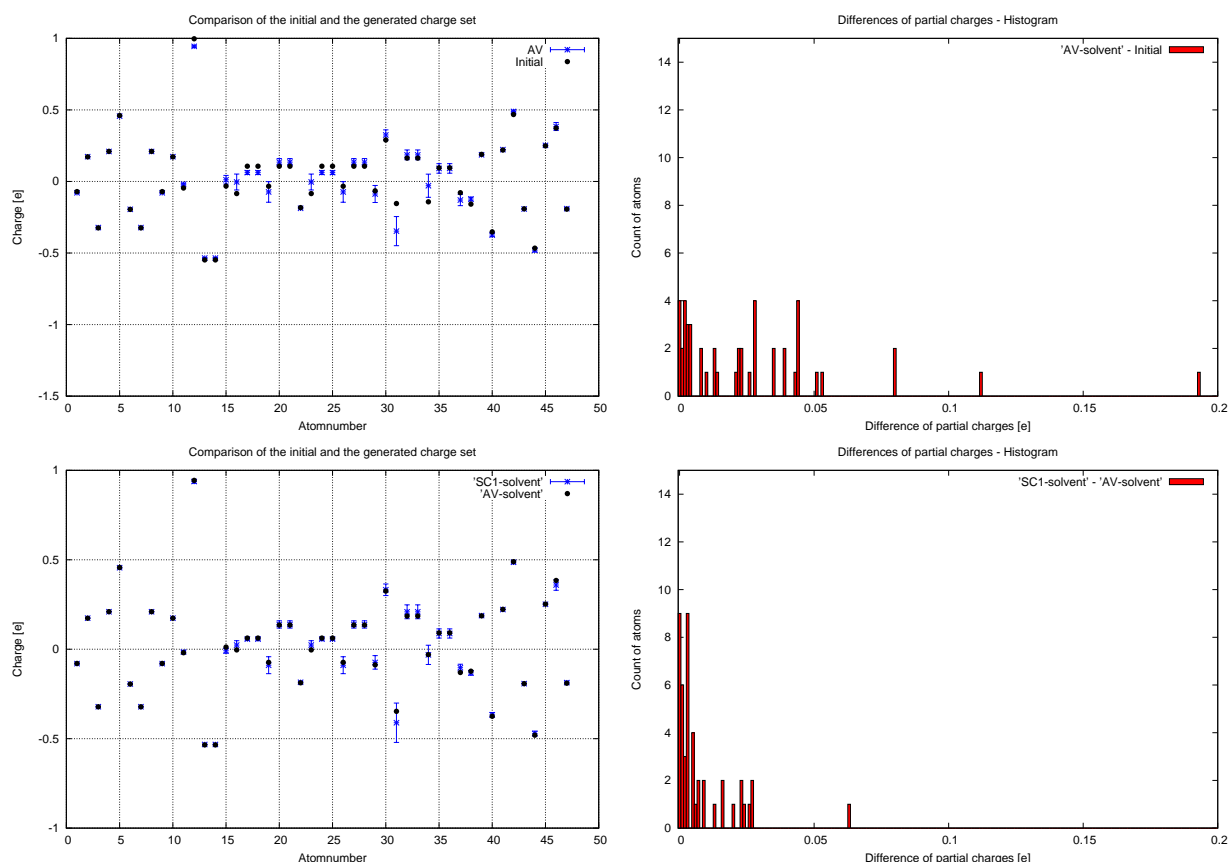


Figure 7.11: The charges differ much less from the initial values if the starting structures are taken from a trajectory with explicit water. The charges converge very rapidly in comparison with the 500 K vacuum approach (cf. fig. 7.10).

A comparison of the initial charges and the charge sets SC2, SC3 and SC1-solvent with each other revealed, that SC3 and SC1-solvent are in nearly complete accordance to each other. Furthermore, SC2 agrees with the initial charges. In the cases of C16 and C23 the partial charges of the SC2 set are closer to the charges from SC1-solvent and SC3 than to the initial ones (cf. fig. 7.12). During the vacuum simulations for the charge sets AV and SC2 the compound fell into a conformation where one of the sulfonyl group's oxygen atom interacted with the hydrogen bound to the central nitrogen. The distance between O14 and H30 stayed stable at 2 Å. The non-aromatic ring changed to a trans-configuration and thereby stabilized this interaction therefore. Lastly, the aromatic ring containing the two fluorine atoms was arranged in a way that the S12-O14 bond pointed central and perpendicular to the plane of the ring. Such a conformation was also seen in the simulation with solvent molecules for AV-solvent, but was not stable suggesting that the solvent destabilizes the molecule's self-interaction.

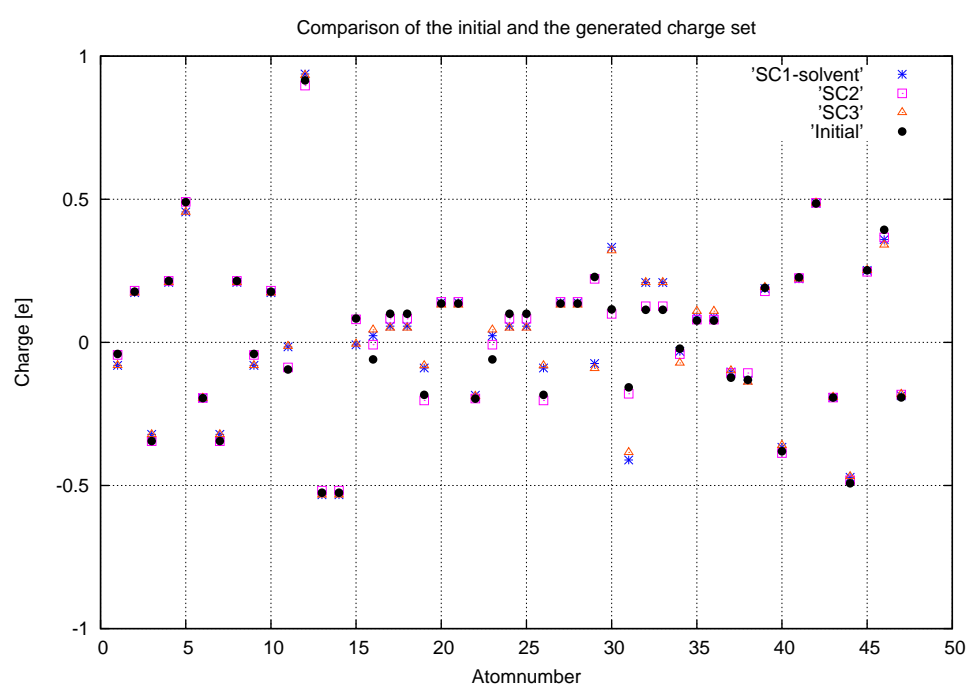


Figure 7.12: Comparison of the final charges with SC2, SC3 and SC1-solvent. SC3 and SC1-solvent are in good accordance to each other, whereas SC2 accord with the initial charges except for C16 and C23.

## 7.8 Conclusions

The TEEREX simulation turned out to be the more advanced sampling method, but it also requires the largest computational effort. Aside from the multiple parallel simulations at different temperatures a calculation of the eigenvalue decomposition of the covariance matrix has to be done. In contrast, the vacuum simulation is a much more simplified approach. The examples showed that for some compounds no average over different conformations is required to obtain a robust set of partial charges. This holds at least for molecules like *4-aminopyridine*, but also for molecules with a much larger configuration space such as *pentamidine*. The vacuum approach may give a reasonable sampling and can allow a convergence of the partial charges in several iteration steps, as was shown by the example of *cisapride*, but the application of this approach on *4-Fluorosulfonylpiperidine* demonstrated that the sampling with explicit water is more accurate and allows a faster convergence of the partial charges. The difference of the initial charge set and the averaged set is up to 0.5 e for *nifedipine*, 0.2 e for *cisapride* and *4-Fluorosulfonylpiperidine* and 0.07 for *pentamidine*. The influence of the electrostatic screening of the chemical environment on the partial charges was investigated indirectly, because the *ab initio* calculations were performed in an environment with a dielectric constant of 1 and did not contain explicit solvent molecules. Therefore, merely the conformational distribution, which was influenced by the chemical environment, contributed to the change of the partial charges. Both the examples of *4-Fluorosulfonylpiperidine* and *pentamidine* suggest that the influence of the solvent on the sampling should not be neglected.

Whether an average over different conformations is required depends on both, the flexibility and the chemical structure of the compound. As *nifedipine* shows, also small conformational changes can cause charge differences of the order of 0.5 e. For most MD simulations it might be sufficient to parameterize a compound twice. Firstly to get *force field parameters* that make an energy minimization possible and secondly after an energy minimization to derive charges that correspond to a probable average state. The generated charges should be sufficient for binding free energy estimations and a range of other approaches, but if the aim is to generate reproducible charges without previously assigning a certain conformation, the process shown here could be a proper procedure. In the case of molecules as TEA, where a relatively high energy barrier divides the conformational space, also the sampling with explicit water at 300 K will be insufficient. If the conformational space is manageable, it could be straightforward to parameterize the ligands in all regions and average the charges weighted with the probability for the compound to populate the respective region. Otherwise, one should accept the effort to set up a more accurate sampling approach like TEEREX.

## Chapter 8

# Potential of Mean Force and the estimation of IC<sub>50</sub> values

Umbrella sampling is a method for the calculation of the free energy landscape in one or more dimensions. Here the method was used for the calculation of the *potential of mean force* (PMF) of a drug with respect to the K<sub>v</sub>1.2-2.1 receptor (PMF) along a one dimensional reaction coordinate which was defined as the pore axis (cf. sec. 5.4.3). After one simulation consisting of up to 200 calculations (also-called windows), the PMF was reconstructed from the data and the IC<sub>50</sub> value was calculated. First of all, proper simulation conditions were estimated (cf. sec. 5.5).

### 8.1 Methods

A weighting or biasing potential  $W(\mathbf{r})$  of the form of eq. 8.1 was used in order to keep the compound in the vicinity of certain points along the reaction coordinate, which was chosen as the pore axis along the z-direction. In this way the compound samples the coordinate from the bulk water to a predefined binding site with a stepsize of 0.25 Å.

$$W(\mathbf{r}) = W_z(r_z) + W_{xy}(\mathbf{r}_{xy}) \quad (8.1)$$

$$W_z(r_z) = k_z (r_z - r_{z0})^2 \quad (8.2)$$

$$W_{xy}(\mathbf{r}_{xy}) = -k_{xy} (\mathbf{r}_{xy} - \mathbf{r}_{xy,c}) H(\mathbf{r}_{xy} - \mathbf{r}_{xy,c}) \quad (8.3)$$

The weighting potential had a harmonical part acting along the z-axis  $W_z(r_z)$  with a force constant  $k_z = 1000 \text{ kJ mol}^{-1} \text{ nm}^{-2}$  and a cylinder-symmetrical potential  $W_{xy}(\mathbf{r}_{xy})$  acting in the x,y-plane.  $H$  is the Heaviside step function and  $\mathbf{r}_{xy}$  the projection of the vector  $\mathbf{r}$  onto the x,y-plane.  $r_z$  denotes the z-coordinate of the vector  $\mathbf{r}$ . The resulting force from the biasing potential within the x,y-plane was 0 within a certain distance  $r_c$  around the pore axis before it rises in a quasi harmonical fashion with a force constant  $k_{xy} = 400 \text{ kJ mol}^{-1} \text{ nm}^{-2}$ . The bias potential was applied on one single atom near the center of mass of the compound. In the case of TEA it was the central nitrogen atom. In that way the compound was allowed to freely sample a slice of the radius  $r_c$  within the x,y-plane around the z-axis, thereby alleviating a sampling problem of the compound in the bulk that would entropically affect the free energy. The PMF then was reconstructed by analyzing the histograms with the *weighted histogram analysis method* (WHAM) [54] which was shown to be a reliable approach to unbiased and recombine the distributions obtained from single *umbrella calculations* [73].

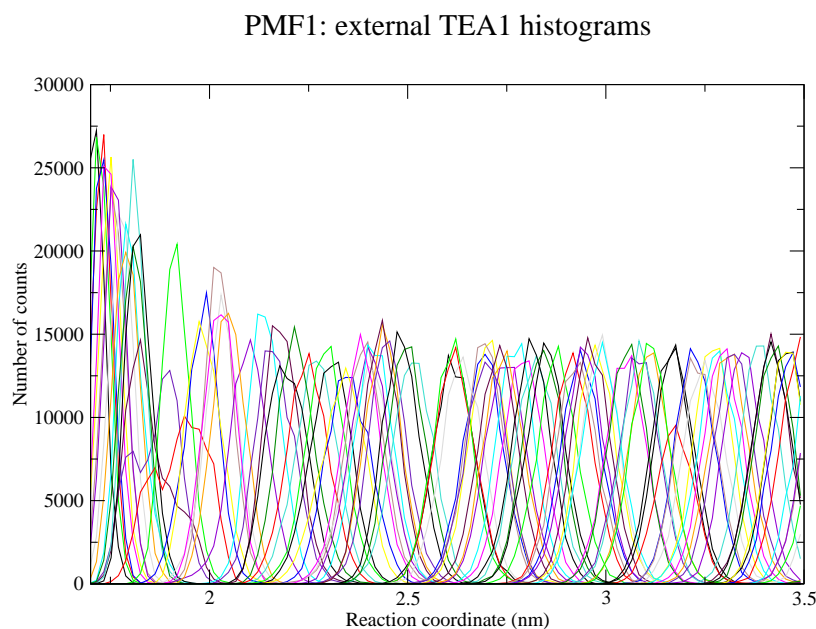


Figure 8.1: The histograms that underly PMF1.

Statistical errors were calculated with a *bootstrap* analysis [36] which randomly takes a number of histograms equal to the number of performed *umbrella calculations* and performs a WHAM analysis. Thereby it is allowed that single histograms are taken into account more than once or never for the analysis. The variability of the generated PMFs gave an estimation for the accuracy of the PMF and were used for a statistical error estimation. For a reasonable profile the WHAM analysis requires mutual overlapping histograms. To avoid gaps between the histograms we splice the histograms in sets of ten consecutive histograms and took randomly ten histograms out of this set. The whole procedure was repeated 30 times. From the generated potential curves a statistical error was calculated. To prevent overestimation of a certain conformation of the receptor, the PMF was calculated by taking many different conformations of the receptor into account. We randomly took the starting frames for the umbrella calculations from equilibration simulations of 10 to 20 ns length. For positively charged compounds, K<sup>+</sup> ions were removed in every starting frame to yield a neutral system. Water molecules which overlapped with the compound were removed. A conjugated gradient energy minimization was performed in ten steps prior to the calculation. The umbrella simulations were carried out for 0.2 to 2 ns, whereby the first 100 ps were finally considered as equilibration and were not taken into account for further analysis.

## 8.2 Binding of TEA on the K<sub>V</sub>1.2-2.1 receptor

### 8.2.1 Calibration of the sampling conditions

In order to calibrate the optimal simulation time per umbrella window, the binding of TEA at the extracellular binding site of K<sub>V</sub>1.2-2.1 was analyzed. This site is easier accessible for the molecule than the inner cavity and the broad extracellular vestibule of the channel pore exhibits fewer interactions than the narrow pore entrance at the intracellular side. The reaction coordinate from the bulk to the binding site was chosen

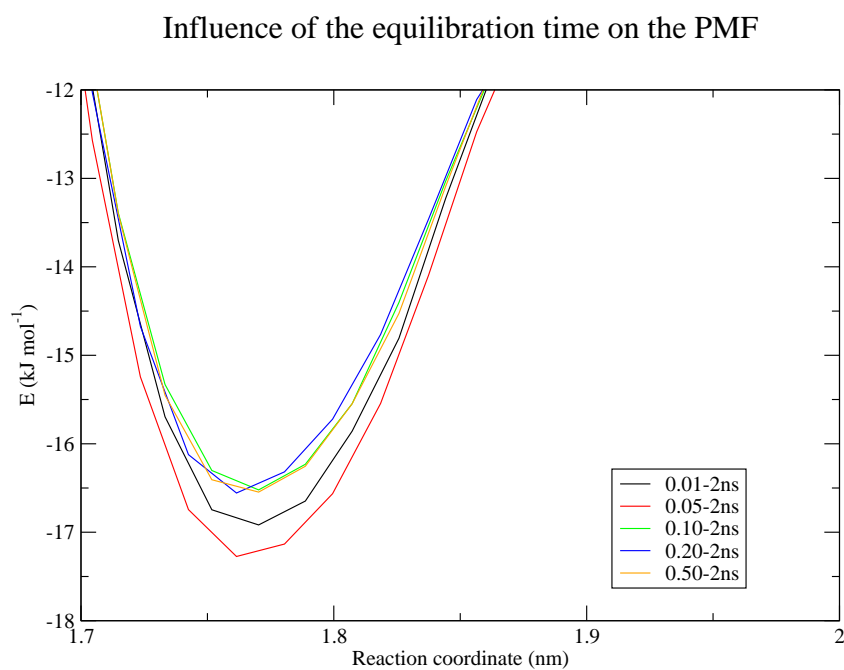


Figure 8.2: Variation of the PMF in dependence of the equilibration time in the beginning of each calculation which was not taken into analysis. An aperture near the binding pocket is shown for clarity. After 100 ps simulation the PMF becomes stable. The variations of the PMF are in the magnitude of  $1 \text{ kJ mol}^{-1}$ .

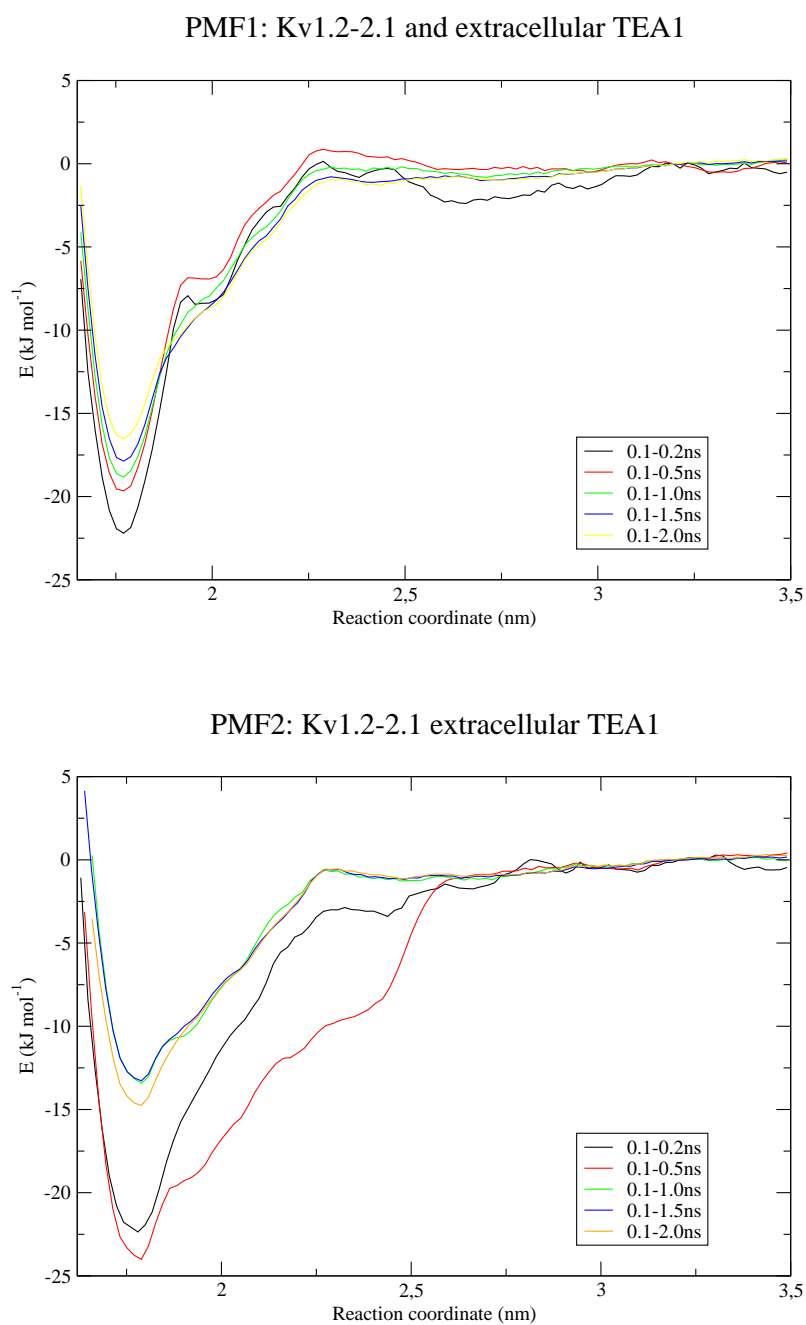


Figure 8.3: Comparison of the development of the PMF for external TEA1. Analysis from 0.1 ns to various times. The PMF varies also after 2 ns of sampling. The depth of the binding pocket decreases in time.

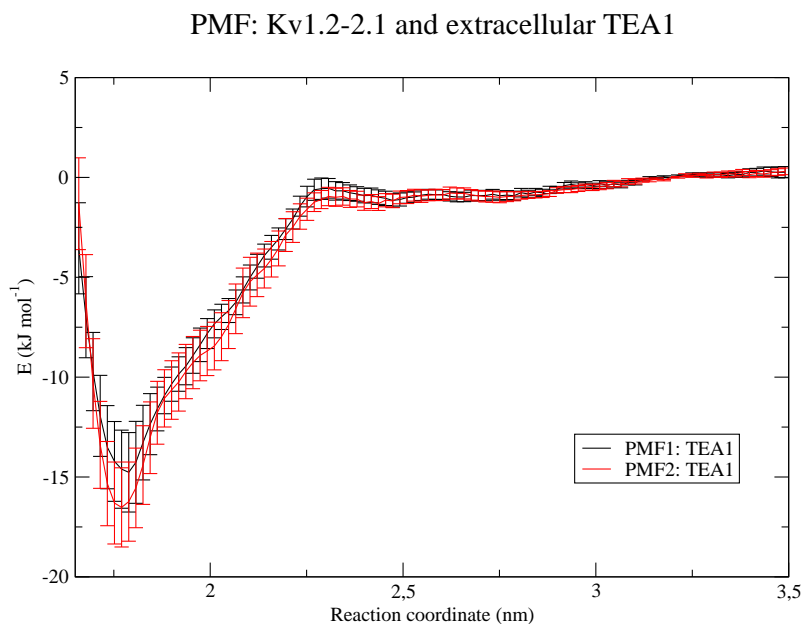


Figure 8.4: PMF1 and PMF2 of TEA1. The calculated potentials agree well within the error bars.

to a length of 3 nm. Two independent umbrella simulations were carried out with a length of 2 ns. The WHAM analysis of this umbrella simulation referred to as PMF1 was evaluated to the very end at 2 ns with variations of the starting time for the analysis. Figure 8.2 shows an aperture of the calculated potentials, which exhibits a variance of  $1 \text{ kJ mol}^{-1}$  at maximum. At first, the calculated potential decreased by about  $0.3 \text{ kJ mol}^{-1}$ . Then it increased to a constant value at equilibration times of 100 ps and longer. The largest differences were observed at values of 1.76 nm of the reaction coordinate belonging to the region directly in front of the entrance of the SF. Here the PMF has a quasi harmonic shape. Such regions are in the following referred to as “binding pocket”. They belong to attractive fix points in phase space. Due to this results the equilibration time in the analysis of further simulations was taken as 100 ps.

In addition to the equilibration time per umbrella window, also the required simulation time per window was assessed. With this aim, the simulations were analyzed from 100 ps to various values between 0.2 and 2 ns, in order to evaluate when the PMF is converged. Figure 8.3 shows how the potential varies with different sampling lengths. The overall shape of the PMF is similar for all sampling times. The potential seems to be composed of a plane region according to the bulk water, a linearly decreasing part and finally a binding pocket. The two PMF’s with the shortest sampling times are less smooth and exhibit a small energy barrier between the bulk and the decreasing part. Furthermore, the 0.1–0.2 ns PMF’s exhibit regularly emerging fluctuations relative to the longer sampled ones. With longer sampling these irregularities smear out. The radial distribution function of  $K^+$  ions in water exhibits maxima at similar distances. Therefore it is possible that these unregularities come from the ion distribution in the bulk that need time for reequilibration. Figure 8.3 shows that the PMF in the binding pocket increases with longer sampling periods which suggest that too short sampling leads to an overestimation of the binding free energy in this case. This effect is likely caused by an *induced fit* mechanism that in this case effects a decrease of the binding free energy. Even after 2 ns sampling, the PMF shows variability. For the evaluation of the reproducibility of the PMF, a second umbrella simulation referred to as PMF2 with exactly the same conditions

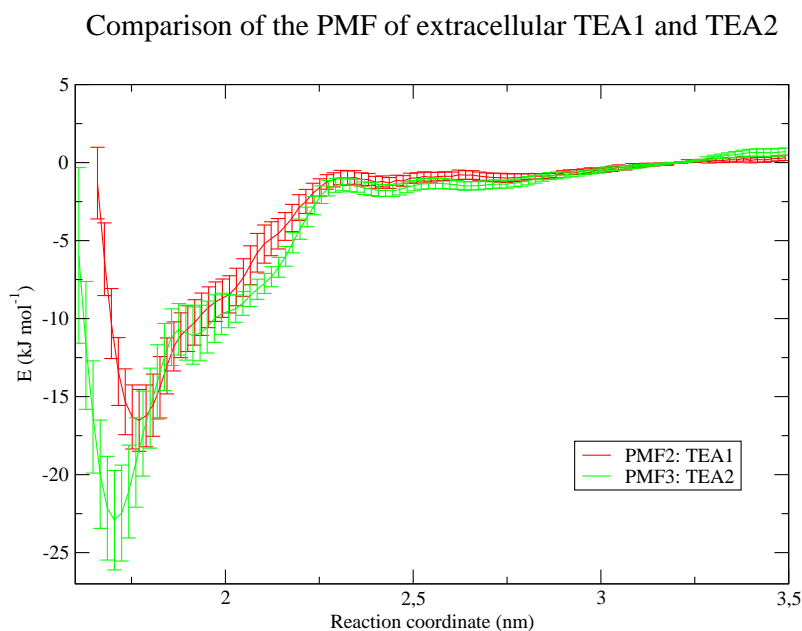


Figure 8.5: PMFs of TEA1 and TEA2 in respect to the extracellular  $K_V1.2-2.1$  receptor site. The potential of TEA2 shows a deeper binding pocket that is located closer to the entrance of the channel's pore entrance by about  $0.7 \text{ \AA}$ .

was carried out. The only difference with PMF1 was the starting configuration for each calculation. The whole simulation with a sampling time of 2 ns was taken into account for the analysis - except for the first 100 ps. Figure 8.5 shows PMF1 and PMF2 with error bars which were estimated using a bootstrap analysis using 10 calculations per window and 30 runs. The PMF's fit well within the error bars as one can see in fig. 8.5. For more accurate conclusions longer simulation times are required.

### 8.2.2 Binding of TEA on the extracellular $K_V1.2-2.1$ receptor site

An umbrella simulation was performed with the same conditions as in PMF1 and PMF2 taking TEA2 as compound. The results are illustrated in fig. 8.5. The binding pocket is about  $7.5 \text{ kJ mol}^{-1}$  deeper than in the case of TEA1 and is located about  $6.5 \text{ \AA}$  closer to the receptor. Both observations match with the results from the MD simulations described in sec. 6.3.2. In the case of TEA1 the molecule was treated as bound for values in respect to the reaction coordinate of 2 nm and below and in the case of TEA2 of 1.85 nm and below. The estimation of the  $IC_{50}$  values according to section 5.5 revealed an  $IC_{50}$  of 12 mM for TEA2 and an  $IC_{50}$  between 27 and 46 mM in the cases of PMF1 and PMF2 for TEA1. Choi et al. [11] have measured an  $IC_{50}$  of 33 mM for Shaker. The high similarity of  $K_V1.2-2.1$  to the Shaker channel in terms of both amino acid sequence and function suggests that results in respect to the  $K_V1.2-2.1$  can be interpreted also for Shaker [84]. If this assumption is valid, the affinity of Shaker and  $K_V1.2-2.1$  are likely similar. Under these conditions the results are encouragingly close to the experimental data.

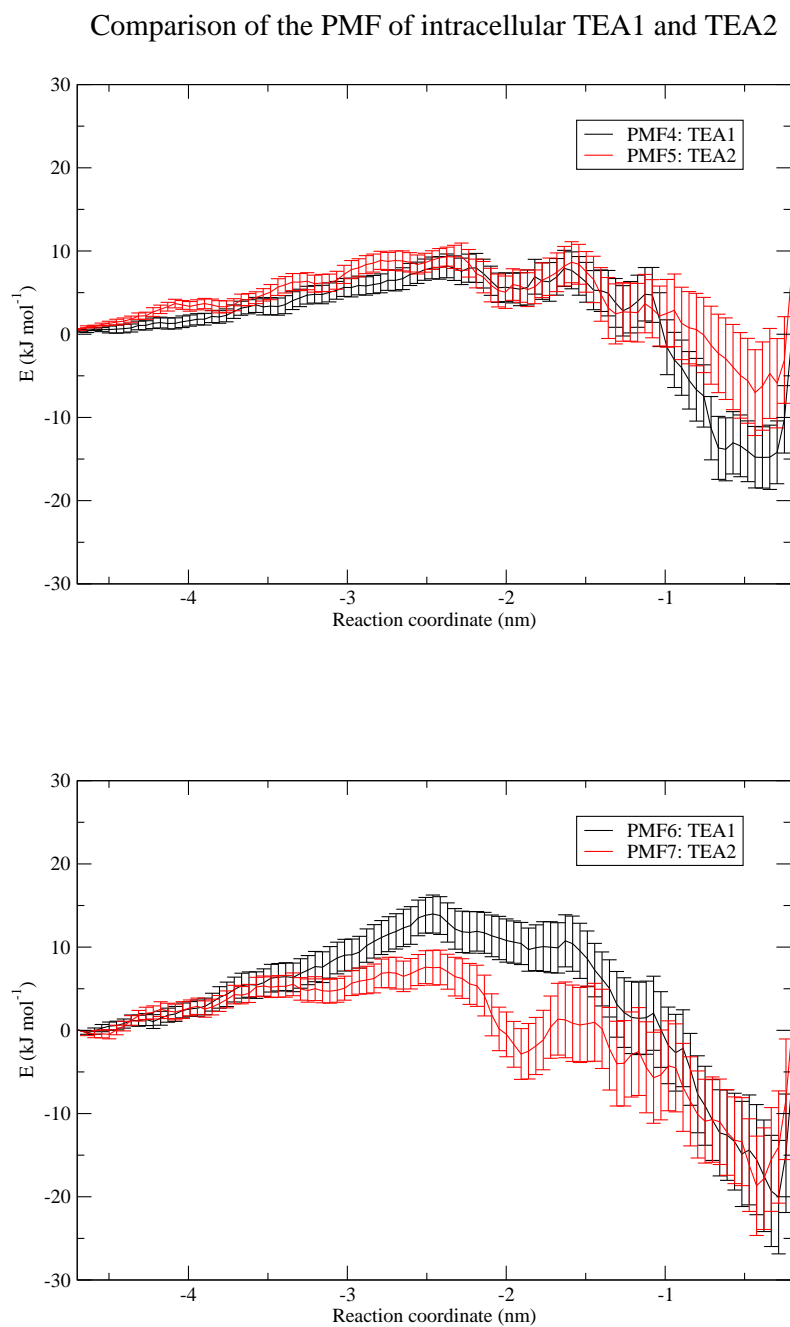


Figure 8.6: The PMFs for TEA1 and TEA2 in respect to the intracellular binding site of the  $K_V1.2-2.1$  receptor site.

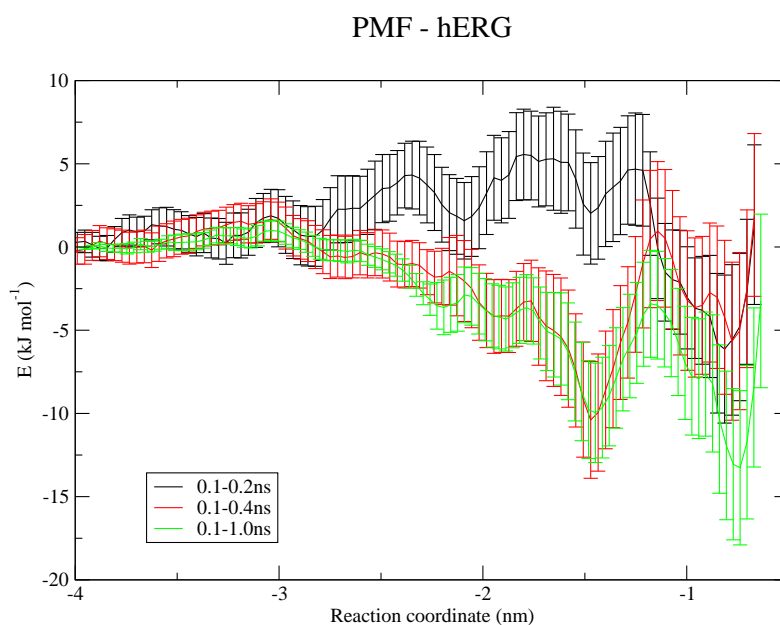


Figure 8.7: The PMF of TEA1 in respect to the intracellular site of the hERG homology model. The three potentials belong to different sampling times (0.2, 0.4 and 1 ns). The potential below  $-1.5$  nm seems to be converged. The binding pocket in direct vicinity of the SF could further increase with longer simulation times. Apparently there are two binding sites for TEA in the hERG channel.

### 8.2.3 Binding of TEA on the intracellular $K_V1.2-2.1$ receptor site

Figure 8.6 shows preliminary PMFs of TEA1 and TEA2 with respect to the intracellular  $K_V1.2-2.1$  receptor site. Starting frames were taken from the same 10 ns equilibration run. In the case of PMF4 and PMF5 structures were taken from the last 8 nanoseconds, whereas in the case of PMF6 and PMF7 only the last 5 ns were taken into account. In both cases the sampling time was only 0.2 ns. In the light of the results in sec. 8.2.1, it was expected that the PMF is not converged yet and that the shape of the PMF would further change with larger sampling times. From MD simulations it was expected that the PMF of TEA2 exhibits a larger barrier than this of TEA1 between the bulk and the cavity, because TEA2 was never seen to diffuse into the inner cavity in contrast to TEA1 (cf. sec. 6.3.2). In the case of PMF6 the potential goes up to  $12 \text{ kJ mol}^{-1}$  with respect to the potential in the bulk phase. In both cases the barrier seems to be higher for TEA1 than for TEA2. The depth of the binding pocket has found to be equal for TEA1 and TEA2 in the case of PMF6 and PMF7. A further observation is the existence of a binding pocket at a value of  $-2$  nm along the reaction coordinate of PMF7. Although the sampling lengths are equal for PMF4 to PMF7 the second pocket is distinct in only one potential. The fact that such a pocket was also seen in the longer sampled PMF for hERG (cf. fig. 8.7) supports the assumption of a second binding site that is located further away from the SF. The second binding site could also be deduced from the free molecular dynamics simulations described in sec. 6.3.2 and was also suggested from physiological experiments [3].

### 8.3 Validation of a hERG-homology model

A further motivation for the estimation of binding affinities and  $IC_{50}$  values not mentioned above is the possibility to use them for the validation of homology models. An *umbrella simulation* with a homology model of the hERG channel was carried out that was built by Anna Stary. The sampling time was chosen to 1 ns, due to limited time. The calculated PMF is depicted in fig. 8.7. It reveals two binding pockets similar as in sec. 8.2.3, where more extensive sampling was used. The first binding pocket is located in direct vicinity of the SF. An analysis according to sec. 5.5 reveals an  $IC_{50}$  of 48 mM. Although still in a preliminary stage, we expect this approach to be useful in the discrimination between multiple homology models of the same target, by comparison of computed affinities to experimentally measured ones.

### 8.4 Conclusions

The first results obtained with *umbrella sampling* were encouraging and sobering at the same time. The experimentally measured  $IC_{50}$  values could be reproduced for TEA for the extracellular binding site of a Shaker related channel within the same order of magnitude as the experimental ones, but the computational effort for the generation of the PMF was quite high. About 200 simulations with a length of 2 ns were performed for a single conformer. Both the extracellular binding site and the compound were very rigid. Therefore, it appears that umbrella sampling is an unsuitable method for the estimation of binding affinities or  $IC_{50}$  values of larger and more flexible molecules as well as for binding sites with higher flexibility. Furthermore, it remains unclear how accurate the estimation of the  $IC_{50}$  values is, if the form of the PMF changes with time due to *induced fit* mechanisms. As it was shown in sec. 6.3.2, the compound and the binding site can adapt to each other. Therefore, the effect of *induced fit* is different at various positions along the reaction coordinate.

## Chapter 9

# Discussion

The aim of this thesis was, on the one hand, to investigate the mechanisms during KTX:KcsA-K<sub>v</sub>1.3 complex formation and, on the other hand, to create a framework for the estimation of binding affinities of drugs to transmembrane channels. Could these aims be achieved? The answer is: in part.

On the side of the toxin-channel complex our investigations led to a more detailed understanding of complex formation and the high affinity's origin. The performed free molecular dynamics simulations provided a reliable model for the chemical shift changes observed with ssNMR upon KTX binding to KcsA-K<sub>v</sub>1.3 and highlighted structural rearrangements that potentially play a crucial role for the binding.

On the side of the estimation of the binding affinities various aims have been reached. An environment was realized that is easy to handle, allowing the parameterization of arbitrary molecules in an automated fashion. The process uses GAFF and generates partial charges at the HF/6-31G\* level. Furthermore, the connection between the conformational space, the chemical composition and the partial charges was investigated. The results suggested a modest dependence of the partial charges on the input structures paving the way towards an automated method for the generation of self-consistent and robust partial charges. However, the combination of AMBER03 and GAFF together with the HF/6-31G\* method is not hundred per cent consistent, because the charges of AMBER03 were generated with the B3LYP/cc-pVTZ//HF//6-31G\*\* method, whereas HF/6-31G\* was used in GAFF.

First steps for the estimation of binding affinities and IC<sub>50</sub> values were realized. The affinity of extracellular TEA could be estimated and the results were close to the experimental data. However, no tests with more complex molecules have been performed so far. These would be the actual targets of further investigations. The *umbrella sampling* approach is not completely automated so far and may turn out challenging for our requirements due to the large computational effort involved.

## Outlook

The results show that umbrella sampling is a very expensive method and for less symmetric and more flexible compounds it is presumably inefficient and perhaps unfeasible. Until now, it remains unclear how accurate binding affinities or IC<sub>50</sub> values can be predicted for more flexible compounds in this way. Especially for potassium channels, the intracellular receptor site is of large interest, because many inhibitors bind from the intracellular side of the membrane. Therefore, other simplified approaches for the estimation of binding affinities such as the *linear interaction energy* (LIE) will be investigated as potential alternative in the future. Further improvement and investigations are possible on the side of the parameterization approach. At first, the B3LYP/cc-pVTZ//HF//6-31G\*\* method for the partial charges corresponding to AMBER03 charges should be implemented. In order to reach highest consistency in

systems with membrane bilayers, partial charges of the lipids should also be generated according to this method. The approach can be further improved by the implementation of parallel charge calculations. Whether a parallel approach is required, depends on the robustness of the B3LYP/cc-pVTZ//HF//6-31G\*\* charges. Further investigations are required to address these questions. Further investigations are required to address these questions. The use of incomplete structures poses another uncertainty on the significance of the results presented here. Even if the whole binding site is modeled, remote parts that are not included in the simulation model could potentially have an influence on the structure that changes the interaction with ligands. That is why we see the need for further clarification.

# Bibliography

- [1] J. Aiyar, J. M. Withka, J. P. Rizzi, D. H. Singleton, G. C. Andrews, W. Lin, J. Boyd, D. C. Hanson, M. Simon, and B. Dethlefs. Topology of the pore-region of a k<sup>+</sup> channel revealed by the nmr-derived structures of scorpion toxins. *Neuron*, 15(5):1169–1181, Nov 1995.
- [2] C. M. Armstrong. Interaction of tetraethylammonium ion derivatives with the potassium channels of giant axons. *J Gen Physiol*, 58(4):413–437, Oct 1971.
- [3] T. Baukrowitz and G. Yellen. Two functionally distinct subsites for the binding of internal blockers to the pore of voltage-activated k<sup>+</sup> channels. *Proc Natl Acad Sci U S A*, 93(23):13357–13361, Nov 1996.
- [4] H. J. C. Berendsen, J. P. M. Postma, W. F. van Gunsteren, A. DiNola, and J. R. Haak. Molecular dynamics with coupling to an external bath. *J. Chem. Phys*, 81:3684–3690, 1984.
- [5] O. Berger, O. Edholm, and F. Jähnig. Molecular dynamics simulations of a fluid bilayer of dipalmitoylphosphatidylcholine at full hydration, constant pressure, and constant temperature. *Biophys J*, 72(5):2002–2013, May 1997.
- [6] S. Bernèche and B. Roux. Energetics of ion conduction through the k<sup>+</sup> channel. *Nature*, 414(6859):73–77, Nov 2001.
- [7] F. Bezanilla. The voltage sensor in voltage-dependent ion channels. *Physiol Rev*, 80(2):555–592, Apr 2000.
- [8] F. Bezanilla and C. M. Armstrong. Negative conductance caused by entry of sodium and cesium ions into the potassium channels of squid axons. *J Gen Physiol*, 60(5):588–608, Nov 1972.
- [9] Denis Bucher, Leonardo Guidoni, and Ursula Rothlisberger. The protonation state of the glu-71/asp-80 residues in the kcsa potassium channel: a first-principles qm/mm molecular dynamics study. *Biophys J*, 93(7):2315–2324, Oct 2007.
- [10] K. L. Choi, R. W. Aldrich, and G. Yellen. Tetraethylammonium blockade distinguishes two inactivation mechanisms in voltage-activated k<sup>+</sup> channels. *Proc Natl Acad Sci U S A*, 88(12):5092–5095, Jun 1991.
- [11] K. L. Choi, C. Mossman, J. Aubé, and G. Yellen. The internal quaternary ammonium receptor site of shaker potassium channels. *Neuron*, 10(3):533–541, Mar 1993.
- [12] D. Choquet and H. Korn. Mechanism of 4-aminopyridine action on voltage-gated potassium channels in lymphocytes. *J Gen Physiol*, 99(2):217–240, Feb 1992.

- [13] Julio F Cordero-Morales, Luis G Cuello, and Eduardo Perozo. Voltage-dependent gating at the kcsa selectivity filter. *Nat Struct Mol Biol*, 13(4):319–322, Apr 2006.
- [14] Julio F Cordero-Morales, Luis G Cuello, Yanxiang Zhao, Vishwanath Jogini, D. Marien Cortes, Benoît Roux, and Eduardo Perozo. Molecular determinants of gating at the potassium-channel selectivity filter. *Nat Struct Mol Biol*, 13(4):311–318, Apr 2006.
- [15] Julio F Cordero-Morales, Vishwanath Jogini, Anthony Lewis, Valeria Vásquez, D. Marien Cortes, Benoît Roux, and Eduardo Perozo. Molecular driving forces determining potassium channel slow inactivation. *Nat Struct Mol Biol*, 14(11):1062–1069, Nov 2007.
- [16] Jason S Cordes, Zhuoqian Sun, David B Lloyd, Jenifer A Bradley, Alan C Opsahl, Mark W Tengowski, Xian Chen, and Jun Zhou. Pentamidine reduces herg expression to prolong the qt interval. *Br J Pharmacol*, 145(1):15–23, May 2005.
- [17] Wendy D. Cornell, Piotr Cieplak, Christopher I. Bayly, Ian R. Gould, Kenneth M. Merz, David M. Ferguson, David C. Spellmeyer, Thomas Fox James W. Caldwell, and Peter A. Kollman. A second generation force field for the simulation of proteins, nucleic acids, and organic molecules. *J. Am. Chem. Soc.*, 117:5179 – 5197, 1995.
- [18] S. Crouzy, S. Bernéche, and B. Roux. Extracellular blockade of k(+) channels by tea: results from molecular dynamics simulations of the kcsa channel. *J Gen Physiol*, 118(2):207–218, Aug 2001.
- [19] Liem X. Dang. Mechanism and thermodynamics of ion selectivity in aqueous solutions of 18-crown-6 ether: A molecular dynamics study. *J. Am. Chem. Soc.*, 117:6954–6960, 1995.
- [20] T Darden, D York, and L Pedersen. Particle mesh ewald: An n log(n) method for ewald sums in large systems. *J. Chem. Phys.*, 98:10089–10092, 1993.
- [21] W.L. DeLano. W.I. the pymol molecular graphics system. *DeLano Scientific San Carlos, CA, USA.*, 2002.
- [22] D. A. Doyle, J. Morais Cabral, R. A. Pfuetzner, A. Kuo, J. M. Gulbis, S. L. Cohen, B. T. Chait, and R. MacKinnon. The structure of the potassium channel: molecular basis of k+ conduction and selectivity. *Science*, 280(5360):69–77, Apr 1998.
- [23] Yong Duan, Chun Wu, Shibasish Chowdhury, Mathew C Lee, Guoming Xiong, Wei Zhang, Rong Yang, Piotr Cieplak, Ray Luo, Taisung Lee, James Caldwell, Junmei Wang, and Peter Kollman. A point-charge force field for molecular mechanics simulations of proteins based on condensed-phase quantum mechanical calculations. *J Comput Chem*, 24(16):1999–2012, Dec 2003.
- [24] S. R. Durell and H. R. Guy. Structural model of the outer vestibule and selectivity filter of the shaker voltage-gated k+ channel. *Neuropharmacology*, 35(7):761–773, 1996.
- [25] H. Ehrenreich. Self-consistent field approach to the many-electron problem. *Phys. Rev*, 115:786 – 790, 1959.
- [26] Mats A L Eriksson and Benoît Roux. Modeling the structure of agitoxin in complex with the shaker k+ channel: a computational approach based on experimental distance restraints extracted from thermodynamic mutant cycles. *Biophys J*, 83(5):2595–2609, Nov 2002.
- [27] Ulrich Essmann, Lalith Perera, Max L. Berkowitz, Tom Darden, Hsing Lee, and Lee G. Pedersen. A smooth particle mesh ewald method. *J. Chem. Phys.*, 103:8577–8592, 1995.

- [28] D. Fedida, N. D. Maruoka, and S. Lin. Modulation of slow inactivation in human cardiac kv1.5 channels by extra- and intracellular permeant cations. *J Physiol*, 515 ( Pt 2):315–329, Mar 1999.
- [29] L. Rebecca Fish, Myra T Gilligan, Alexander C Humphries, Magnus Ivarsson, Tammy Ladduwahetty, Kevin J Merchant, Desmond O’Connor, Smita Patel, Elisabeth Philipps, Hugo M Vargas, Peter H Hutson, and Angus M MacLeod. 4-fluorosulfonylpiperidines: selective 5-ht<sub>2a</sub> ligands for the treatment of insomnia. *Bioorg Med Chem Lett*, 15(16):3665–3669, Aug 2005.
- [30] G. E. Flynn and W. N. Zagotta. Conformational changes in s6 coupled to the opening of cyclic nucleotide-gated channels. *Neuron*, 30(3):689–698, Jun 2001.
- [31] Peter L Freddolino, Anton S Arkhipov, Steven B Larson, Alexander McPherson, and Klaus Schulten. Molecular dynamics simulations of the complete satellite tobacco mosaic virus. *Structure*, 14(3):437–449, Mar 2006.
- [32] M. L. Garcia, Y. Gao, O. B. McManus, and G. J. Kaczorowski. Potassium channels: from scorpion venoms to high-resolution structure. *Toxicon*, 39(6):739–748, Jun 2001.
- [33] George A Gutman, K. George Chandy, John P Adelman, Jayashree Aiyar, Douglas A Bayliss, David E Clapham, Manuel Covarriubias, Gary V Desir, Kiyoshi Furuichi, Barry Ganetzky, Maria L Garcia, Stephan Grissmer, Lily Y Jan, Andreas Karschin, Donghee Kim, Sabina Kuperschmidt, Yoshihisa Kurachi, Michel Lazdunski, Florian Lesage, Henry A Lester, David McKinnon, Colin G Nichols, Ita O’Kelly, Jonathan Robbins, Gail A Robertson, Bernardo Rudy, Michael Sanguinetti, Susumu Seino, Walter Stuehmer, Michael M Tamkun, Carol A Vandenberg, Aguan Wei, Heike Wulff, Randy S Wymore, and International Union of Pharmacology. International union of pharmacology. xli. compendium of voltage-gated ion channels: potassium channels. *Pharmacol Rev*, 55(4):583–586, Dec 2003.
- [34] L. Heginbotham, Z. Lu, T. Abramson, and R. MacKinnon. Mutations in the k<sup>+</sup> channel signature sequence. *Biophys J*, 66(4):1061–1067, Apr 1994.
- [35] L. Heginbotham and R. MacKinnon. The aromatic binding site for tetraethylammonium ion on potassium channels. *Neuron*, 8(3):483–491, Mar 1992.
- [36] A. Ralph Henderson. The bootstrap: a technique for data-driven statistics. using computer-intensive analyses to explore experimental data. *Clin Chim Acta*, 359(1-2):1–26, Sep 2005.
- [37] Berk Hess, Henk Bekker, Herman J. C. Berendsen, and Johannes G. E. M. Fraaije. Lincs: A linear constraint solver for molecular simulations. *J. Comput. Chem.*, 18:1463–1472, 1997.
- [38] P. Hidalgo and R. MacKinnon. Revealing the architecture of a k<sup>+</sup> channel pore through mutant cycles with a peptide inhibitor. *Science*, 268(5208):307–310, Apr 1995.
- [39] Bertil Hille. *Ion Channels of Excitable Membranes 3rd ed.* Sinauer Associates, Inc., 2001.
- [40] A. L. HODGKIN and A. F. HUXLEY. A quantitative description of membrane current and its application to conduction and excitation in nerve. *J Physiol*, 117(4):500–544, Aug 1952.
- [41] T. Hoshi, W. N. Zagotta, and R. W. Aldrich. Biophysical and molecular mechanisms of shaker potassium channel inactivation. *Science*, 250(4980):533–538, Oct 1990.
- [42] Craig Jamieson, Elizabeth M Moir, Zoran Rankovic, and Grant Wishart. Medicinal chemistry of herg optimizations: Highlights and hang-ups. *J Med Chem*, 49(17):5029–5046, Aug 2006.

- [43] L. Y. Jan and Y. N. Jan. Voltage-gated and inwardly rectifying potassium channels. *J Physiol*, 505 (Pt 2):267–282, Dec 1997.
- [44] Donald H Jenkinson. Potassium channels—multiplicity and challenges. *Br J Pharmacol*, 147 Suppl 1:S63–S71, Jan 2006.
- [45] Youxing Jiang, Alice Lee, Jiayun Chen, Martine Cadene, Brian T Chait, and Roderick MacKinnon. Crystal structure and mechanism of a calcium-gated potassium channel. *Nature*, 417(6888):515–522, May 2002.
- [46] Youxing Jiang, Alice Lee, Jiayun Chen, Vanessa Ruta, Martine Cadene, Brian T Chait, and Roderick MacKinnon. X-ray structure of a voltage-dependent k<sup>+</sup> channel. *Nature*, 423(6935):33–41, May 2003.
- [47] W. L. Jorgensen, D.S. Maxwell, and J. Tirado-Rives. Development and testing of the opls all-atom force field on conformational energetics and properties of organic liquids. *J. Am. Chem. Soc.*, 118(45):11225–11236, 1996.
- [48] William L. Jorgensen, Jayaraman Chandrasekhar, Jeffrey D. Madura, Roger W. Impey, and Michael L. Klein. Comparison of simple potential functions for simulating liquid water. *J. Chem. Phys.* 79, 79:926, 1983.
- [49] Susan I V Judge and Christopher T Bever. Potassium channel blockers in multiple sclerosis: neuronal kv channels and effects of symptomatic treatment. *Pharmacol Ther*, 111(1):224–259, Jul 2006.
- [50] Peter Kollman. Free energy calculations: Applications to chemical and biochemical phenomena. *Chem. Rev.*, 93(7):2395–2417, 1993.
- [51] Sebastian Kraszewski, Céline Boiteux, Marek Langner, and Christophe Ramseyer. Insight into the origins of the barrier-less knock-on conduction in the kcsa channel: molecular dynamics simulations and ab initio calculations. *Phys Chem Chem Phys*, 9(10):1219–1225, Mar 2007.
- [52] Elmar Krieger, Tom Darden, Sander B Nabuurs, Alexei Finkelstein, and Gert Vriend. Making optimal use of empirical energy functions: force-field parameterization in crystal space. *Proteins*, 57(4):678–683, Dec 2004.
- [53] Marcus B Kubitcki and Bert L de Groot. Molecular dynamics simulations using temperature-enhanced essential dynamics replica exchange. *Biophys J*, 92(12):4262–4270, Jun 2007.
- [54] Shankar Kumar, John M. Rosenberg, Djamel Bouzida, Robert H. Swendsen, and Peter A. Kollman. The weighted histogram analysis method for free-energy calculations on biomolecules. i. the method. *J. of Comput. Chem.*, 13:1011–1021, 1992.
- [55] Anling Kuo, Jacqueline M Gulbis, Jennifer F Antcliff, Tahmina Rahman, Edward D Lowe, Jochen Zimmer, Jonathan Cuthbertson, Frances M Ashcroft, Takayuki Ezaki, and Declan A Doyle. Crystal structure of the potassium channel kirbac1.1 in the closed state. *Science*, 300(5627):1922–1926, Jun 2003.
- [56] Harley T Kurata and David Fedida. A structural interpretation of voltage-gated potassium channel inactivation. *Prog Biophys Mol Biol*, 92(2):185–208, Oct 2006.

- [57] Yuri A Kuryshv, Eckhard Ficker, Lu Wang, Peter Hawryluk, Adrienne T Dennis, Barbara A Wible, Arthur M Brown, Jiesheng Kang, Xiao-Liang Chen, Kaoru Sawamura, William Reynolds, and David Rampe. Pentamidine-induced long qt syndrome and block of hERG trafficking. *J Pharmacol Exp Ther*, 312(1):316–323, Jan 2005.
- [58] Esin Kutluay, Benoît Roux, and Lise Heginbotham. Rapid intracellular TEA block of the KcsA potassium channel. *Biophys J*, 88(2):1018–1029, Feb 2005.
- [59] Adam Lange, Karin Giller, Sönke Hornig, Marie-France Martin-Eauclaire, Olaf Pongs, Stefan Becker, and Marc Baldus. Toxin-induced conformational changes in a potassium channel revealed by solid-state NMR. *Nature*, 440(7086):959–962, Apr 2006.
- [60] Andrew R. Leach. *Molecular Modelling Principles and Applications*. Longman, 1996.
- [61] C. Legros, V. Pollmann, H. G. Knaus, A. M. Farrell, H. Darbon, P. E. Bougis, M. F. Martin-Eauclaire, and O. Pongs. Generating a high affinity scorpion toxin receptor in KcsA-Kv1.3 chimeric potassium channels. *J Biol Chem*, 275(22):16918–16924, Jun 2000.
- [62] Michael J Lenaeus, Magdalini Vamvouka, Pamela J Focia, and Adrian Gross. Structural basis of TEA blockade in a model potassium channel. *Nat Struct Mol Biol*, 12(5):454–459, May 2005.
- [63] Stephen B Long, Xiao Tao, Ernest B Campbell, and Roderick MacKinnon. Atomic structure of a voltage-dependent K<sup>+</sup> channel in a lipid membrane-like environment. *Nature*, 450(7168):376–382, Nov 2007.
- [64] V. B. Luzhkov and J. Aqvist. Mechanisms of tetraethylammonium ion block in the KcsA potassium channel. *FEBS Lett*, 495(3):191–196, Apr 2001.
- [65] R. MacKinnon, S. L. Cohen, A. Kuo, A. Lee, and B. T. Chait. Structural conservation in prokaryotic and eukaryotic potassium channels. *Science*, 280(5360):106–109, Apr 1998.
- [66] R. MacKinnon and C. Miller. Mutant potassium channels with altered binding of charybdotoxin, a pore-blocking peptide inhibitor. *Science*, 245(4924):1382–1385, Sep 1989.
- [67] Shuichi Miyamoto and Peter A. Kollman. Settle: An analytical version of the shake and rattle algorithm for rigid water models. *J. of Comp. Chem.*, 13:952–962, 1992.
- [68] E. Müller, Jochen Hub, Helmut Grubmüller, and Bert de Groot. Is TEA an inhibitor for human aquaporin-1? *Pflugers Arch*, 456(4):663–669, Jul 2008.
- [69] Stephen Neal, Alex M Nip, Haiyan Zhang, and David S Wishart. Rapid and accurate calculation of protein 1h, 13c and 15n chemical shifts. *J Biomol NMR*, 26(3):215–240, Jul 2003.
- [70] Uta-Maria Ohndorf and Roderick MacKinnon. Construction of a cyclic nucleotide-gated KcsA K<sup>+</sup> channel. *J Mol Biol*, 350(5):857–865, Jul 2005.
- [71] Chunyang Peng, Philippe Y. Ayala, H. Bernhard Schlegel, and Michael J. Frisch. Using redundant internal coordinates to optimize equilibrium geometries and transition states. *J. Comput. Chem.*, 17:49 – 56, 1996.
- [72] R. Ranganathan, J. H. Lewis, and R. MacKinnon. Spatial localization of the K<sup>+</sup> channel selectivity filter by mutant cycle-based structure analysis. *Neuron*, 16(1):131–139, Jan 1996.

- [73] Benoît Roux. The calculation of the potential of mean force using computer simulations. *Computer Physics Communications*, 91:275–282, 1994.
- [74] Benoît Roux. Ion conduction and selectivity in k(+) channels. *Annu Rev Biophys Biomol Struct*, 34:153–171, 2005.
- [75] S. N. Russell, N. G. Publicover, P. J. Hart, A. Carl, J. R. Hume, K. M. Sanders, and B. Horowitz. Block by 4-aminopyridine of a kv1.2 delayed rectifier k+ current expressed in xenopus oocytes. *J Physiol*, 481 ( Pt 3):571–584, Dec 1994.
- [76] Mark S P Sansom, Indira H Shrivastava, Joanne N Bright, John Tate, Charlotte E Capener, and Philip C Biggin. Potassium channels: structures, models, simulations. *Biochim Biophys Acta*, 1565(2):294–307, Oct 2002.
- [77] H. Bernhard Schlegel. Optimization of equilibrium geometries and transition structures. *J. Comput. Chem.*, 3:214 – 218, 1982.
- [78] U. Chandra Singh and Peter A. Kollman. An approach to computing electrostatic charges for molecules. *J. Comp. Chem.*, 5:129–145, 1984.
- [79] Shirley W I Siu, Robert Vácha, Pavel Jungwirth, and Rainer A Böckmann. Biomolecular simulations of membranes: physical properties from different force fields. *J Chem Phys*, 128(12):125103, Mar 2008.
- [80] R. H. Smith, W. L. Jorgensen, J. Tirado-Rives, M. L. Lamb, P. A. Janssen, C. J. Michejda, and M. B. Kroeger Smith. Prediction of binding affinities for tibo inhibitors of hiv-1 reverse transcriptase using monte carlo simulations in a linear response method. *J Med Chem*, 41(26):5272–5286, Dec 1998.
- [81] Christopher D Snow, Eric J Sorin, Young Min Rhee, and Vijay S Pande. How well can simulation predict protein folding kinetics and thermodynamics? *Annu Rev Biophys Biomol Struct*, 34:43–69, 2005.
- [82] Eric J Sorin and Vijay S Pande. Exploring the helix-coil transition via all-atom equilibrium ensemble simulations. *Biophys J*, 88(4):2472–2493, Apr 2005.
- [83] David Van Der Spoel, Erik Lindahl, Berk Hess, Gerrit Groenhof, Alan E Mark, and Herman J C Berendsen. Gromacs: fast, flexible, and free. *J Comput Chem*, 26(16):1701–1718, Dec 2005.
- [84] Xiao Tao and Roderick MacKinnon. Functional analysis of kv1.2 and paddle chimera kv channels in planar lipid bilayers. *J Mol Biol*, 382(1):24–33, Sep 2008.
- [85] Brett A Tounge, Ramkumar Rajamani, Ellen W Baxter, Allen B Reitz, and Charles H Reynolds. Linear interaction energy models for beta-secretase (bace) inhibitors: Role of van der waals, electrostatic, and continuum-solvation terms. *J Mol Graph Model*, 24(6):475–484, May 2006.
- [86] W.F. van Gunsteren and H.J.C. Berendsen. Computer simulation of molecular dynamics: Methodology, applications, and perspectives in chemistry. *Angew. Chem. Int. Ed. Engl.*, 29:992–1023, 1990.
- [87] Wilfred F van Gunsteren, Dirk Bakowies, Riccardo Baron, Indira Chandrasekhar, Markus Christen, Xavier Daura, Peter Gee, Daan P Geerke, Alice GlÄd’ttli, Philippe H HÄijnenberger, Mika A Kastenholtz, Chris Oostenbrink, Merijn Schenk, Daniel Trzesniak, Nico F A van der Vegt, and Haibo B

- Yu. Biomolecular modeling: Goals, problems, perspectives. *Angew Chem Int Ed Engl*, 45(25):4064–4092, Jun 2006.
- [88] Junmei Wang, Piotr Cieplak, and Peter A. Kollman. How well does a restrained electrostatic potential (resp) model perform in calculating conformational energies of organic and biological molecules? *J. comput. chem.*, 21:1049 – 1074, 2000.
- [89] Junmei Wang, Wei Wang, Peter A Kollman, and David A Case. Automatic atom type and bond type perception in molecular mechanical calculations. *J Mol Graph Model*, 25(2):247–260, Oct 2006.
- [90] Junmei Wang, Romain M Wolf, James W Caldwell, Peter A Kollman, and David A Case. Development and testing of a general amber force field. *J Comput Chem*, 25(9):1157–1174, Jul 2004.
- [91] Alan Wickenden. K(+) channels as therapeutic drug targets. *Pharmacol Ther*, 94(1-2):157–182, 2002.
- [92] G. Yellen, M. E. Jurman, T. Abramson, and R. MacKinnon. Mutations affecting internal tea blockade identify the probable pore-forming region of a k+ channel. *Science*, 251(4996):939–942, Feb 1991.
- [93] S.O. Yesylevskyy and V.N. Kharkyanen. Barrier-less knock-on conduction in ion channels: peculiarity or general mechanism? *Chem. Phys.*, 312:127–133, 2005.
- [94] Frank H Yu, Vladimir Yarov-Yarovoy, George A Gutman, and William A Catterall. Overview of molecular relationships in the voltage-gated ion channel superfamily. *Pharmacol Rev*, 57(4):387–395, Dec 2005.
- [95] Ulrich Zachariae, Robert Schneider, Phanindra Velisetty, Adam Lange, Daniel Seeliger, Sören J. Wacker, Yasmin Karimi-Nejad, Gert Vriend, Stefan Becker, Olaf Pongs, Marc Baldus, and Bert L de Groot. The molecular mechanism of toxin-induced conformational changes in a potassium channel: relation to c-type inactivation. *Structure*, 16(5):747–754, May 2008.
- [96] Yong Zhao, Todd Scheuer, and William A Catterall. Reversed voltage-dependent gating of a bacterial sodium channel with proline substitutions in the s6 transmembrane segment. *Proc Natl Acad Sci U S A*, 101(51):17873–17878, Dec 2004.
- [97] Yong Zhao, Vladimir Yarov-Yarovoy, Todd Scheuer, and William A Catterall. A gating hinge in na+ channels; a molecular switch for electrical signaling. *Neuron*, 41(6):859–865, Mar 2004.
- [98] Y. Zhou, J. H. Morais-Cabral, A. Kaufman, and R. MacKinnon. Chemistry of ion coordination and hydration revealed by a k+ channel-fab complex at 2.0 a resolution. *Nature*, 414(6859):43–48, Nov 2001.

# Danksagung

Mein größter Dank gilt Bert de Groot. Er hat mir zum Einen die vorliegende Arbeit ermöglicht und zum Anderen in unendlicher Geduld, mit gewissenhafter Detailpflege die vielen kleinen und großen Fehler korrigiert und mit seinen unzähligen konstruktiven Vorschlägen und Kritiken zu Inhalt und Stil den Ertrag dieser Arbeit immens gesteigert. Seine Unterstützung machte es mir möglich diese Arbeit in der englischen Sprache zu verfassen.

Der Dank gilt ebenso Prof. Dr. Helmut Grubmüller für sein Lob und mehr noch für die sehr hilfreiche Kritik sowie Dr. Ulrich Zachariae für die tolle Zusammenarbeit und die Vorbereitung auf die Welt der Grundlagenforschung in der Anfangsphase meiner Diplomarbeit.

Ebenso aufrichtiger Dank gilt den Mitgliedern der Abteilung für theoretische und computergestützte Biophysik. Besonders möchte ich Nicole Doelker danken. Ihr regelmäßiges Feedback sowie die kontinuierliche und aktive Vermittlung chemischer und nicht-chemischer Sachverhalte hat mir sehr geholfen. Insbesondere Markus Kubitzki und Jochen Hub danke ich, für die kompetenten Beratungen und Diskussionen sowie die technische Hilfe beim Erstellen der TEEREX und Umbrella-Simulationen. Außerdem danke ich Christian Kappel für den ausgiebigen technischen Support und die regelmäßigen "Zwangspausen". Danke Anna, für die schöne Zusammenarbeit!

Ganz herzlichen Dank richte ich an meine Lektoren Ann-Kathrin, Nicole und Rudolfo für das Korrekturlesen und die hilfreichen Vorschläge. Die letzte Etappe meines Studiums ist nicht denkbar ohne die Unterstützung seitens meiner Familie und all den wunderbaren Menschen die ich meine Freunde nennen darf.

Nicht zuletzt möchte ich Prof. Dr. Norbert Dragon und Prof. Dr. Hermann Schulz von der Universität Hannover danken, die mich im Verlauf meines Studiums von der Seite der Professoren wohl am stärksten geprägt und inspiriert sowie mir das Handwerkszeug für meinen weiteren Werdegang mit auf den Weg gegeben haben, sowie Prof. Dr. Harald Lesch von der Universität München, der mit seiner lebhaften Art und Weise physikalisches Weltbild zu vermitteln mir stets Vorbild im Gespräch mit Nicht-Physikern war.

Und schließlich: Danke René!!! Von der ersten Vorlesungsstunde bis heute, hast Du mich begleitet und mich mit deiner Menschlichkeit und deiner einzigartigen Kreativität beflügelt. Danke, mein Freund!